NTNU
Innovation and Creativity

Integrated Model Based Control of Topside Process and Production Wells

Martin Berger Stange

Master of Science in Engineering Cybernetics
Submission date: June 2007
Supervisor: Ole Morten Aamo, ITK
Co-supervisor: Vidar Alstad, Hydro Olje og Energi Forskningssenter

Norwegian University of Science and Technology
Department of Engineering Cybernetics

BACKGROUND

Production systems for oil and gas are often split into two main parts with regard to optimization and control. The production wells transport the reservoir fluids from the reservoir to the processing unit at the platform. The wells are controlled manually by the operators, while the topside process is controlled using a decentralized control system.

The production rates are set at the inlet of the topside process by use of the stroke position of the production chokes for each well. There is no automatic feedback from the process to where the production rates are set. The feedback is handled manually by the operators and the performance will naturally vary depending on the operators. Especially, when one or more of the wells show natural variation in the feed rates, the feedback is slow and not optimal with respect to process utilization.

The process constraints (which limit the throughput) are typically located in the processing unit and the operational objective is to utilize the available capacity (constraint control) dynamically. Since the production rate is set at the wells, introducing automatic feedback control from the constraints to the feed stream to the process is assumed to have great economic potentials in term of plant efficiency.

The number of feed points (wells, multivariable nature) and different routing options (binary decision variables) make regular decentralized feedback control difficult to implement.

The main objective of this Master thesis is to show the potential of integrated automatic control of wells and topside processes using model based control.
The following points should be addressed:

1. MODELING

The first task of the thesis is to establish a simplified dynamic model of a generic topside process including the main unit operations. Matlab/Simulink is the preferred simulation environment. Model input will be provided by Hydro.

Next, a dynamic model of a subset of the production wells should be coupled with the dynamic model of the process. OLGA or a simplified PDE based multi-phase model is to be used as the simulation model for the wells (supplied by Hydro). The coupling of the well simulator and the simplified topside model is one important project target.
It is assumed that the constraint of the process is the available processing capacity for gas. The limits of the process are treated as hard constraints.

A disturbance scenario is to be defined in cooperation with Hydro R&D which is used as a base case for the dynamic simulations.

2. CONTROLLER IMPLEMENTATION

Two control structures should be compared with respect to robustness and performance for the predefined disturbance scenario.

The decentralized control structure should be implemented without any model in closed loop (should be possible to implement in existing DCS). The flow of gas in the compressor train should provide feedback to the choke valve for one or more of the wells. The control structure for the topside process should follow a typical offshore Hydro implementation. Back off from the constraints should be adjusted so that the operation is inside the allowable region of operation for the disturbance scenario simulated.

As an alternative control structure, an MPC controller is to be utilized for the manipulation of the well choke valves and possibly also of key set points of the topside controllers. It is assumed that there is no measurement of the flow rates from the wells. A linear model is to be used for the model of the wells in the MPC controller.

Alternative implementations should be investigated and proposed by the candidate.

3. SIMULATION

The two control structures should be compared with respect to robustness and performance for a defined disturbance signal. An economic objective should be used to evaluate the performance of the two implementations.

Abstract

In offshore production systems for oil and gas, the wells are usually controlled manually, while the topside process is controlled using a decentralized control system. It is clear that this control structure may not be economically optimal.

In the work of this thesis, one decentralized and two MPC based control systems were designed, integrating the control of the production wells and the topside process of an offshore production system. The performance of the controllers was tested in a simulation study with three different disturbance scenarios, defined in collaboration with Hydro. The simulations were also carried out using a manual control scheme, enabling a performance comparison between the designed controllers and the control conventions of today.

The automatic controllers showed a significant increase in oil throughput over the manual control scheme, while performing quite similarly when compared to each other. It is however expected that the MPCs will outperform the decentralized control system in a case with a larger number of wells than was used in the simulations of this thesis. The potential of achieving additionally smoothened topside outflow rates by applying a supervisory MPC for topside setpoint manipulation was also demonstrated.

Preface

This Master's thesis concludes my Master of Science studies at the Department of Engineering Cybernetics, the Norwegian University of Science and Technology (NTNU).

I would like to thank my primary supervisor Ole Morten Aamo at the Department of Engineering Cybernetics for dedicating a considerable amount of time throughout the last semester to our weekly meetings. His input has been greatly appreciated, and the high frequency of our meetings has helped drive the progress of the thesis work.

I would also like to thank my co-supervisor Vidar Alstad at the Norsk Hydro Oil and Energy Research Centre in Porsgrunn, Norway for the collaboration which started during my summer internship at Hydro last summer, and for taking the time flying to Trondheim for our meetings throughout the last two semesters. Finally, I would also like to thank him for constructive input and for reading through the final draft of my thesis.

Both of the above persons have shown a cheerful and down to earth attitude, which has helped keeping the work morale high throughout the thesis work.

Trondheim, June 14th, 2007

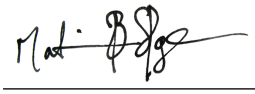

Martin Berger Stange

Contents

Chapter 1

Introduction

In many offshore production systems for oil and gas, the wells and the topside process are separated with respect to control and optimization. The flow from each well passes through a choke valve at the inlet to the topside process. Thereafter the well flows are mixed in the manifold and sent to the separators. The purpose of the topside process is to secure the quality of the exported oil and gas.

The gas processing capacity is assumed to be the main operational constraint of the topside process examined in this thesis. Utilizing this capacity can be achieved by balancing the production rate at the choke valves. While too high production rates may lead to process shut downs and flaring of gas, mainly due to excessive separator tank pressures, lower than optimal production rates obviously yield a loss of income due to lower production rates.

Usually, the topside process is controlled using a decentralized control structure, while the wells are controlled manually by the operators through the choke valve stroke positions. Although this control strategy may not be optimal with respect to utilizing the full processing capacity of the platform, its high operational reliability due to low design complexity is a favorable advantage.

The well dynamics can be difficult to predict. In addition to the natural variation in the flow rates and the multi-phase flow in each well, its dynamics are affected by the choke valve position and the gas lift rate. Also, there is the additional complexity introduced by using multiple production wells with individual dynamics and compositions. Add the dynamics of the topside process to this, and it is obvious that it may be difficult for a human operator to control the production chokes in an optimal manner.

The integrated control of topside and wells becomes more important when the process disturbances become larger (e.g. slugging wells). With unstable wells present, the platform operators tend to back off from the process capacity constraints in order to avoid process shut downs and flaring of gas in the event of excessive slugs entering the topside process. This does however yield lower production rates which lead to a loss of income. With automatic well and topside control, it is likely that we will be able to operate closer to the process constraints also with process disturbances such as slugging wells present in the system.

1.1 Compressor capacity limitation

The gas mass flow rate through the compressors can be represented using a second order compressor flow approximation as given in equation (1.1), where $f(u)$ is proportional to the shaft speed control signal u, and $c_2 < 0$. The models will be dealt with in more detail in Section 2.1.

$$w = \frac{-c_1 f(u) - \sqrt{(c_1 f(u))^2 - 4c_2[c_0 f(u)^2 - (P_{out} - P_{in})]}}{2c_2} \quad \text{[kg/s]} \tag{1.1}$$

In the following, assume that the compressor outlet pressure is given. The mass flow rate through a compressor as a function of inlet pressure and shaft speed control signal is illustrated in Figure 1.1. As can be seen in the right plot of said figure, the gas mass flow rate increases with increasing shaft speeds. This explains why the compressors often are operated at full speed[1], when recalling that the main limiting factor of the topside process often is the gas processing system.

The left plot shows that a higher compressor inlet pressure, that is, a lower pressure difference over the compressor, yields a higher mass flow rate through the compressor. However, with an upper limit on the compressor inlet pressure (which is given by the highest allowed separator tank pressure), it follows that there is an upper limitation on the attainable gas mass flow rate through the compressor when its outlet pressure is given. Thus, it seems reasonable to control the gas inflow rate to the topside process in order to avoid excessive process pressure increases. More specifically, the gas inflow rate from the wells should typically not exceed the maximum possible gas outflow rate from the gas compression train. For the above purpose, the gas inflow rate can be controlled through the production choke valves, and if we place a constraint on the compressor gas flow rate at a level lower than the circle in the left plot of Figure 1.1, the compressor should be able to keep the pressure down to a corresponding level to the left of the circle in the said plot.

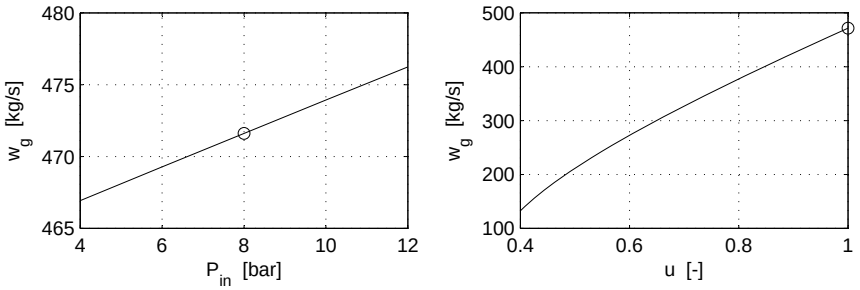

Figure 1.1: Illustration of compressor gas mass flow rates. The compressor data are taken from the second stage compressor used in later simulations. $P_{out} = 80$ bar. Constant values in the plots: Left: $u = 1$. Right: $P_{in} = 8$ bar.

1.2 Master's thesis objectives

In this Master's thesis, two main choke valve control structures will be examined. The studies are to be performed on a generic model of a topside process and its production wells. The operational objective is to maximize the oil production rate while not exceeding capacity constraints in the gas processing train.

$$\max_{u_{chokes}} \sum_{i=1}^{N_{wells}} w_{o,i} \quad s.t. \quad \sum_{i=1}^{N_{wells}} w_{g,i} \leq \bar{w}_g \tag{1.2}$$

[1]Note that with the gas compressors being the main tank pressure control devices, this means that many platforms are in effect operating without any tank pressure control, at least within certain limits.

1.2.1 Decentralized control

The first control structure to be examined is traditional decentralized control. One of the advantages of this approach is that such controllers can be easily implemented in the existing distributed control system (DCS) of the platform. Since the main operational constraint of the topside process is assumed to be the gas processing capacity, it is presumed that measurements in the gas compression train should represent good candidates for the feedback signal to the decentralized choke valve controllers. It is however assumed that the distribution of the production between the different production wells will not be straight forward in the decentralized control approach. One possibility would be to use the choke valves of one or a selection of the wells which produce significant amounts of gas for constraint control, and keep the other choke valves at constant openings.

1.2.2 Model predictive control

In the second approach, a model predictive controller (MPC) is to be used. In addition to setting choke valve positions, the MPC may be used to set control reference points for the local separator tank and compressor controllers. The advantage of employing an MPC is the prospect of achieving near optimal plantwide operation, given that the plant model and problem formulation is chosen appropriately. Further, it eliminates the eventual need of a multivariable analysis for plants with multivariable couplings. The basic PI controllers and the MPC can be considered to be situated in different layers in the control system hierarchy, namely the regulatory and supervisory control layer, respectively. Care must be taken in order to achieve a sufficient time scale separation between the two layers. That is, the supervisory control layer must operate on a slower time scale than the lower regulatory control layer. The time scale separation means that the controllers are not expected to interfere with each other stabilization wise. Note however that the MPC will operate directly on the choke valves, so this control system layering will only apply to the topside process.

1.2.3 Model requirements

For the MPC to be implemented, there is a need for a linear model of the topside process. A simplified nonlinear topside model was provided by Hydro at project startup, see Figure 1.2. Thus, there is need for linearizing the provided process model.

Further, for the well dynamics to be taken into consideration by the MPC, a linear model of the wells should also be developed. An OLGA well model was provided by Hydro. Although the OLGA model will not be used in the MPC directly due to its high complexity, it will be used for representing the physical wells in the simulations, providing a more realistic simulation case. There is thus still a need for a simplified, robust well model for use in the MPC. The behavior of the simplified well model will be verified in a comparison with the OLGA model response.

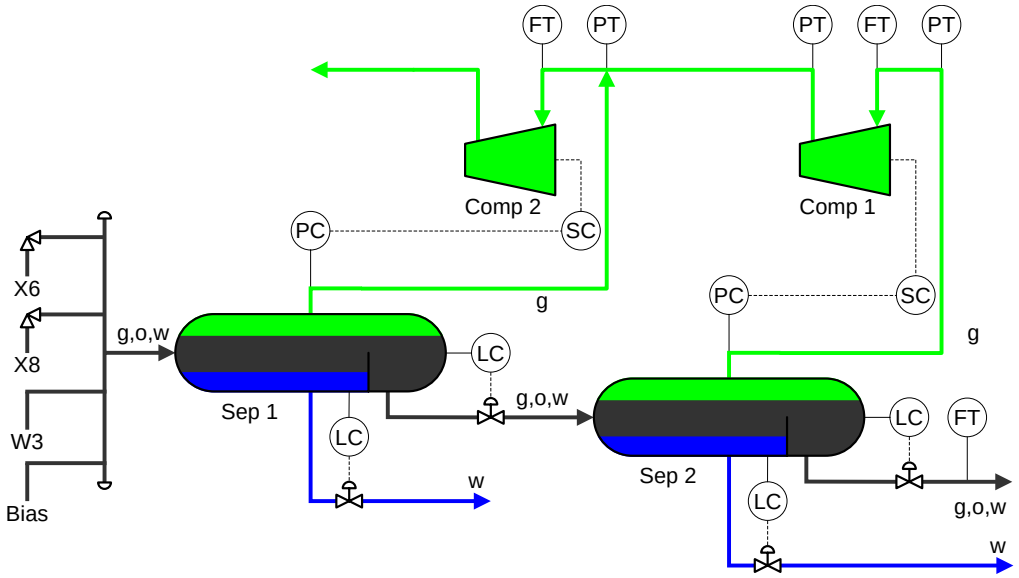

Figure 1.2: MATLAB model process elements - simplified topside process. Wells *X6* and *X8* are simulated in OLGA. *W3* is an inflow disturbance which changes between the various simulation cases. *Bias* represents the other production wells and is added to bring the inflow rates to realistic levels.

Chapter 2

Models

In this chapter, the system models will be presented. First, the nonlinear model of the topside process is introduced. Further on, the OLGA well models are presented. After this, the linearization of the well models will be presented, followed by an introduction of the disturbance well models used in the simulation cases to be introduced in Chapter 4. Note that although the topside process model and OLGA well models were provided by Hydro at project startup, the well models did not operate in a stable flow regime upon delivery, so some model adjustment was needed.

2.1 Nonlinear topside process model

The nonlinear topside process model was provided by Hydro at project startup. In the following, an outline of the model will be presented. For additional details on the model, consult the enclosed MATLAB code. Look to Appendix A for the key parameter values of the topside process.

The mass holdup of gas, oil and water in the two separator tanks define the six states of the nonlinear topside process model. The topside process is depicted in Figure 1.2.

The state vector of tank i is

$$x_i = \begin{bmatrix} m_{g,i} \\ m_{o,i} \\ m_{w,i} \end{bmatrix} \qquad [\text{kg}] \tag{2.1}$$

The mass balance of tank i is computed as follows. Note that each w_j is a 3×1 vector defining the mass flow of each of the three phases (gas, oil and water, respectively) through the different tank inlets and outlets.

$$\dot{x}_i = w_{in,i} - w_{out,g,i} - w_{out,o,i} - w_{out,w,i} \qquad [\text{kg/s}] \tag{2.2}$$

For the first separator tank, the inflow w_{in} is set by a well flow defined by a simulation performed in OLGA added on top of a bias representing the other wells. The inflow w_{in} to the second separator tank is set equal to the oil valve outflow $w_{out,o}$ from the first separator tank (easily verified by a quick glance at Figure 1.2)

$$\begin{array}{lcll} w_{in,1} & = & \text{(well outflow)} & [\text{kg/s}] \\ w_{in,2} & = & w_{out,o,1} & [\text{kg/s}] \end{array} \tag{2.3}$$

$w_{out,w}$ is the outflow passing through the water valve, and is given by equation (2.4). Note that this outflow consists of pure water, meaning that no oil mixes into the water layer of the tank. The tank pressure p is calculated in a flash equation where constant volume and temperature is assumed. The downstream pressure $p_{ext,w}$ is defined as a constant (given by the platform produced water treatment facilities, not included in the model). $K_{v,w}$ is a valve sizing constant, ρ_w is the water mass density, and u_w is the valve opening control signal.

$$w_{out,w,i} = \begin{bmatrix} 0 \\ 0 \\ 1 \end{bmatrix} \cdot u_{w,i} K_{v,w,i} \sqrt{\rho_w (p_i - p_{ext,w})} \qquad [\text{kg/s}] \tag{2.4}$$

Similarly, $w_{out,o}$ is the outflow passing through the oil valve, and is given by equation (2.5). This is a true three phase flow, due to water and gas mixing into the tank oil layer. The flow phase composition is given by x_2 in equation (2.6). ρ_2 is the average mass density of the oil layer and is different from the oil density due to water blending into the oil (gas contribution is neglected due to its low mass density). For the first separator tank, the downstream pressure is set equal to the pressure p of the second separator tank. For the second separator tank, the downstream pressure is set at a constant level (given by the oil export line inlet pressure).

$$w_{out,o,i} = x_{2,i} \cdot u_{o,i} K_{v,o,i} \sqrt{\rho_{2,i} \Delta p_i} \qquad [\text{kg/s}] \tag{2.5}$$

with

$$\begin{array}{lcl} \Delta p_1 & = & p_1 - p_2 \\ \Delta p_2 & = & p_2 - p_{ext,o,2} \end{array}$$

The phase composition x_2 of the outflow through the oil valves, equal to the phase composition in the tank oil layers, is given in equation (2.6). m_o is the mass holdup of oil in the tank. m_{wo} is the mass holdup of water in the oil phase, and is only greater than zero if the tank water level surpasses the tank weir height. m_s is the mass of the gas contained in the oil phase due to pressure conditions, and is computed from the results of the flash equation used to compute the tank pressure p. m_2 is the total mass of the holdup in the tank oil layer. Gas is neglected also here due to its relatively low mass density.

$$x_{2,i} = \frac{1}{m_{2,i}} \cdot \begin{bmatrix} m_{s,i} \\ m_{o,i} \\ m_{wo,i} \end{bmatrix} \qquad , \qquad m_{2,i} = m_{o,i} + m_{wo,i} \tag{2.6}$$

The mass flow of gas through compressor stage 1 and 2 (referring to Figure 1.2) is modeled as given below. c_0, c_1 and c_2 are parameters defining the compressor characteristics in a second order polynomial approximation. Note that $c_2 < 0$.

$$w_{g,c,i} = \frac{-u_{a,i} c_{1,i} - \sqrt{(u_{a,i} c_{1,i})^2 - 4 c_{2,i} [c_{0,i} u_{a,i}^2 - \Delta p_i]}}{2 c_{2,i}} \qquad [\text{kg/s}] \tag{2.7}$$

with

$$\begin{array}{lcl} \Delta p_1 & = & p_1 - p_2 \\ \Delta p_2 & = & p_{ext,g} - p_1 \end{array}$$

where $u_{a,i} \in [N_{min,i},\ N_{max,i}]$ is the actual input as given below, with $u_i \in [0,\ 1]$ being the control signal

$$u_{a,i} = u_i(N_{max,i} - N_{min,i}) + N_{min,i}$$

The gas outflow $w_{out,g}$ from the tanks is then as given in equation (2.8). The outflow through the gas outlet of the second separator tank is equal to the gas flow through the first compressor stage. Further, since the total gas outflow from the gas compression train is equal to the the flow through the second compressor, it follows that the difference between the mass flow through the second and first compressor has to come from the first separator tank.

$$\begin{array}{lcll} w_{out,g,1} & = & w_{g,c,2} - w_{g,c,1} & [\text{kg/s}] \\ w_{out,g,2} & = & w_{g,c,1} & [\text{kg/s}] \end{array} \tag{2.8}$$

2.2 OLGA well model

The inflow of gas, oil and water from the controlled wells to the topside process was to be simulated with two dynamic OLGA well models with an inflow bias added on top of the OLGA output in order to heighten the inflow rates to a realistic level. This bias represented the rest of the "thought" wells connected to the platform.

Two separate OLGA well models (to be denoted *X6* and *X8*) were provided by Hydro at project startup. Their geometry is presented in Figure 2.1.

For practical reasons, it was decided to replace the so called OLGA *PVT files* with the OLGA *Blackoil module*. These entities are used in the phase composition calculations of the model, and abandoning the PVT files allowed for easier model adjustments and a larger dynamic model range without the need of making new PVT files as the pressure and temperature operating points changed. This did however mean that the simulations would take more time to complete as the fluid properties would have to be calculated in stead of simply looked up in a table.

Note that the two wells were equipped with gas lift systems. These were left at 3000 and 3300 Sm^3/h for *X6* and *X8*, respectively, and will not be manipulated throughout the project. Therefore, we will not go into further details on these.

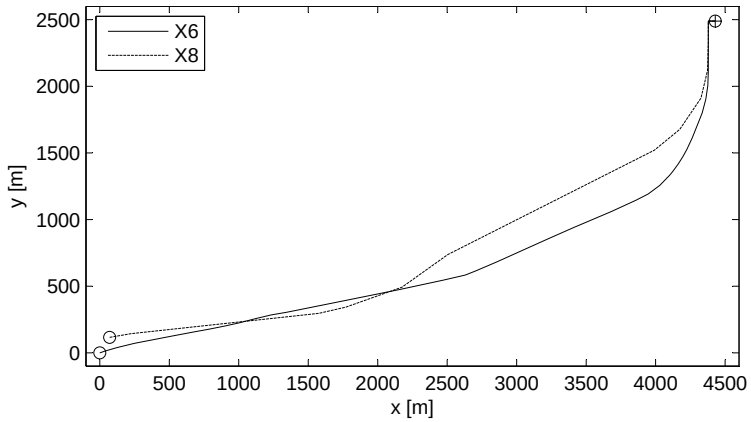

Figure 2.1: Geometry of wells *X6* and *X8*

2.2.1 Phase composition

The models would have to be scaled in order to provide a useful simulation case. First, their phase compositions were adjusted to have different gas-to-liquid ratios and water cuts. With maximization of the oil production rates being the objective of the optimization, and gas rates being the limiting factor, it would be interesting to have one well producing relatively large amounts of both oil and gas compared to the other well. Otherwise, it would seem quite obvious that the solution to gas processing capacity problems would be to choke down on the well which produced more gas. Consequently, it was decided that *X6* would have a larger oil and gas production than *X8*.

Table 2.1: Chosen GLR and w_c for the two wells. Computed at standard conditions.

Well	$GLR = \frac{Q_g}{Q_o+Q_w}$	$w_c = \frac{Q_w}{Q_o+Q_w}$
X6	800	0.75
X8	600	0.85

2.2.2 Flow rates

Thereafter, the production rates were scaled using the reservoir pressure p_r and productivity index PI as tuning parameters. The maximum capacity of the second gas compressor at the given pressure operating point (inlet pressure 8 bar, outlet pressure 80 bar) is about 470 kg/s, as is illustrated in Figure 1.1. After tuning, the wells had a maximum gas outflow rate of about 19 kg/s at full valve opening. Using this number as an average well gas flow rate, we need a total number of about 25 thought wells in order to fill the process capacity of 470 kg/s.

Table 2.2: Chosen p_r and PI for the two wells.

Well	p_r $[bar]$	PI $[Sm^3/d/bar]$
X6	140	290
X8	160	210

Table 2.3: Maximum well outflow rates, in kg/s, with outlet pressure 8 bar. At full choke valve opening.

Well	$\bar{w}_g$	$\bar{w}_o$	$\bar{w}_w$
X6	20.2	4.2	15.5
X8	17.0	2.8	19.3
Average	18.6	3.5	17.4

2.2.3 Model combination

The two models were combined in a single OLGA model file in order to get less simulation overhead. They shared the same output boundary condition, which was set equal to the dynamic pressure of the first separator tank.

2.2.4 Choke valve stroke time

The choke valve stroke time, defined as the time the valve uses to go from fully closed to fully open, was set to 8 minutes, and was introduced as follows. First, a manual controller was defined per choke valve in the OLGA model. For each choke valve, a controller was assigned (and the valve *time* parameter was left blank). The stroke time was set as a parameter in the controllers. The controllers would then receive and simply pass through control commands (valve opening setpoints) from the controllers implemented in MATLAB to their assigned valves.[1]

2.3 Linear well model

A linear time invariant (LTI) well model was needed for use in the MPCs, relating the choke valve openings to the combined well outflow. The step response of the OLGA simulated wells is illustrated in Figure 2.2, showing the well flow response to stepwise choke valve opening changes. Note that the steady state gain decreases nonlinearly with increasing valve openings (approximately quadratically, see Figure 2.3). The model to be found was of the form

$$\begin{aligned} x_{k+1} &= A^w x_k + B^w u_k \\ y_k &= C^w x_k + D^w u_k \end{aligned} \tag{2.9}$$

In the above, the w indicate that the matrices represent the well model. The control input is the choke valve openings of choke valves *X6* and *X8*, and the measurement vector is the mass flow rate of gas, oil and water out of the combined wells

$$u_k = \begin{bmatrix} u_{X6,k} \\ u_{X8,k} \end{bmatrix} \quad , \quad y_k = \begin{bmatrix} y_{1,k} \\ y_{2,k} \\ y_{3,k} \end{bmatrix} = \begin{bmatrix} w_g \\ w_o \\ w_w \end{bmatrix} \tag{2.10}$$

Mainly two approaches to the well modeling were considered. The first involved use of the *System identification toolbox* of MATLAB. It did however prove a bit difficult to achieve good model characteristics with low model orders using the said toolbox, as the main desired characteristics of the model were not necessarily the ones being weighted the most by the toolbox routines. Thus, after a while, a manual modeling approach was carried out. This approach was much more successful, cutting the number of model states in half, if not down to one third.

2.3.1 Model design principle

It was decided to model the response for an input step change from 20 to 25% valve openings (indicated in Figure 2.2 with thick lines). At this operating point, both the steady state gain and the transient response could be considered to be around the average over the whole spectrum of valve openings, not being too extreme in any direction.

Prior to the modeling, the linearization point of the input u_k (valve openings) and the measurement y_k (flow rates) were stored in the vectors u^N and y^N, respectively, such that

$$\begin{aligned} u_k &= \Delta u_k + u^N \\ y_k &= \Delta y_k + y^N \end{aligned} \tag{2.11}$$

[1] Note that there is also the possibility of assigning a stroke time parameter directly to the valve objects in OLGA models, but this parameter is restricted for use only with separator tank drain valves and does not comply with our case.

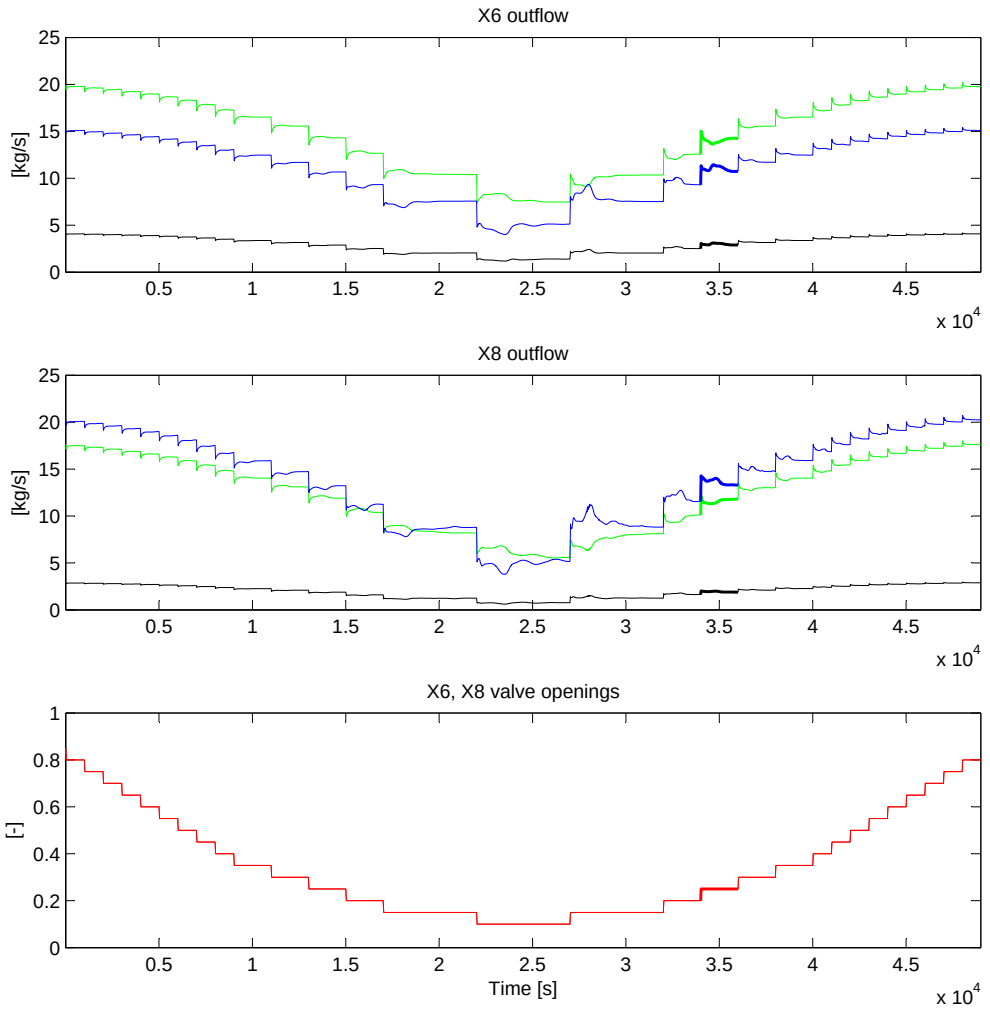

Figure 2.2: Response of well *X6* and *X8* to choke valve opening steps of magnitude 5%. Note the nonlinear steady state gain, and the approximate symmetry when comparing the response to increasing and decreasing valve openings. The thick lines around $t = 35,000\ s$ indicate the responses used in the linearization of the wells. Green-gas, black-oil, blue-water.

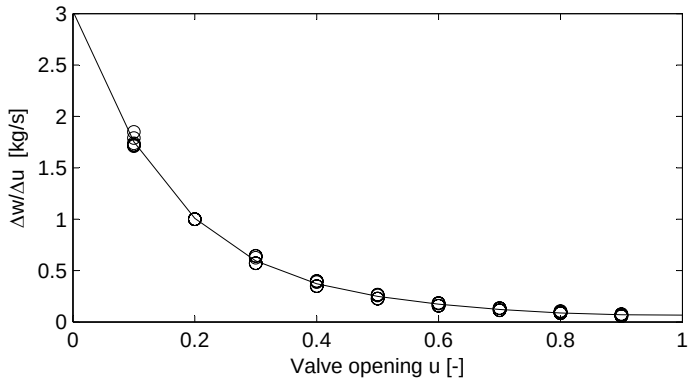

Figure 2.3: Flow rate steady state gain at different valve openings. Relative to gain at linearization point $u = 0.2$. Circles: gain of the six different inflows (three from *X6*, three from *X8*). Solid line: The mean response.

The nonlinear responses were then shifted to an initial value of zero by subtracting y^N from the

measurements.

The two OLGA wells would be modeled separately. For each well, it seemed that the oil and water phase flow could share dynamics, only to be distinguished by different measurement gains. The individual dynamic responses were modeled as a low-pass filtered first order plus delayed second order transfer function. The delay of the second order response was realized with a first order Padé approximation, requiring one additional state. The low-pass filtering of the first order response was included in order to represent the valve stroke time and gave a strictly proper transfer function (meaning that the input signal would not pass directly through to the measurement).

The inverse response introduced by the right-half plane zero of the Padé approximation would call for some additional tuning. As an alternative to the Padé approximation, one could have introduced time shifting states in the discrete system. This solution would however necessarily introduce quite a considerable amount of extra model states and was avoided.

With a total of five states per dynamic well outflow, the model would require a total of twenty states for the representation of the six phase flows before model reduction. The transfer functions took the form of equation (2.12), and the principle is illustrated in Figure 2.4.

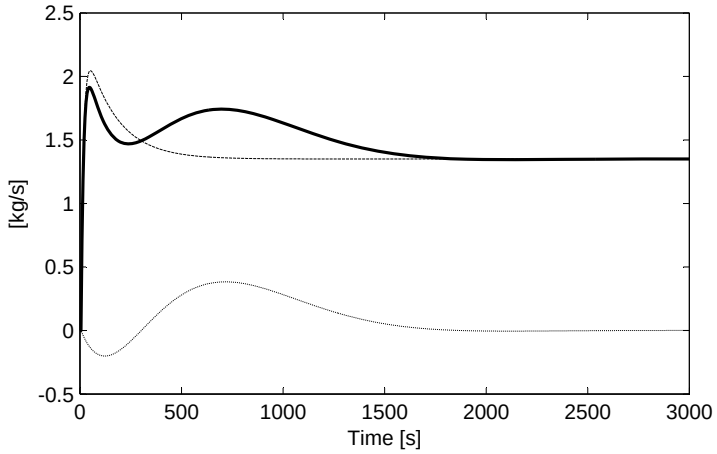

Figure 2.4: Design principle. Well flow model (thick, solid) is the sum of a low-pass filtered first order (dashed) and delayed second order (dotted) transfer function. Inverse response is due to Padé approximation.

$$y(s) = \left(\left(\frac{K_1 s}{1 + T_1 s} + y_f \right) \cdot \frac{1}{1 + T_2 s} + \frac{K_2 s}{1 + 2\zeta \frac{s}{\omega_0} + (\frac{s}{\omega_0})^2} \cdot \frac{1 - \frac{\theta}{2} s}{1 + \frac{\theta}{2} s} \right) u \tag{2.12}$$

2.3.2 Model tuning

The model tuning was carried out as follows, and was performed as a combination of calculations based on plot measurements and tweaking through examination of the resulting plots. While reading through the following section, it could be handy to keep an eye on the response of the original nonlinear system and the response of the resulting model, shown in Figure 2.6.

y_0 and y_f were found as the height of the initial peak and the steady state gain, respectively. A first order response was fitted to the first part of the plot, falling from y_0 to y_f. T_1 was found as the time constant of this response.

An approximate of K_1 was found by applying the initial value theorem to the first parenthesis of equation (2.12), setting the initial value equal to y_0

$$\lim_{s\to\infty} \frac{K_1}{1+T_1 s} + y_f = \frac{K_1}{T_1} + y_f = y_0 \Rightarrow K_1 = T_1(y_0 - y_f) \tag{2.13}$$

The low-pass filter was introduced with T_2 set such that the well flow estimate would closely resemble the physical flow response at the time of the next MPC iteration, e.g. $20s$ into the response if using $20s$ as the MPC sampling interval. After introducing the low-pass filter, the gain K_1 would need some adjustments due to the low-pass filter lowering the overall gain of the filtered model. While the filter would mean that the initial peak of the response would be smoothened out, it was included due to the importance of getting a more accurate MPC prediction of particularly the first upcoming flow rate.

Then, the delay θ before the start of the second order response was found by plot examination. The damping factor ζ was initially set to 0.7. Lowering this value would lead to a more distinct second order response, but would also give more oscillations and also increase the inverse response effect of the Padé delay approximation. ω_0 was chosen such that $1/\omega_0 + \theta$ resembled the approximate desired time of the maximum of the second order response (this point is slightly before the exact maximum, see Figure 2.5 for an illustration without the time delay added).

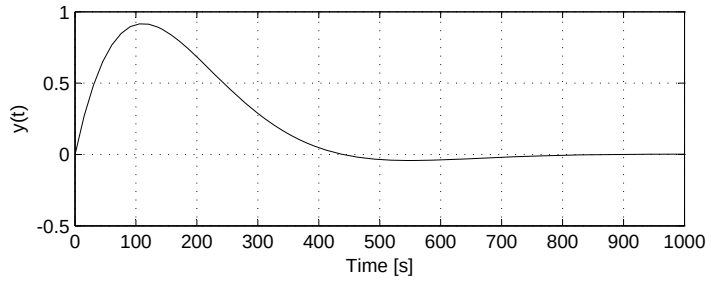

Figure 2.5: Step response of $K_2 s/(1 + 2\zeta\frac{s}{\omega_0} + (\frac{s}{\omega_0})^2)$. $\omega_0 = 1/100$, $K_2 = 200$, $\zeta = 0.7$. Maximum occurs close to $t = 100\ s$.

Finally, an approximate of K_2 was found by taking the inverse Laplace transform of the non-delayed second order response after exciting it with a unit step input

$$\begin{aligned} y(t) &= L^{-1}\left\{\frac{K_2 s}{1+2\zeta\frac{s}{\omega_0}+(\frac{s}{\omega_0})^2}\cdot\frac{1}{s}\right\} \\ &= K_2\omega_0 \mathrm{e}^{-t\zeta\omega_0}\sinh\left(t\omega_0\sqrt{\zeta^2-1}\right)\frac{1}{\sqrt{\zeta^2-1}} \end{aligned} \tag{2.14}$$

As stated earlier (see Figure 2.5), an approximate maximum of the above function can be found at $t = 1/\omega_0$

$$y(t = 1/\omega_0) = K_2\omega_0\mathrm{e}^{-\zeta}\sinh\left(\sqrt{\zeta^2-1}\right)\frac{1}{\sqrt{\zeta^2-1}} \tag{2.15}$$

Defining $y_{\omega_0} = y(t = 1/\omega_0)$, we get the following for calculating the gain which sets the approximate maximum of the second order response equal to the desired y_{ω_0}

$$K_2 = \frac{y_{\omega_0}\sqrt{\zeta^2-1}}{\omega_0\mathrm{e}^{-\zeta}\sinh\left(\sqrt{\zeta^2-1}\right)} \tag{2.16}$$

After some tuning, the parameters for the wells were found as follows.

Table 2.4: Parameters used in the transfer functions as given in equation (2.12)

Parameter	*X6g*	*X6w,o*	*X8g*	*X8w,o*
y_f	33.2	27	30	37
K_1	868	2850	360	4200
T_1	35	150	20	200
T_2	13	13	13	13
K_2	-3656.5	4940.3	-8776.6	11834.0
ζ	0.9	0.7	0.75	0.65
$1/\omega_0$	200	250	350	350
θ	350	600	130	500

2.3.3 The resulting model

The combined water and oil models were modeled for the water flow. Then, the individual gas and water models were taken over to state space form and discretized. Following this, the water state space model was duplicated to represent the oil model and the oil measurement matrices C and D were scaled down in accordance with the ratio *(steady state gain oil)/(steady state gain water)*. The two A and B matrices were combined in a block-diagonal form, and the three C and D measurement matrices were stacked vertically. The model before model order reduction was then

$$\begin{aligned} \Delta x_{k+1} &= \begin{bmatrix} A_g & 0 \\ 0 & A_{o,w} \end{bmatrix} \Delta x_k + \begin{bmatrix} B_g & 0 \\ 0 & B_{o,w} \end{bmatrix} \Delta u_k \\ \Delta y_k &= \begin{bmatrix} C_g \\ C_o \\ C_w \end{bmatrix} \Delta x_k + \begin{bmatrix} D_g \\ D_o \\ D_w \end{bmatrix} \Delta u_k \end{aligned} \tag{2.17}$$

Lastly, the model order was reduced by two states using the MATLAB function `minreal`, bringing the model order down from twenty to eighteen for representing the six well outflows. The step response of the resulting model is shown in Figure 2.6, and the reduced order model is repeated below

$$\begin{aligned} \Delta x_{k+1} &= A^w \Delta x_k + B^w \Delta u_k \\ \Delta y_k &= C^w \Delta x_k + D^w \Delta u_k \end{aligned} \tag{2.18}$$

with

$$\begin{aligned} u_k &= \Delta u_k + u^N \\ y_k &= \Delta y_k + y^N \end{aligned} \tag{2.19}$$

As a final note on the models, one could have considered including a second second order response in the oil and water flow models, representing the first minor top which happens between approximately 100 and 400 s in Figure 2.6. However, with the linear model being tuned at one operating point and the transient response being somewhat different at other points, it would not necessarily improve the overall controller performance much. There would still be model errors present in the system either way.

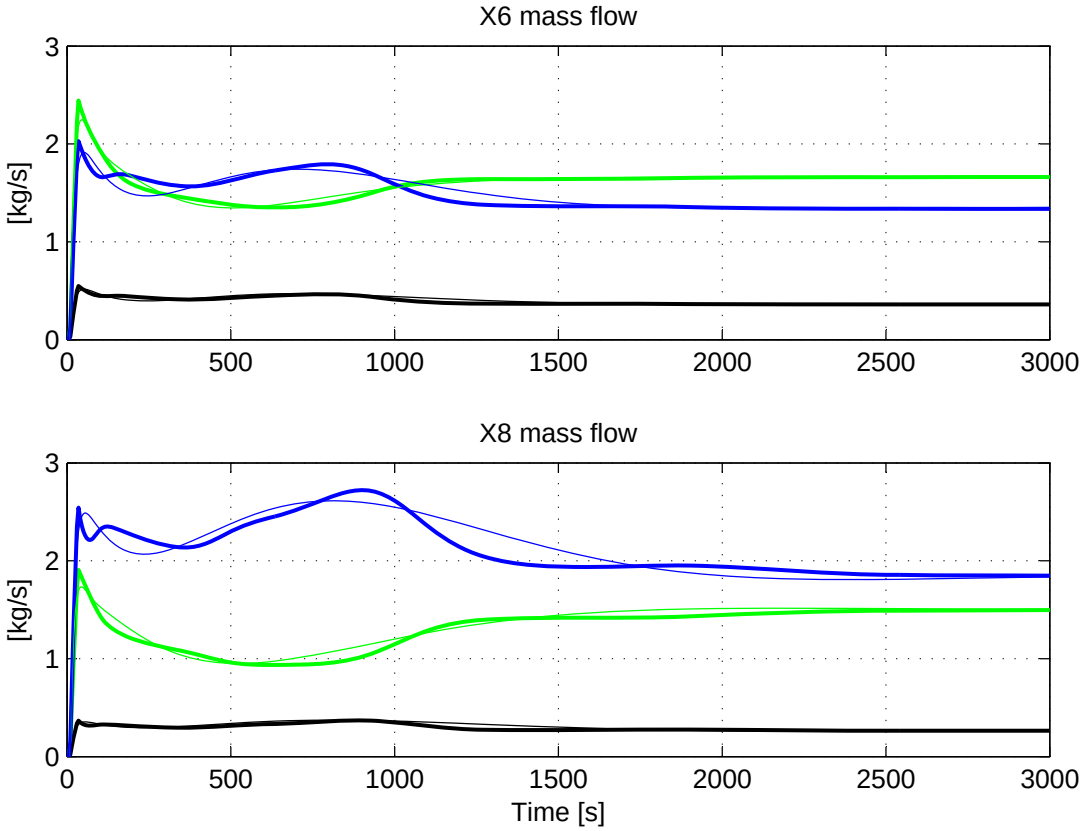

Figure 2.6: Resulting linearized model, shifted down to initial value zero for easier comparison. Response to a valve opening step change from 20 to 25%. Thick lines: actual nonlinear well response. Thin lines: linear model. Green-gas, black-oil, blue-water.

2.4 Well startup model

In the simulation case to be denoted as *case 1* in Chapter 4, the well *W3* in Figure 1.2 will be simulated using OLGA. The well will be opened for production after some time, and the *W3* choke valve will be held at a constant level thereafter. This change in production will be known in advance, and with a model of the startup dynamics of *W3*, the controllers will perform a feedforward compensation in advance of and during the production change in order to try to avoid breaking any constraints and try keeping the production as optimal as possible.

W3 has the same geometry and properties as the well *X6* (see Section 2.2), albeit with its *GLR* set to 700 and its gas lift rate set to 1980 Sm^3/h.

The startup dynamics of the third well will be introduced to the controllers through logging data from previous startups (in our case from previous simulations). If no inflow rate measurement logs are available in a practical implementation (for instance due to lack of instrumentation at the well outlet), they could be generated from other plant measurements using a model based estimator such as a Kalman filter, or the data could be generated using simulation software such as OLGA.

The logging data to be used for feedforward in later simulations are shown in Figure 2.7. The choke valve is opened from 0 to 15% after $2000s$. The *W3* gas lift is started at $t = 0s$, building up pressure before the valve is opened, as is standard practice. In some cases, a simplified model based on the logging data will be fed forward, more about this later.

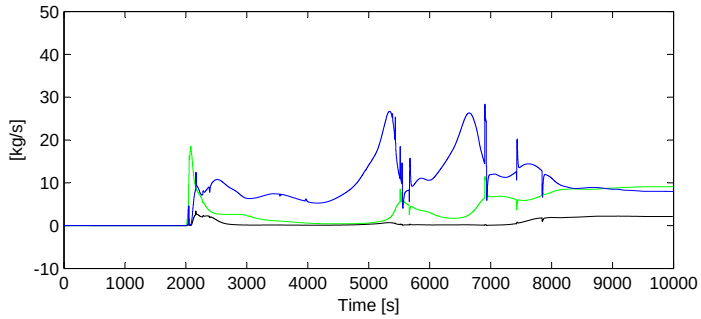

Figure 2.7: Startup of well *W3*. Choke valve moves from 0 to 15% at $t = 2000s$. Gas lift is started at $t = 0s$. Green-gas, black-oil, blue-water.

Figure 2.8 shows the outflow from *W3* if the choke valve opening is postponed from the initial $t = 2000s$, as shown in Figure 2.7, to $t = 4000s$, thereby allowing a further pressure and mass buildup prior to the valve opening. Although the trend is quite similar in the two cases, there is still some difference, especially in the gas flow rate peak amplitude, and the figures hint at the importance of applying the right startup model depending on the actual operating conditions.

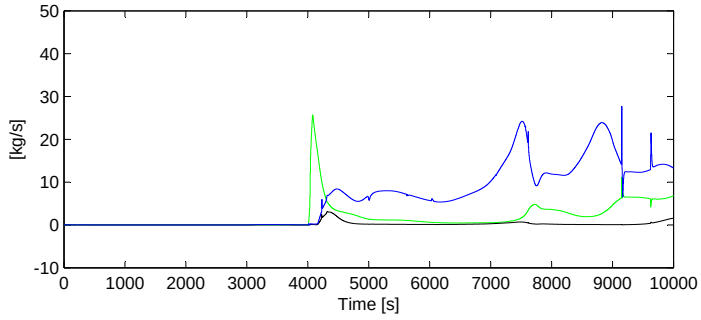

Figure 2.8: Startup of well *W3*. Choke valve moves from 0 to 15% at $t = 4000s$. Gas lift is started at $t = 0s$. Green-gas, black-oil, blue-water.

2.5 Slugging well model

In the simulation case to be denoted as *case 2* in Chapter 4, the well *W3* in Figure 1.2 will be defined by a pre-generated inflow vector, representing a slugging well. The inflow disturbance, shown in Figure 2.9, will not be known in advance.

While we will not try to control the slugging well itself, we will examine how the other controlled wells and the topside process can be used to compensate for the disturbances which are introduced to the system.

The maximum amplitude of the *W3* gas, oil and water mass flow rates were set equal to the average maximum flow rate of wells *X6* and *X8*, as given in Table 2.3 on page 8. If the inflow rates had been set too high, the two controlled wells and the topside process would not have been able to compensate adequately for the disturbance. The same applies if the inflow disturbance rate was too rapidly changing.

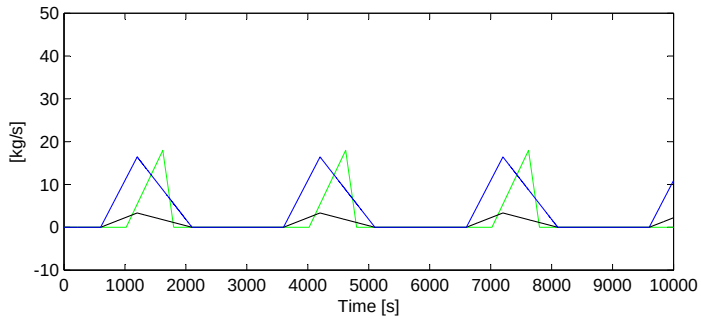

Figure 2.9: Process disturbance - slugging well. Slug period time 50 minutes. Green-gas, black-oil, blue-water.

Chapter 3

Controllers

In this chapter, the various controller approaches will be presented. Simulation results follow in Chapter 4.

The MPC implementations will use the compressed formulation of Maciejowski (2002). Using this formulation, the optimization state vector consists exclusively of the future control input changes (and eventual augmented parameters needed for soft constraints, more about this later). The system model is substituted into the objective function and the constraints, thereby eliminating the need for additional equality constraints. The result is a computationally efficient MPC structure with a relatively small optimization state vector. Note that with the well model being stable, and the topside process being marginally stable (integrating tanks), there is no need for prestabilizing the process for the MPCs to function properly, see page 22 of Maciejowski (2002).

In the following, the tuning of the topside PI controllers will be presented. Following this, the basic structure common to all the realized MPCs will be introduced. Thereafter, we turn the focus to the specific MPCs and decentralized controllers.

3.1 Topside PI controller tuning

For control system setups relying solely on PI controllers for controlling the topside process (all realized controllers except for the one to be denoted *MPC2*), the tank level controllers should be loosely tuned in order to utilize the buffering capacity of the tanks. The tank level controllers were therefore in these cases tuned using the smooth tuning rules of Skogestad (2006) for averaging tank level control.

The separator tank pressures were in all controller setups controlled using PI controllers alone, the tuning of which was leaning towards a fast response.

The level controller tuning was performed as part of the project, while the pressure controllers were adequately tuned upon model delivery from Hydro. Therefore, in the following, tuning details will only be presented for the level controllers. The parameters of the other controllers will be presented, but not discussed in any more detail.

3.1.1 Smooth tuning for averaging level control

From equation (18) and the equation after equation (23) in Skogestad (2006), we have for controller i

$$K_{c,i} = \frac{|\Delta q_{0,i}|}{|\Delta h_{max,i}|} = \frac{|\Delta w_i|}{\rho_i |\Delta h_{max,i}|} \tag{3.1}$$

and

$$\tau_{I,i} = 4\tau_{tank,i} = 4\frac{|\Delta V_i|}{|\Delta q_{0,i}|} = 4L_i D_i \frac{|\Delta h_{max,i}|}{|\Delta q_{0,i}|} = \frac{4L_i D_i}{K_{c,i}} \tag{3.2}$$

in the above, $|\Delta q_0|$ [m^3/s] is the maximum expected inflow disturbance flow rate, and $|\Delta h_{max}|$ [m] is the maximum allowed level control deviation. The tank residence time τ_{tank} [s] is equal to the tank volume ΔV [m^3] available for liquid buffering divided by the maximum inflow disturbance rate Δq_0 [m^3/s]. L and D are tank lengths and widths as illustrated in Figure 3.1.

In the following, we have assumed that the maximum inflow disturbance rate is equal to the magnitude of one average well, as given in Table 2.3 on page 8. For the oil level controllers, we must also include the water inflow disturbances in the calculations, since the oil floats on top of the water and is thus directly affected by the water disturbances. With parameters as given in Table 3.1, we get the tunings of Table 3.2.

Table 3.1: Parameters used for smooth level control tuning. See Figure 3.1 for reference. The difference between the oil surface length of separator tank 1 and 2 is due to different tank lengths.

	D_i [m]	L_i [m]	$\Delta h_{max,i}$ [m]	Δw_i [kg/s]	ρ_i [kg/m^3]
Sep1,o	3.0	8.47	0.4	3.5+18.6=22.1	$\frac{3.5 \cdot 800 + 18.6 \cdot 1000}{3.5+18.6} = 968.3$
Sep1,w	2.2	5.54	0.2	18.6	1000
Sep2,o	3.0	5.89	0.4	3.5+18.6=22.1	$\frac{3.5 \cdot 800 + 18.6 \cdot 1000}{3.5+18.6} = 968.3$
Sep2,w	2.2	5.54	0.2	18.6	1000

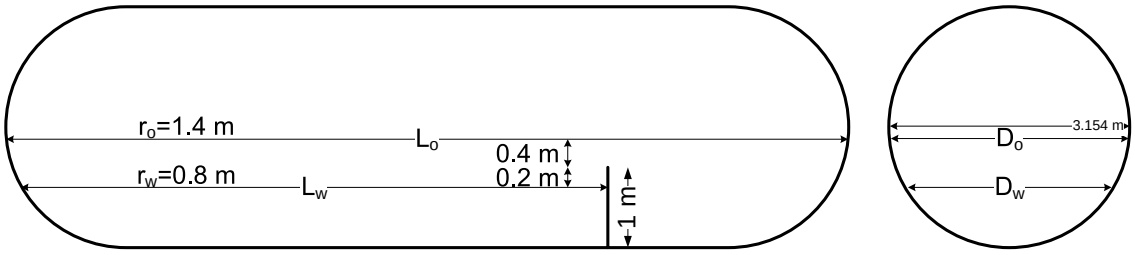

Figure 3.1: Tuning parameter reference illustration. For use with Table 3.1. Separator tank schematic view. First and second separator tanks have different lengths, but same weir positions.

Table 3.2: Final PI controller tunings

Parameter	*Value*
$K_{c,sep1,p}$	0.5
$K_{c,sep2,p}$	0.5
$\tau_{I,sep1,p}$	100
$\tau_{I,sep2,p}$	100
$K_{c,sep1,o}$	0.0512
$K_{c,sep2,o}$	0.0512
$K_{c,sep1,w}$	0.0822
$K_{c,sep2,w}$	0.0822
$\tau_{I,sep1,o}$	1986
$\tau_{I,sep2,o}$	1382
$\tau_{I,sep1,w}$	593
$\tau_{I,sep2,w}$	593

3.2 Common MPC structure

The state and measurement updates of the linearized model are (the size and structure of the A, B, C and D matrices will vary in the different MPC implementations)

$$\begin{aligned} \Delta x_{k+1} &= A\Delta x_k + B\Delta u_k \\ \Delta y_k &= C\Delta x_k + D\Delta u_k \end{aligned}$$

Reserving the Δ character for input changes between two iterations, we write the following in stead in order to avoid confusion

$$\begin{aligned} \tilde{x}_{k+1} &= A\tilde{x}_k + B\tilde{u}_k \\ \tilde{y}_k &= C\tilde{x}_k + D\tilde{u}_k \end{aligned} \tag{3.3}$$

Introducing $\Delta u_{k+i} = \tilde{u}_{k+i} - \tilde{u}_{k+i-1}$, we have

$$\begin{aligned} \tilde{x}_{k+1} &= A\tilde{x}_k + B(\tilde{u}_{k-1} + \Delta u_k) \\ \tilde{y}_k &= C\tilde{x}_k + D(\tilde{u}_{k-1} + \Delta u_k) \end{aligned} \tag{3.4}$$

For the next iteration, we get

$$\begin{aligned} \tilde{x}_{k+2} &= A\tilde{x}_{k+1} + B\tilde{u}_{k+1} \\ &= A(A\tilde{x}_k + B(\tilde{u}_{k-1} + \Delta u_k)) + B(\tilde{u}_{k-1} + \Delta u_k + \Delta u_{k+1}) \\ &= A^2\tilde{x}_k + (B + AB)\tilde{u}_{k-1} + (B + AB)\Delta u_k + B\Delta u_{k+1} \\ \tilde{y}_{k+1} &= C\tilde{x}_{k+1} + D\tilde{u}_{k+1} \\ &= C(A\tilde{x}_k + B(\tilde{u}_{k-1} + \Delta u_k)) + D(\tilde{u}_{k-1} + \Delta u_k + \Delta u_{k+1}) \\ &= CA\tilde{x}_k + (D + CB)\tilde{u}_{k-1} + (D + CB)\Delta u_k + D\Delta u_{k+1} \end{aligned} \tag{3.5}$$

3.2.1 Prediction

With prediction horizon H_p and control horizon H_u, we get the following prediction of the next H_p measurements after some straight forward substitutions similar to the ones done between equations (3.4) and (3.5). Note that the control input is held constant for all $k > H_u$.

$$\begin{bmatrix} \tilde{y}_{k+1} \\ \tilde{y}_{k+2} \\ \vdots \\ \tilde{y}_{k+H_u} \\ \vdots \\ \tilde{y}_{k+H_p} \end{bmatrix} = \begin{bmatrix} CA \\ CA^2 \\ \vdots \\ CA^{H_u} \\ \vdots \\ CA^{H_p} \end{bmatrix} \tilde{x}_k + \begin{bmatrix} D + CB \\ D + CAB \\ \vdots \\ D + C\sum_{i=0}^{H_u-1} A^i B \\ \vdots \\ D + C\sum_{i=0}^{H_p-1} A^i B \end{bmatrix} \tilde{u}_{k-1} +$$

$$\left[\begin{array}{cccc} D + CB & D & 0 & \cdots \\ D + CB + CAB & D + CB & D & \ddots \\ \vdots & & & \ddots \\ \vdots & & & \\ D + C\sum_{i=0}^{H_u-1} A^i B & & & \cdots \\ \hline \vdots & & & \\ \vdots & & & \\ D + C\sum_{i=0}^{H_p-1} A^i B & & & \cdots \end{array}\right.$$

$$\left.\begin{array}{c} 0 \\ \\ 0 \\ D \\ D + CB \\ \hline D + CB + CAB \\ \vdots \\ D + C\sum_{i=0}^{H_p-H_u} A^i B \end{array}\right] \begin{bmatrix} \Delta u_k \\ \Delta u_{k+1} \\ \vdots \\ \vdots \\ \Delta u_{k+H_u-1} \end{bmatrix} \tag{3.6}$$

More compactly written, we have

$$\tilde{\mathcal{Y}}_k = \underbrace{\Psi \tilde{x}_k + \Upsilon \tilde{u}_{k-1}}_{past} + \underbrace{\Theta \Delta \mathcal{U}_k}_{future} \tag{3.7}$$

Note that the first two parts of the left hand side of equation (3.7) are given by the past states and control inputs and cannot be influenced. Thus, the only free variables in the optimization are the ones being contained in the $\Delta\mathcal{U}_k$ vector. Also note that although the said vector contains predicted control input changes H_u steps into the future, only the first input (Δu_k) will actually be used. After this iteration, the prediction and control horizons will recede, and the optimization will be performed again, after updating $\tilde{x}_k$ and $\tilde{u}_{k-1}$ with new values.

3.2.2 Integral action for offset-free control

Dealing with a nonlinear system, the predictions from the linear model will not be correct. For example, there is a nonlinear steady state gain in the well outflow rate response to the changing choke valve openings, see Section 2.3. Also, there are the nonlinearities of the topside process, see Section 2.1.

For the constraint control to be offset-free, we need to compensate for the mismatching model and eventual unmeasured process disturbances. This can be done by adding the discrepancy between the physical plant output and the predicted plant output to the next prediction (see page 18 in Maciejowski (2002)). This is commonly known as MPC integral action and can be realized with the following simple modification to equation (3.7)

$$\tilde{\mathcal{Y}}_k = \Psi \tilde{x}_k + \Upsilon \tilde{u}_{k-1} + \Theta \Delta \mathcal{U}_k + \Phi d_k \tag{3.8}$$

where

$$d_k = y_k - \hat{y}_{k|k-1} \tag{3.9}$$

and

$$\Phi = \begin{bmatrix} I \\ \vdots \\ I \end{bmatrix} \tag{3.10}$$

3.2.3 Vector and matrix dimensions

H_p and H_u are the prediction and control horizons, respectively. The MPC vector and matrix dimensions are given in Table 3.3.

Table 3.3: MPC vector and matrix dimensions

$\tilde{x}_k$	$n_x \times 1$
$\tilde{u}_k$	$n_u \times 1$
$\tilde{y}_k$	$n_y \times 1$
$\tilde{d}_k$	$n_y \times 1$
$\tilde{\mathcal{Y}}_k$	$n_y H_p \times 1$
$\Delta\mathcal{U}_k$	$n_u H_u \times 1$
Ψ	$n_y H_p \times n_x$
Υ	$n_y H_p \times n_u$
Θ	$n_y H_p \times n_u H_u$
Φ	$n_y H_p \times n_y$

3.3 *MPC1* - Direct choke valve control

The MPC1 control system is structured as shown in Figure 3.2, using an MPC for well control and a decentralized control system for tank level and pressure control.

The MPC used a plant model consisting of a linearized well model and a simple topside model. The topside model simply consisted of the steady state gain relation between the outflow rate from the wells and the outflow rate from the topside process for the gas and oil phases. It only modeled those two phases since the objective function only focused on those two topside outflow rates for constraint control and production maximization. Also, with the close connection between the oil and water phase flows, smoothing the oil outflow rate translates directly to the same effect for the water flow rate.

Figure 3.3 shows the flow rate of gas and oil out of compressor stage two and the second separator tank, respectively, when the topside process is subjected to a 2.5% step increase in the inflow rates of the two said phases from the wells. The figure demonstrates that a simple gain model is a good representation of the gas input-output dynamics of the topside process.

Although transient dynamics are present in the oil input-output relation of the topside process, these dynamics were not modeled in this particular MPC implementation, for a few reasons. First of all, what is needed for maximizing the oil production, is simply for the MPC to know

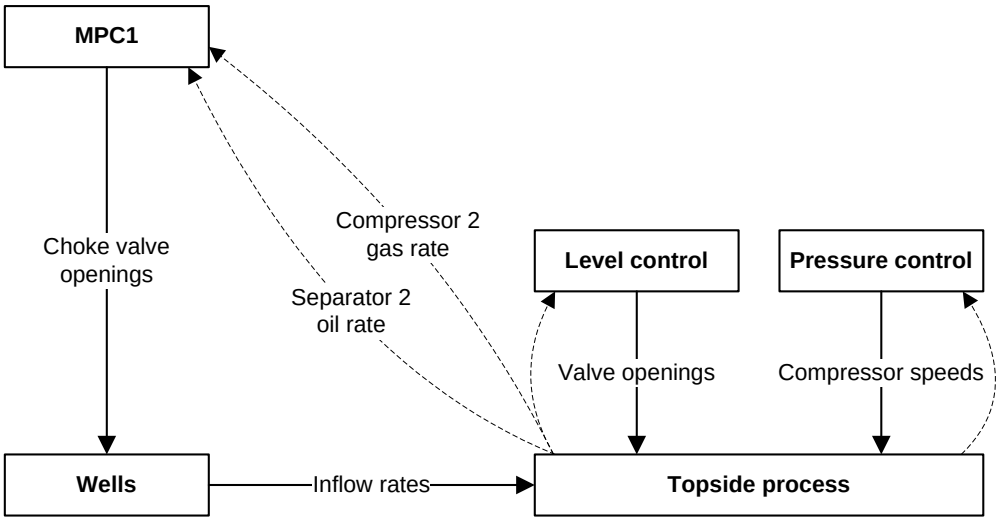

Figure 3.2: Structure of control system *MPC1*. Feedback to level and pressure control system is tank level and pressure measurements, respectively.

that ultimately, more oil inflow means more oil outflow. The focus of the MPC with respect to the oil outflow is mainly that of flow maximization; there is no reference trajectory to be followed. This can be taken care of using a simple gain model. There is however the aspect of outflow smoothing for the protection and easier operation of downstream process facilities. This is realized in the MPC by a cost on changes in the outflow from the topside process. However, smoothing the outflow rate using a simple steady state gain model for the topside oil outflow rate, means that the actual outflow rate will be even smoother than predicted in the MPC. Thus, a simple gain model was used also for the oil flow rate, thereby saving a few model states.

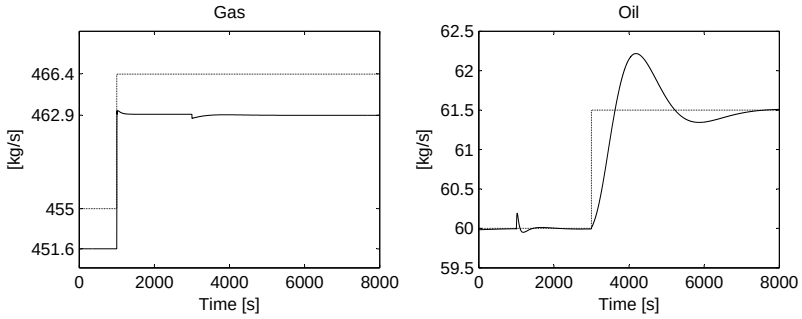

Figure 3.3: Left: Gas outflow rate from second compressor stage (solid) when subjected to a 2.5% increase in the gas inflow rate from the wells (dotted). Right: Oil outflow rate from second separator tank (solid) when subjected to a 2.5% increase in the oil inflow rate from the wells (dotted).

In the following, the structure of *MPC1* will be presented.

3.3.1 Overall plant model

The overall plant input was chosen to be the choke valve opening of the wells *X6* and *X8*. The plant measurements were the gas mass flow rate out of the second compressor and the oil mass flow rate out of the second separator tank

$$u_k = \begin{bmatrix} u_{X6,k} \\ u_{X8,k} \end{bmatrix} \quad , \quad y_k = \begin{bmatrix} w_{g,c2,k} \\ w_{o,s2,k} \end{bmatrix} \tag{3.11}$$

The input and measurement vectors of the linear well model were as given in equation (2.10) on page 9. With the topside model consisting of a steady state gain for the gas and oil flow rates, we get the following plant model

$$\begin{aligned} \Delta x_{k+1} &= A\Delta x_k + B\Delta u_k \\ \Delta y_k &= C\Delta x_k + D\Delta u_k \end{aligned} \tag{3.12}$$

with

$$A = A^w \quad , \quad B = B^w \quad , \quad C = C_{P1}C^w \quad , \quad D = C_{P1}D^w \tag{3.13}$$

where

$$C_{P1} = \begin{bmatrix} g_g & 0 & 0 \\ 0 & g_o & 0 \end{bmatrix} \tag{3.14}$$

The w indicates matrices from the well model presented in equation (2.18) on page 13. The steady state gains g_g and g_o of the topside process were found to be as given below, after dividing the outflow steady state flow rates on the inflow steady state flow rates of the same phase in the plots of Figure 3.3. Note that the reason why g_g is less than 1.0 is that the rest of the gas stays with the oil, exiting through the second separator oil outflow valve.

$$g_g = 0.99 \quad , \quad g_o = 1.00 \tag{3.15}$$

C_{P1} is the gain matrix transforming the three well outflow rates $[w_{g,in} \ , \ w_{o,in} \ , \ w_{w,in}]^T$ to the topside outflow rates $[w_{g,c2} \ , \ w_{o,s2}]^T$.

3.3.2 Feedforward from known future inflow disturbances

In simulation *case 1*, to be introduced in Chapter 4, a third well will be opened for production a while into the simulation run (the well is denoted as *W3* in the model overview given in Figure 1.2). This production change is known in advance and will be compensated for using feedforward control. The following augmentation to the last term of equation (3.8) implements the feedforward from the disturbance, adding the predicted changes to the topside outflow rate prediction. C_{P1}, defined in equation (3.14), transforms the predicted topside inflow rates to predictions of the topside outflow rates.

$$(\Phi d_k)_{\text{new}} = \Phi d_k + \begin{bmatrix} C_{P1} & & \\ & \ddots & \\ & & C_{P1} \end{bmatrix} \begin{bmatrix} w_{W3,g,k} \\ w_{W3,o,k} \\ w_{W3,w,k} \\ \vdots \\ w_{W3,g,k+H_p-1} \\ w_{W3,o,k+H_p-1} \\ w_{W3,w,k+H_p-1} \end{bmatrix} \tag{3.16}$$

Two different approaches will be taken to the inflow predictions, see below.

MPC1 FF1 - First feedforward scheme

In the first feedforward approach, to be denoted as *MPC1* FF1, logging data from previous startups of *W3* will be used for model representation, see Section 2.4. The data to be fed forward are shown in Figure 2.7.

MPC1 FF2 - Second feedforward scheme

In the second feedforward approach, only the first large, abrupt change in the gas inflow rate is included in the inflow prediction. The idea is that the rest of the startup dynamics will be handled by MPC integral action, saving modeling effort. The abrupt inflow change is included in the prediction data because the choke valve cannot be expected to be able to compensate for this large, sudden inflow change using feedback control alone due to the long choke valve stroke time. The data being fed forward using the *MPC1* FF2 scheme are shown in Figure 3.4, while the original data are shown in Figure 2.7.

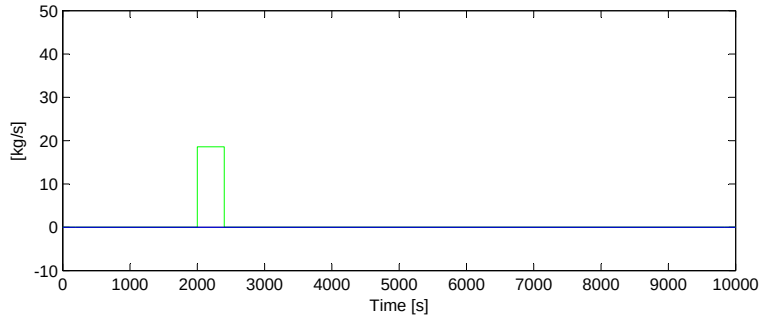

Figure 3.4: Simplified inflow disturbance data used in the *MPC1* FF2 feedforward scheme (only gas rates are nonzero). Green-gas, black-oil, blue-water.

3.3.3 Optimization state vector with constraint softening

In order to guarantee feasibility during operation, the constraint on the gas rate (to be introduced in equation (3.26)) needed to be softened. Consequently, the optimization vector was chosen as follows

$$\mathcal{X}_k = \begin{bmatrix} \Delta\mathcal{U}_k \\ \mathcal{E}_k \end{bmatrix} \in (n_u H_u + 1) \times 1 \tag{3.17}$$

This also meant that Θ of equation (3.6) needed to be augmented

$$\Theta = \begin{bmatrix} \Theta & 0 \end{bmatrix} \in n_y H_p \times (n_u H_u + 1) \tag{3.18}$$

3.3.4 Cost function

We want to maximize the future oil outflow from the second separator stage. The oil flow rate measurement is the second element of the measurement vector y_k defined in equation (3.11). Further, we also want to minimize the valve control input changes and the changes in the topside process outflow rate. Lastly, relaxing the gas outflow rate constraint, meaning that $\mathcal{E}_k$ is set to a nonzero value by the optimizer, should be penalized heavily. Thus,

$$\min_{\Delta\mathcal{U}_k,\mathcal{E}_k} V_1 \;=\; -\mathcal{Q}^T\tilde{\mathcal{Y}}_k \;+\; \|\Delta\mathcal{U}_k\|^2_{\mathcal{R}} \;+\; \|\mathcal{E}_k\|^2_{R_\mathcal{E}} \;+\; \|\Delta\tilde{\mathcal{Y}}_k\|^2_{\mathcal{S}} \tag{3.19}$$

with

$$\Delta\tilde{\mathcal{Y}}_k = \begin{bmatrix} \tilde{y}_{k+2} - \tilde{y}_{k+1} \\ \vdots \\ \tilde{y}_{k+H_p} - \tilde{y}_{k+H_p-1} \end{bmatrix} = \underbrace{\begin{bmatrix} -I & I & 0 & \cdots & 0 \\ 0 & -I & I & \ddots & \vdots \\ \vdots & \ddots & \ddots & \ddots & 0 \\ 0 & \cdots & 0 & -I & I \end{bmatrix}}_{W\in\, n_y(H_p-1)\times n_yH_p} \begin{bmatrix} \tilde{y}_{k+1} \\ \vdots \\ \tilde{y}_{k+H_p} \end{bmatrix} = W\tilde{\mathcal{Y}}_k \tag{3.20}$$

and

$$\begin{aligned}
\mathcal{Q} &= \begin{bmatrix} Q_1 \\ \vdots \\ Q_{H_p} \end{bmatrix} \quad , \quad Q_i = \begin{bmatrix} q_1 \\ \vdots \\ q_{n_y} \end{bmatrix} = \begin{bmatrix} 0 \\ q \end{bmatrix} \\
\mathcal{R} &= \begin{bmatrix} R_1 & & 0 \\ & \ddots & \\ 0 & & R_{H_u} \end{bmatrix} \quad , \quad R_i = \begin{bmatrix} r_1 & & 0 \\ & \ddots & \\ 0 & & r_{n_u} \end{bmatrix} = \begin{bmatrix} r_1 & 0 \\ 0 & r_2 \end{bmatrix} \\
\mathcal{S} &= \begin{bmatrix} S_1 & & 0 \\ & \ddots & \\ 0 & & S_{H_p-1} \end{bmatrix} \quad , \quad S_i = \begin{bmatrix} s_1 & & 0 \\ & \ddots & \\ 0 & & s_{n_y} \end{bmatrix} = \begin{bmatrix} s_1 & 0 \\ 0 & s_2 \end{bmatrix} \\
R_\mathcal{E} &= \begin{bmatrix} R_{\mathcal{E},1} & & 0 \\ & \ddots & \\ 0 & & R_{\mathcal{E},n_\mathcal{E}} \end{bmatrix} = r_\mathcal{E}
\end{aligned} \tag{3.21}$$

In the above, q, r_i, s_i and $r_\mathcal{E}$ are tuning parameters used while setting up the MPC.

Cost function in terms of optimization vector $\mathcal{X}_k$

With the overall aim being to express the cost function in terms of the new optimization vector $\mathcal{X}_k$, we start by expressing $\tilde{\mathcal{Y}}_k$ and $\Delta\tilde{\mathcal{Y}}_k$ as functions of $\Delta\mathcal{U}_k$. We have

$$\tilde{\mathcal{Y}}_k = \Psi\tilde{x}_k + \Upsilon\tilde{u}_{k-1} + \Theta\Delta\mathcal{U}_k + \Phi d_k \tag{3.22}$$

With $\tilde{x}_k$, $\tilde{u}_{k-1}$ and d_k being given by the past control inputs, there is nothing the optimizer can do with these terms in the future. We therefore get the following term for $\tilde{\mathcal{Y}}_k$ in the cost function V_1

$$\tilde{\mathcal{Y}}_k = \Theta\Delta\mathcal{U}_k \tag{3.23}$$

From equation (3.20) we have that $\Delta\tilde{\mathcal{Y}}_k = W\tilde{\mathcal{Y}}_k$. We can then rewrite $\|\Delta\tilde{\mathcal{Y}}_k\|^2_{\mathcal{S}}$ as follows

$$\begin{aligned}
\|\Delta\tilde{\mathcal{Y}}_k\|^2_{\mathcal{S}} &= (W\tilde{\mathcal{Y}}_k)^T\mathcal{S}W\tilde{\mathcal{Y}}_k = \tilde{\mathcal{Y}}_k^TW^T\mathcal{S}W\tilde{\mathcal{Y}}_k \\
&= (\Psi\tilde{x}_k + \Upsilon\tilde{u}_{k-1} + \Theta\Delta\mathcal{U}_k + \Phi d_k)^TW^T\mathcal{S}W(\Psi\tilde{x}_k + \Upsilon\tilde{u}_{k-1} + \Theta\Delta\mathcal{U}_k + \Phi d_k) \\
&= 2(\Psi\tilde{x}_k + \Upsilon\tilde{u}_{k-1} + \Phi d_k)^TW^T\mathcal{S}W\Theta\Delta\mathcal{U}_k + \Delta\mathcal{U}_k^T\Theta^TW^T\mathcal{S}W\Theta\Delta\mathcal{U}_k + c
\end{aligned} \tag{3.24}$$

In the above, c is a constant which cannot be affected by the control input and is therefore disregarded in the following. With $\mathcal{X}_k$ as defined in equation (3.17), we can finally rewrite the cost function of equation (3.19) as given below, using the results of equations (3.23) and (3.24)

$$\begin{aligned} V_1 &= \left[\begin{array}{cc} -\mathcal{Q}^T\Theta + 2(\Psi\tilde{x}_k + \Upsilon\tilde{u}_{k-1} + \Phi d_k)^T W^T \mathcal{S} W \Theta & 0 \end{array} \right] \mathcal{X}_k \\ &\quad + \mathcal{X}_k^T \left[\begin{array}{cc} \mathcal{R} + \Theta^T W^T \mathcal{S} W \Theta & 0 \\ 0 & R_{\mathcal{E}} \end{array} \right] \mathcal{X}_k \\ &= h_k^T \mathcal{X}_k + \mathcal{X}_k^T H \mathcal{X}_k \end{aligned} \tag{3.25}$$

3.3.5 Constraints

There were three constraints in this MPC implementation - one on the absolute valve openings, one on the rate of change of the valve openings (dictated by the valve stroke times) and one on the gas flow rates through the second compressor (measurement $y_{1,k}$). The latter one was softened for feasibility. The two other constraints needed no softening since they were free variables chosen by the controller, that is, they were not governed by any system equalities

$$\begin{array}{rcll} |\Delta u_k| & \leq & \Delta\bar{u} & [-] \\ 0 & \leq & u_k \ \leq \ 1 & [-] \\ y_{1,k} & \leq & \bar{w}_{g,c2} + \mathcal{E}_k & [\text{kg/s}] \end{array} \tag{3.26}$$

The first constraint can be written as follows in terms of the optimization state vector $\mathcal{X}_k = [\Delta\mathcal{U}_k^T \ , \ \mathcal{E}_k^T]^T$, with $I \in \ n_u H_u \times n_u H_u$ and $\mathbf{1} = [1 \ \cdots \ 1]^T \in \ n_u H_u \times 1$. With a 8 minute valve stroke time, we have $\Delta\bar{u} = \frac{h}{8 \cdot 60}$ with h equal to the MPC sampling time, e.g. 40 s

$$\underbrace{\left[\begin{array}{cc} I & 0 \\ -I & 0 \end{array} \right]}_{E} \mathcal{X}_k \leq \underbrace{\left[\begin{array}{c} \mathbf{1}\Delta\bar{u} \\ \mathbf{1}\Delta\bar{u} \end{array} \right]}_{e} \tag{3.27}$$

The second constraint can be written as given below, with $I \in \ n_u \times n_u$ and $\mathbf{1} = [1 \ \cdots \ 1]^T \in \ n_u \times 1$. u^N is the control input linearization point ($u_k = u^N + \tilde{u}_k$), e.g. $u^N = [0.2 \ , \ 0.2]^T$

$$\underbrace{\left[\begin{array}{ccccc} I & 0 & \cdots & 0 & 0 \\ \vdots & \ddots & \ddots & \vdots & \vdots \\ \vdots & & \ddots & 0 & \vdots \\ I & \cdots & \cdots & I & 0 \\ -I & 0 & \cdots & 0 & 0 \\ \vdots & \ddots & \ddots & \vdots & \vdots \\ \vdots & & \ddots & 0 & \vdots \\ -I & \cdots & \cdots & -I & 0 \end{array} \right]}_{F} \mathcal{X}_k \leq \underbrace{\left[\begin{array}{c} \mathbf{1} - u^N - \tilde{u}_{k-1} \\ \vdots \\ \vdots \\ \mathbf{1} - u^N - \tilde{u}_{k-1} \\ u^N + \tilde{u}_{k-1} \\ \vdots \\ \vdots \\ u^N + \tilde{u}_{k-1} \end{array} \right]}_{f_k} \tag{3.28}$$

The third constraint is developed as follows. Introducing the matrix $\mathcal{C}$, we can select the gas

rates from the measurement vector

$$\mathcal{C} = \begin{bmatrix} c_1 & & 0 \\ & \ddots & \\ 0 & & c_{H_p} \end{bmatrix}, \; c_i = \begin{bmatrix} 1 & 0 \end{bmatrix} \tag{3.29}$$

We can now write the below, inserting $\tilde{\mathcal{Y}}_k$ as given in equation (3.22), and defining $\mathbf{1} = [1 \cdots 1]^T \in H_p \times 1$ and $I_1 = [I \cdots I]^T \in n_y H_p \times n_y$. $\mathcal{E}_k$ is introduced for constraint softening

$$\mathcal{C}(\tilde{\mathcal{Y}}_k + I_1 y^N) = \mathcal{C}(\Psi \tilde{x}_k + \Upsilon \tilde{u}_{k-1} + \Theta \Delta \mathcal{U}_k + \Phi d_k + I_1 y^N) \leq \mathbf{1}(\bar{w}_{g,c2} + \mathcal{E}_k) \tag{3.30}$$

This can be written

$$\mathcal{C}\Theta\Delta\mathcal{U}_k - \mathbf{1}\mathcal{E}_k \leq \mathbf{1}\bar{w}_{g,c2} - \mathcal{C}(\Psi \tilde{x}_k + \Upsilon \tilde{u}_{k-1} + \Phi d_k + I_1 y^N) \tag{3.31}$$

Finally, we once again introduce $\mathcal{X}_k = [\Delta\mathcal{U}_k^T \; , \; \mathcal{E}_k^T]^T$, and get the third constraint

$$\underbrace{\begin{bmatrix} \mathcal{C}\Theta & -\mathbf{1} \end{bmatrix}}_{G} \mathcal{X}_k \leq \underbrace{\mathbf{1}\bar{w}_{g,c2} - \mathcal{C}(\Psi \tilde{x}_k + \Upsilon \tilde{u}_{k-1} + \Phi d_k + I_1 y^N)}_{g_k} \tag{3.32}$$

In the different controllers, a constraint on the mass flow rate of gas through the second compressor was defined. This constraint was due to a capacity limitation in the compressor. With a pressure increase from 8 to 80 bar, the flow rate of the second compressor is limited to 471.6 kg/s when operating at full speed, see Figure 1.1 on page 2. However, due to the nonlinearity of the process together with the simplified topside model for the gas flow rate, a certain safety margin should be kept when introducing this constraint to the linear MPC. Therefore, the constraint to be denoted as $\bar{w}_{g,c2}$ in the specific controller introductions of the upcoming sections, was set to 468 kg/s.

3.3.6 Summary

To sum it all up, we have the following optimization problem

$$\min_{\mathcal{X}_k} \; h_k^T \mathcal{X}_k + \mathcal{X}_k^T H \mathcal{X}_k \quad s.t. \quad \begin{bmatrix} E \\ F \\ G \end{bmatrix} \mathcal{X}_k \leq \begin{bmatrix} e \\ f_k \\ g_k \end{bmatrix} \tag{3.33}$$

where h_k^T and H are given in equation (3.25), e and E in (3.27), f_k and F in (3.28) and g_k and G are given in equation (3.32).

The matrix and vector dimensions are as given in Table 3.4. See also Table 3.3 on page 21.

Table 3.4: *MPC1* vector and matrix dimensions

n_x	18
n_u	2
n_y	2
n_d	2
$n_{\mathcal{E}}$	1
$\Delta\mathcal{U}_k$	$n_u H_u \times 1$
$\mathcal{E}_k$	$n_{\mathcal{E}} \times 1$
$\mathcal{X}_k$	$n_u H_u + n_{\mathcal{E}} \times 1$
E	$2n_u H_u \times n_u H_u + n_{\mathcal{E}}$
F	$2n_u H_u \times n_u H_u + n_{\mathcal{E}}$
G	$H_p \times n_u H_u + n_{\mathcal{E}}$
e	$2n_u H_u \times 1$
f_k	$2n_u H_u \times 1$
g_k	$H_p \times 1$

3.3.7 Kalman filter for well state vector estimation

The MPC needed an estimate of the state vector $\tilde{x}_k$ in equation (3.22). This was found using a discrete linear Kalman filter. In a noise free environment, one could also have used a simple Luenberger state observer. A Kalman filter has however the advantage that it is easily adapted to a noisy environment. Also, with a Kalman filter, one does not have to deal with pole placement issues explicitly. The physical system as seen from the Kalman filter is presented in equation (3.34). The process disturbance v_k can be thought to represent the difference between the linear system response and the response of the actual nonlinear system. w_k is the measurement noise.

$$\begin{aligned} \tilde{x}_{k+1} &= A\tilde{x}_k + B\tilde{u}_k + \Omega v_k \\ \tilde{y}_k &= C\tilde{x}_k + D\tilde{u}_k + w_k \end{aligned} \tag{3.34}$$

The Kalman filter equations are presented below in equations (3.35) and (3.36). W is the covariance matrix of the measurement noise and V is the covariance matrix of the unmeasured process disturbances. These two matrices were set during the initialization of the simulations. When simulating with no measurement noise added, W was set very small relative to V. When not specified otherwise, $\Omega = I$ was used. This means that it was not assumed to be any coupling between the process disturbance to the different states.

Prediction

$$\begin{aligned} \bar{\tilde{x}}_{k+1} &= A\hat{\tilde{x}}_k + B\tilde{u}_k \\ \bar{X} &= A\hat{X}A^T + \Omega V \Omega^T \end{aligned} \tag{3.35}$$

Filtering

$$\begin{aligned} \hat{\tilde{x}}_k &= \bar{\tilde{x}}_k + K(\tilde{y}_k - C\bar{\tilde{x}}_k - D\tilde{u}_k) \\ \hat{X} &= (I - KC)\bar{X} \\ K &= \bar{X}C^T(C\bar{X}C^T + W)^{-1} \end{aligned} \tag{3.36}$$

In the above, the filtered state vector, $\hat{\tilde{x}}_k$, was used as an estimate of $\tilde{x}_k$.

3.4 *MPC2* - Direct choke valve and topside flow rate setpoint control

In the control system setup denoted *MPC1*, only the wells were controlled using an MPC, while the topside process was left to an ordinary decentralized PI control system. With *MPC2*, we will also set some key setpoints in the topside process using an MPC, namely the flow rates through the topside oil and water valves. The tank levels will be allowed to vary around a nominal level setpoint, albeit at a penalty introduced in the cost function. The aim is to achieve a better flow smoothing by utilizing the buffering capacity of the separator tanks better. The structure of the *MPC2* control system is shown in Figure 3.5.

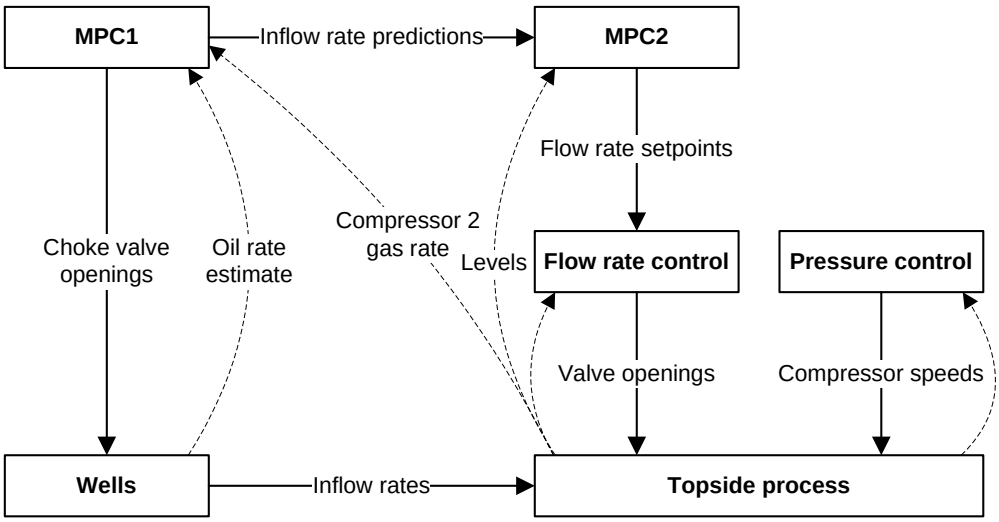

Figure 3.5: Structure of control system *MPC2*. Feedback to flow rate and pressure control system is valve flow rate estimate and pressure measurements, respectively.

A slightly modified version of *MPC1* will be used for controlling the wells. Flow rate setpoints for the four topside water and oil valves (see Figure 1.2) will be issued from *MPC2*, operating on the supervisory control layer, down to the PI flow rate controllers situated in the regulatory control layer. The PI flow rate controllers will in effect linearize the valves as seen from the MPC. The separator tank pressure control will still be handled by the decentralized system alone.

The control system setup denoted as *MPC2* will be comprised of two different MPCs. Keeping the well and topside controllers separated as specified above may lead to less optimal operation than what might have been possible with one, large MPC controlling everything alone. On the other hand, the separation into smaller MPCs should allow for easier tuning of the cost functions, which is an advantage.

By introducing flow rate controllers to the topside process, we will need measurements of the flow rates to be controlled, and, as Figure 1.2 illustrates, there are quite few flow rate measurements in the topside process. The flow rates may however be obtained using a model based estimator, such as a Kalman filter. Unfortunately, there was no time to develop these estimators within the project time frame. Thus, for the simulations, it was assumed that these measurements were readily available, and they were extracted directly from the model. Stange (2006) looks at the application of an extended Kalman filter for flow rate measurements in three phase separator

tanks, and represents a possible starting point in the development of the required flow rate estimators.

Note that depending on the context, *MPC2* may in the following mean either the isolated MPC for topside flow rate control, or the overall control system setup combining *MPC1* for well control and *MPC2* for topside flow rate control.

The structure of *MPC2* is presented below.

3.4.1 Overall plant model

The state vector x [kg] is defined to be the oil and water mass holdups in each separator tank, the input vector u [kg/s] is the flow rate setpoints for the four topside oil and water valves, and the measurement vector y [m] is the oil and water levels in the two separator tanks. $w_{in,k}$ [kg/s] is a vector containing the oil and water inflow rates to the first separator tank

$$x_k = \begin{bmatrix} x_{1o,k} \\ x_{1w,k} \\ x_{2o,k} \\ x_{2w,k} \end{bmatrix} \quad , \quad u_k = \begin{bmatrix} w_{1o,k} \\ w_{1w,k} \\ w_{2o,k} \\ w_{2w,k} \end{bmatrix} \quad , \quad y_k = \begin{bmatrix} L_{1o} \\ L_{1w} \\ L_{2o} \\ L_{2w} \end{bmatrix} \quad , \quad w_{in,k} = \begin{bmatrix} w_{1o,in,k} \\ w_{1w,in,k} \\ 0 \\ 0 \end{bmatrix} \tag{3.37}$$

The mass balance of the two separator tanks was then found to be as given in equation (3.38), where $w_{i,in}$ is the topside inflow rate from the wells and h is the MPC sampling time.

$$x_{k+1} = \underbrace{\begin{bmatrix} 1 & 0 & 0 & 0 \\ 0 & 1 & 0 & 0 \\ 0 & 0 & 1 & 0 \\ 0 & 0 & 0 & 1 \end{bmatrix}}_{A} x_k + \underbrace{\begin{bmatrix} -h & 0 & 0 & 0 \\ -hk_{1w} & -h & 0 & 0 \\ h & 0 & -h & 0 \\ hk_{1w} & 0 & -hk_{2w} & -h \end{bmatrix}}_{B} u_k + hw_{in,k} \tag{3.38}$$

In equation (3.38), k_{1w} and k_{2w} is the amount of water passing through the first and second separator tank oil outlet valves per *kg* of oil passing through the valve in question. The two parameters, which were found to be quite constant in all the simulations to be performed in Chapter 4, are given in Table 3.5. They were found by averaging the tank outflow rates in the simulation depicted in Figure 4.3 (the simulation will be introduced in the said chapter). The flow rates in question are depicted in Figure 3.6.[1]

Table 3.5: Calculation of k_{1w} and k_{2w}. Data from Figure 3.6.

Outflow	$\bar{w}_o$	$\bar{w}_w$	$k_{iw} = \bar{w}_o/\bar{w}_w$
Sep1	89.12	69.02	0.77
Sep2	89.12	33.51	0.38

[1]Note that in an actual topside process, there is usually an electrostatic water separator in the end of the oil train in order to clear out much of the remaining water contained in the oil flow. Thus, the final oil outflow will usually be purer than the one obtained here.

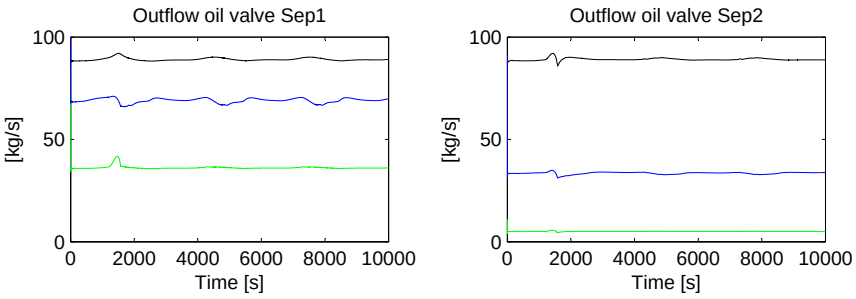

Figure 3.6: Flow rates out of the two separator tanks. Data from the simulation in Figure 4.3. Green-gas, black-oil, blue-water.

With $\tilde{y}_k = y_k - y^N$, $\tilde{x}_k = x_k - x^N$ and $\tilde{u}_k = u_k - u^N$, we have the following system (y^N, x^N and u^N are the linearization points, and in this case, $u^N = 0$). The measurement matrix C was found by model perturbation [2]

$$\begin{aligned} \tilde{x}_{k+1} &= A\tilde{x}_k + B\tilde{u}_k + hw_{in,k} \\ \tilde{y}_k &= C\tilde{x}_k \end{aligned} \tag{3.39}$$

3.4.2 MPC predictions

The structure of the topside MPC is mainly as given in Section 3.2. There is however a slight difference due to the $w_{in,k}$ term in equation (3.39).

Introducing $\Delta u_{k+i} = \tilde{u}_{k+i} - \tilde{u}_{k+i-1}$ as before, we have

$$\begin{aligned} \tilde{x}_{k+1} &= A\tilde{x}_k + B(\tilde{u}_{k-1} + \Delta u_k) + hw_{in,k} \\ \tilde{y}_{k+1} &= C\tilde{x}_{k+1} \\ &= C(A\tilde{x}_k + B(\tilde{u}_{k-1} + \Delta u_k) + hw_{in,k}) \end{aligned} \tag{3.40}$$

Further, we have

$$\begin{aligned} \tilde{x}_{k+2} &= A\tilde{x}_{k+1} + B(\tilde{u}_{k-1} + \Delta u_k + \Delta u_{k+1}) + hw_{in,k+1} \\ &= A(A\tilde{x}_k + B(\tilde{u}_{k-1} + \Delta u_k) + hw_{in,k}) + B(\tilde{u}_{k-1} + \Delta u_k + \Delta u_{k+1}) + hw_{in,k+1} \\ &= A^2\tilde{x}_k + (B + AB)\tilde{u}_{k-1} + (B + AB)\Delta u_k + B\Delta u_{k+1} + Ahw_{in,k} + hw_{in,k+1} \\ \\ \tilde{y}_{k+2} &= C[A^2\tilde{x}_k + (B + AB)\tilde{u}_{k-1} + (B + AB)\Delta u_k + B\Delta u_{k+1} + Ahw_{in,k} + hw_{in,k+1}] \end{aligned} \tag{3.41}$$

The structure of the topside MPC can then be written as given below, with $\tilde{\mathcal{Y}}_k$, Ψ, Υ, Θ and $\Delta\mathcal{U}_k$ as defined in Section 3.2 (note that in the case of *MPC2*, D is a zero matrix)

$$\tilde{\mathcal{Y}}_k = \Psi\tilde{x}_k + \Upsilon\tilde{u}_{k-1} + \Theta\Delta\mathcal{U}_k + \Gamma\mathcal{W}_{in,k} \tag{3.42}$$

[2] As before, we use $\tilde{y}_k$, $\tilde{x}_k$ and $\tilde{u}_k$ instead of the normal convention Δy_k, Δx_k and Δu_k in order to reserve Δ for control input moves in the MPC.

with

$$\mathcal{W}_{in,k} = \begin{bmatrix} w_{in,k} \\ w_{in,k+1} \\ \vdots \\ w_{in,k+H_p-1} \end{bmatrix} \in n_x H_p \times 1 \tag{3.43}$$

and

$$\Gamma = \begin{bmatrix} Ch & 0 & \cdots & 0 \\ CAh & Ch & \ddots & \vdots \\ \vdots & & \ddots & 0 \\ CA^{H_p-1}h & & \cdots & Ch \end{bmatrix} \in n_y H_p \times n_x H_p \tag{3.44}$$

MPC integral action is applied as given in Section 3.2, yielding

$$\tilde{\mathcal{Y}}_k = \Psi \tilde{x}_k + \Upsilon \tilde{u}_{k-1} + \Theta \Delta \mathcal{U}_k + \Gamma \mathcal{W}_{in,k} + \Phi d_k \tag{3.45}$$

3.4.3 Optimization state vector with constraint softening

As for *MPC1*, constraint softening was included for feasibility reasons. If the constraints had not been softened, the MPC would have halted with an error message if a constraint was broken during run-time.

Introducing constraint softeners for the four level constraints (to be presented in more detail shortly), the optimization state vector was chosen as follows

$$\mathcal{X}_k = \begin{bmatrix} \Delta \mathcal{U}_k \\ \mathcal{E}_{Lo1,k} \\ \mathcal{E}_{Lw1,k} \\ \mathcal{E}_{Lo2,k} \\ \mathcal{E}_{Lw2,k} \end{bmatrix} = \begin{bmatrix} \Delta \mathcal{U}_k \\ \mathcal{E}_{2,k} \end{bmatrix} \in (n_u H_u + 4) \times 1 \tag{3.46}$$

As for MPC1, this meant that Θ of equation (3.42) needed to be stuffed with zeros in order to fit with the optimization vector

$$\Theta = \begin{bmatrix} \Theta & 0 & 0 & 0 & 0 \end{bmatrix} \in n_y H_p \times (n_u H_u + 4) \tag{3.47}$$

3.4.4 Cost function

The cost function of the topside MPC is as follows

$$\min_{\Delta \mathcal{U}_k, \mathcal{E}_k} V_2 \;=\; \|\Delta \mathcal{U}_k\|^2_{\mathcal{R}_2} \;+\; \|\mathcal{E}_k\|^2_{R_{\mathcal{E}2}} \;+\; \|\tilde{\mathcal{Y}}_k\|^2_{\mathcal{P}_2} \tag{3.48}$$

with

$$\mathcal{R}_2 = \begin{bmatrix} R_{2,1} & & 0 \\ & \ddots & \\ 0 & & R_{2,H_u} \end{bmatrix} \quad , \quad R_{2,i} = \begin{bmatrix} r_{2,1} & & 0 \\ & \ddots & \\ 0 & & r_{2,n_u} \end{bmatrix} = \begin{bmatrix} r_{2,1} & & & 0 \\ & r_{2,2} & & \\ & & r_{2,3} & \\ 0 & & & r_{2,4} \end{bmatrix}$$

$$\mathcal{P}_2 = \begin{bmatrix} P_{2,1} & & 0 \\ & \ddots & \\ 0 & & P_{2,H_p} \end{bmatrix} \quad , \quad P_{2,i} = \begin{bmatrix} p_{2,1} & & 0 \\ & \ddots & \\ 0 & & p_{2,n_y} \end{bmatrix} = \begin{bmatrix} p_{2,1} & & & 0 \\ & p_{2,2} & & \\ & & p_{2,3} & \\ 0 & & & p_{2,4} \end{bmatrix}$$

$$\mathcal{R}_{\mathcal{E}2} = \begin{bmatrix} R_{\mathcal{E}2,1} & & 0 \\ & \ddots & \\ 0 & & R_{\mathcal{E}2,n_{\mathcal{E}2}} \end{bmatrix} = \begin{bmatrix} r_{\mathcal{E}2,1} & & & 0 \\ & r_{\mathcal{E}2,2} & & \\ & & r_{\mathcal{E}2,3} & \\ 0 & & & r_{\mathcal{E}2,4} \end{bmatrix} \tag{3.49}$$

Cost function in terms of optimization vector $\mathcal{X}_k$

In order to write the cost function V_2 of equation (3.48) in terms of the new optimization state vector $\mathcal{X}_k$, we must rewrite $\tilde{\mathcal{Y}}_k$ to a function of $\Delta\mathcal{U}_k$. In the below result, c is a constant not given by future input moves $\Delta\mathcal{U}_k$, and can thus be removed from the MPC equations

$$\begin{aligned} \| \tilde{\mathcal{Y}}_k \|^2_{\mathcal{P}_2} &= (\tilde{\mathcal{Y}}_k)^T \mathcal{P}_2 \tilde{\mathcal{Y}}_k \\ &= (\Psi\tilde{x}_k + \Upsilon\tilde{u}_{k-1} + \Theta\Delta\mathcal{U}_k + \Gamma\mathcal{W}_{in,k} + \Phi d_k)^T \\ &\quad \cdot\mathcal{P}_2(\Psi\tilde{x}_k + \Upsilon\tilde{u}_{k-1} + \Theta\Delta\mathcal{U}_k + \Gamma\mathcal{W}_{in,k} + \Phi d_k) \\ &= 2(\Psi\tilde{x}_k + \Upsilon\tilde{u}_{k-1} + \Gamma\mathcal{W}_{in,k} + \Phi d_k)^T \mathcal{P}_2\Theta\Delta\mathcal{U}_k + \Delta\mathcal{U}_k^T\Theta^T\mathcal{P}_2\Theta\Delta\mathcal{U}_k + c \end{aligned} \tag{3.50}$$

With $\mathcal{X}_k$ as defined in equation (3.46), we finally get the following cost function

$$\begin{aligned} V_2 &= \begin{bmatrix} 2(\Psi\tilde{x}_k + \Upsilon\tilde{u}_{k-1} + \Gamma\mathcal{W}_{in,k} + \Phi d_k)^T\mathcal{P}_2\Theta & 0 \end{bmatrix} \mathcal{X}_k \\ &\quad + \mathcal{X}_k^T \begin{bmatrix} \mathcal{R}_2 + \Theta^T\mathcal{P}_2\Theta & 0 \\ 0 & R_{\mathcal{E}2} \end{bmatrix} \mathcal{X}_k \\ &= h_{2,k}^T\mathcal{X}_k + \mathcal{X}_k^T H_2 \mathcal{X}_k \end{aligned} \tag{3.51}$$

3.4.5 Constraints

There were two types of constraints in this MPC implementation, namely an input constraint and a constraint on the separator tank levels.

$$\begin{aligned} \underline{u} &\leq u_k \leq \bar{u} && [-] \\ y_k &\leq \bar{L} + \mathcal{E}_{2k} && [\text{m}] \\ y_k &\geq \underline{L} - \mathcal{E}_{2k} && [\text{m}] \end{aligned} \tag{3.52}$$

With $\mathcal{X}_k$ as defined in equation (3.46), we can write the input constraint as follows, where $I \in n_u \times n_u$

$$\underbrace{\begin{bmatrix} I & 0 & \cdots & 0 & 0_{n_u \times n_{\mathcal{E}2}} \\ \vdots & \ddots & \ddots & \vdots & \vdots \\ \vdots & & \ddots & 0 & \vdots \\ I & \cdots & \cdots & I & 0_{n_u \times n_{\mathcal{E}2}} \\ -I & 0 & \cdots & 0 & 0_{n_u \times n_{\mathcal{E}2}} \\ \vdots & \ddots & \ddots & \vdots & \vdots \\ \vdots & & \ddots & 0 & \vdots \\ -I & \cdots & \cdots & -I & 0_{n_u \times n_{\mathcal{E}2}} \end{bmatrix}}_{F_2} \mathcal{X}_k \leq \underbrace{\begin{bmatrix} \bar{u} - u^N - \tilde{u}_{k-1} \\ \vdots \\ \vdots \\ \bar{u} - u^N - \tilde{u}_{k-1} \\ -\underline{u} + u^N + \tilde{u}_{k-1} \\ \vdots \\ \vdots \\ -\underline{u} + u^N + \tilde{u}_{k-1} \end{bmatrix}}_{f_{2,k}} \tag{3.53}$$

Defining $I_2 = [I_1 \cdots I_{H_p}]^T \in n_y H_p \times n_y = n_{\mathcal{E}_2} H_p \times n_{\mathcal{E}_2}$, we can write the following for the upper tank level constraint

$$\begin{aligned} \mathcal{Y}_k = \tilde{\mathcal{Y}}_k + I_2 y^N &\leq I_2 \bar{L} + I_2 \mathcal{E}_{2k} \\ \Psi \tilde{x}_k + \Upsilon \tilde{u}_{k-1} + \Theta \Delta \mathcal{U}_k + \Gamma \mathcal{W}_{in,k} + \Phi d_k + I_2 y^N &\leq I_2 \bar{L} + I_2 \mathcal{E}_{2k} \end{aligned} \tag{3.54}$$

Once again introducing $\mathcal{X}_k$, we can write the above as

$$\underbrace{\begin{bmatrix} \Theta & -I_2 \end{bmatrix}}_{G_{21}} \mathcal{X}_k \leq \underbrace{I_2(\bar{L} - y^N) - (\Psi \tilde{x}_k + \Upsilon \tilde{u}_{k-1} + \Gamma \mathcal{W}_{in,k} + \Phi d_k)}_{g_{21,k}} \tag{3.55}$$

For the lower tank level constraint, we have

$$\begin{aligned} -\mathcal{Y}_k = -(\tilde{\mathcal{Y}}_k + I_2 y^N) &\leq -I_2 \underline{L} + I_2 \mathcal{E}_{2k} \\ -(\Psi \tilde{x}_k + \Upsilon \tilde{u}_{k-1} + \Theta \Delta \mathcal{U}_k + \Gamma \mathcal{W}_{in,k} + \Phi d_k + I_2 y^N) &\leq -I_2 \underline{L} + I_2 \mathcal{E}_{2k} \end{aligned} \tag{3.56}$$

which in terms of $\mathcal{X}_k$ finally yields

$$\underbrace{\begin{bmatrix} -\Theta & -I_2 \end{bmatrix}}_{G_{22}} \mathcal{X}_k \leq \underbrace{I_2(-\underline{L} + y^N) + (\Psi \tilde{x}_k + \Upsilon \tilde{u}_{k-1} + \Gamma \mathcal{W}_{in,k} + \Phi d_k)}_{g_{22,k}} \tag{3.57}$$

3.4.6 Summary

In summary, we have the following optimization problem

$$\min_{\mathcal{X}_k} \; h_{2,k}^T \mathcal{X}_k + \mathcal{X}_k^T H_2 \mathcal{X}_k \quad s.t. \quad \begin{bmatrix} F_2 \\ G_{21} \\ G_{22} \end{bmatrix} \mathcal{X}_k \leq \begin{bmatrix} f_{2,k} \\ g_{21,k} \\ g_{22,k} \end{bmatrix} \tag{3.58}$$

where $h_{2,k}^T$ and H_2 are defined in equation (3.51), F_2 and $f_{2,k}$ in (3.53), G_{21} and $g_{21,k}$ in (3.55), and G_{22} and $g_{22,k}$ are defined in equation (3.57).

The vector and matrix dimensions of the topside MPC2 controller are shown in Table 3.6. See also Table 3.3 on page 21.

Table 3.6: *MPC2* vector and matrix dimensions

n_x	4
n_u	4
n_y	4
n_d	4
$n_{\mathcal{E}2}$	4
$\Delta\mathcal{U}_k$	$n_u H_u \times 1$
$\mathcal{E}_{2,k}$	$n_{\mathcal{E}2} \times 1$
$\mathcal{X}_k$	$n_u H_u + n_{\mathcal{E}2} \times 1$
F_2	$2n_u H_u \times n_u H_u + n_{\mathcal{E}2}$
G_{21}	$n_y H_p \times n_u H_u + n_{\mathcal{E}2}$
G_{22}	$n_y H_p \times n_u H_u + n_{\mathcal{E}2}$
$f_{2,k}$	$2n_u H_u \times 1$
$g_{21,k}$	$n_y H_p \times 1$
$g_{22,k}$	$n_y H_p \times 1$
$\mathcal{W}_{in,k}$	$n_x H_p \times 1$
Γ	$n_y H_p \times n_x H_p$

3.4.7 Kalman filter for tank mass holdup estimation

The topside MPC controller in *MPC2* needs an estimate of the current tank mass holdups of oil and water for level constraint handling. Since the mass holdups are not measured directly, they will be estimated using a linear Kalman filter. The topside inflow $w_{in,k}$ in the below also needs to be estimated.[3] The linear model used for representing the system in the Kalman filter is given below. v_k is an unmeasured process disturbance and can be thought to be caused by a mismatching model in particular. w_k is measurement noise.

$$\begin{aligned} \tilde{x}_{k+1} &= A\tilde{x}_k + B\tilde{u}_k + hw_{in,k} + \Omega v_k \\ \tilde{y}_k &= C\tilde{x}_k + D\tilde{u}_k + w_k \end{aligned} \tag{3.59}$$

The Kalman filter structure is as given below. W and V are the covariance matrices of the measurement noise and the unmeasured process disturbance, respectively.

Prediction

$$\begin{aligned} \bar{\tilde{x}}_{k+1} &= A\hat{\tilde{x}}_k + B\tilde{u}_k + hw_{in,k} \\ \bar{X} &= A\hat{X}A^T + \Omega V \Omega^T \end{aligned} \tag{3.60}$$

Filtering

$$\begin{aligned} \hat{\tilde{x}}_k &= \bar{\tilde{x}}_k + K(\tilde{y}_k - C\bar{\tilde{x}}_k) \\ \hat{X} &= (I - KC)\bar{X} \\ K &= \bar{X}C^T(C\bar{X}C^T + W)^{-1} \end{aligned} \tag{3.61}$$

The filtered state vector, $\hat{\tilde{x}}_k$, is used as the estimate of the tank mass holdups.

[3] As stated earlier, designing a Kalman filter for the topside flow rate estimates was unfortunately not possible within the project time frame. See Stange (2006) for a study in the design of such Kalman filters.

3.4.8 PI flow rate controller tuning

The topside PI flow rate controllers were tuned as follows. Note that relatively large costs on MPC input changes means that the flow rate setpoints will vary slowly, and the purpose of the PI controllers is merely that of sustaining the flow rate prescribed by the MPC.

The tuning was performed by choosing an initial controller gain approximately equal to the inverse of the maximum achievable flow rate through the valve in question. The integral time was initially set to $10s$. The maximum steady state flow rate through the valves was computed according to equation (3.62), setting $u = 1$, ρ equal to the average mass density of the phase flowing through the valve, while Δp was set equal to the steady state pressure difference over the valve

$$w = uK_v\sqrt{\rho\Delta p} \quad [\text{kg/s}] \tag{3.62}$$

After some tuning, the parameters of Table 3.7 was chosen. The integral time was decreased from $10s$ to $3s$, as it yielded a lower flow rate variance through faster setpoint tracking. In a more noisy environment, the integral time might need an increase, and the controller gain may be further decreased.

Table 3.7: Parameters used in the topside PI flow rate controllers of the *MPC2* control system setup

Controller	*Initial gain*	*Tuned gain*	*Integral time*
Sep1 oil	$1/320 = 0.00313$	0.00210	3
Sep1 water	$1/750 = 0.00133$	0.000653	3
Sep2 oil	$1/204 = 0.00490$	0.00330	3
Sep2 water	$1/46 = 0.0217$	0.0107	3

3.4.9 Changes to the *MPC1* well controller

As stated earlier, the *MPC2* control system used two separate MPCs for well and topside control. An overview of the *MPC2* control system structure is shown in Figure 3.5 on page 29. The well control system *MPC1* could be used almost without changes from the setup presented in Section 3.3.

First of all, there was no need to change the topside process model in *MPC1*. The gas dynamics were controlled with the same decentralized pressure controller as before, yielding much the same closed loop dynamics as before. Further, the oil flow rate dynamics were previously represented by a simple gain of 1 (meant to represent the oil flow rate steady state gain from the inlet to the outlet of the topside process), which still would hold now that *MPC1* was predicting the oil outflow rate from the wells.

One slight modification was needed however, namely in the calculation of the prediction error d_k. Previously, when *MPC1* predicted the oil outflow from the topside process, it could use the topside oil outflow rate measurement for prediction corrections as this was readily available in the process. There is however no flow rate measurements available at the well outlet. Thus, there was need for a topside inflow rate estimate. However, as stated before, it turned out that it would not be possible to design such estimators within the project time frame. Thus, the topside inflow rate estimates were instead obtained by extracting the needed parameters from the topside simulation model directly. Stange (2006) looks at the development of the required flow rate estimator based on an extended Kalman filter.

3.5 *DC1* - Decentralized choke valve control

The second gas compressor stage has been established as the main limiting factor of the topside process model (in other words, this compressor stage can be looked at as the process bottleneck). Setting the production rate at the bottleneck is a common way of maximizing the process throughput. This practise is discussed in more detail in Skogestad (2004).

The purpose of *DC1* is to control the gas feed rate of the second compressor stage by manipulating the choke valves at the topside process inlet, thereby attempting to maximize the process throughput. *DC1* was realized using two simple PI controllers (one per controlled well), both using measurements of the second compressor gas flow rates as feedback, albeit with different flow rate setpoints (to be explained shortly). The tank level and pressure PI controllers were configured similarly as in the case of *MPC1*. See Figure 3.7 for an overview of the *DC1* control system structure.

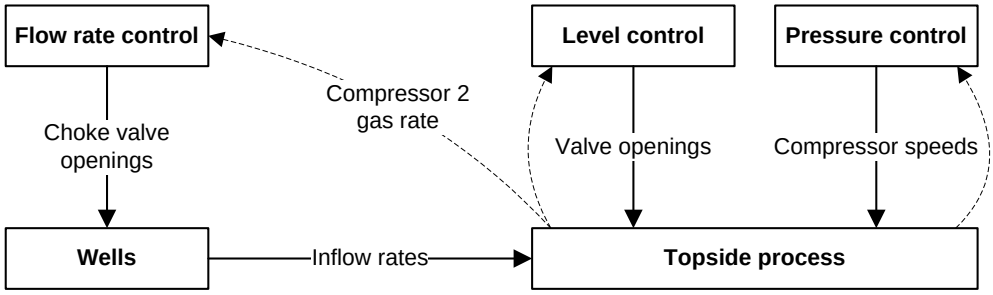

Figure 3.7: Structure of control system *DC1*. Feedback to level and pressure control system is tank level and pressure measurements, respectively.

3.5.1 Design principle

The basic idea for *DC1* is to use the choke valve of the well with the highest GOR (gas-oil ratio, $GOR = Q_g/Q_o$) for gas flow rate control under normal conditions, while letting the other controlled well stay at maximum production. However, when closing in on the gas rate constraint, for instance due to excessive disturbances, the other controlled well will also have to act in order to keep the process within its bounds.

Design principle example

Assume for a moment that *X8* is controlled using a PI controller FIC1, while *X6* is kept constantly at full production. See Figure 3.8 for an illustration. The flow rate setpoint of FIC1 is set somewhat backed off from the highest allowable gas flow rate. FIC1 will control the valve of *X8* in order to sustain the wanted gas flow rate. However, for the simulation case depicted in the said figure, we get a pressure increase in the separator tanks around *t=1200s*. The reason for this is that there is too much gas entering the second compressor. Although the *X8* valve is choking the inflow down, it is not able to compensate fast enough due to its slow stroke time. Thus, there is need for additional compensation from the valve of *X6*, which will be controlled by FIC2. By setting the flow rate setpoint of FIC2 above the setpoint of FIC1, but still below the defined gas rate constraint, we get the desired effect. *X6* will normally operate with full production, but if the second compressor gas rate exceeds a threshold level, the valve of *X6* starts choking down.

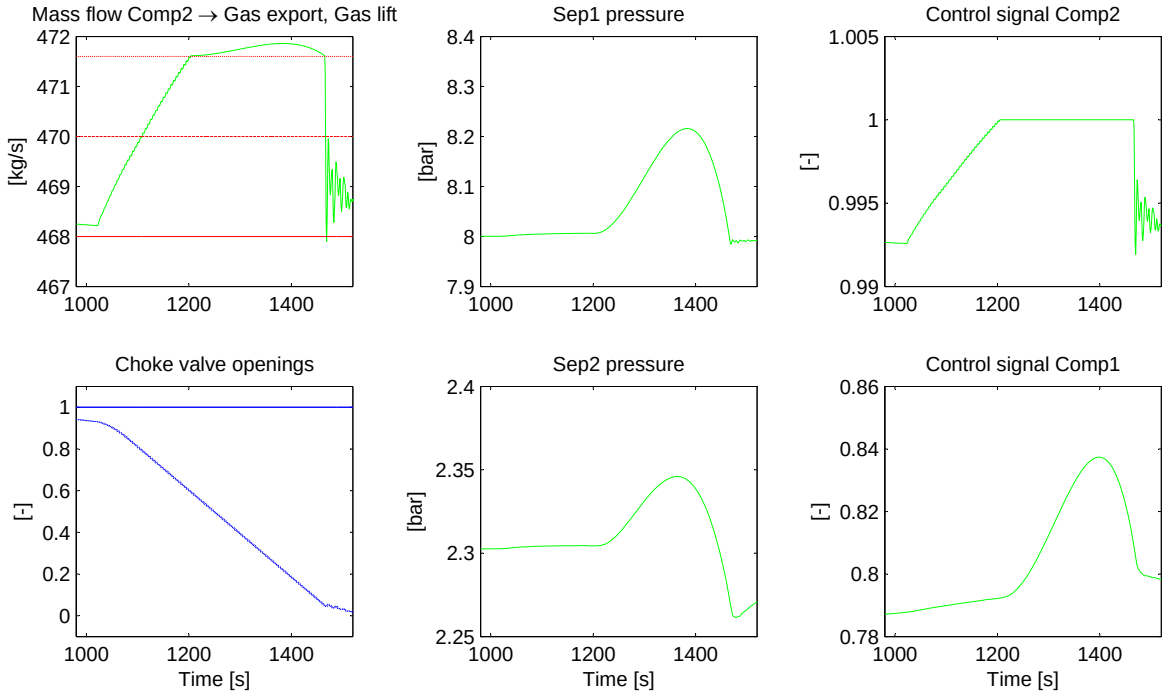

Figure 3.8: Close-up view of a portion of the simulation of Figure 4.13. *X6* is kept constantly at full opening, while *X8* is used for constraint control. Red lines: (Solid: FIC1 setpoint), (Dashed: FIC2 setpoint), (Dotted: Maximum flow rate capacity of second compressor without tank pressure increases). Choke valve control signals: *X6* solid, *X8* dotted. Note that although the setpoint of FIC2 is shown here, FIC2 is not actually used in this simulation, as its output is kept constantly at maximum.

Design principle summary

See Figure 3.9 for an illustration. We need one PI flow rate controller for each controlled well. The gas flow rate in the second gas compressor is the measurement for both controllers. The resulting controller can thus be categorized as a SIMO controller (single input, multiple output). The well with the highest GOR will be used for flow rate control under normal conditions, and its flow rate setpoint is somewhat backed off from the desired gas rate constraint. The well with the lower GOR will only be choked down if necessary. This is ensured by setting its flow rate setpoint less backed off than that of the other well.

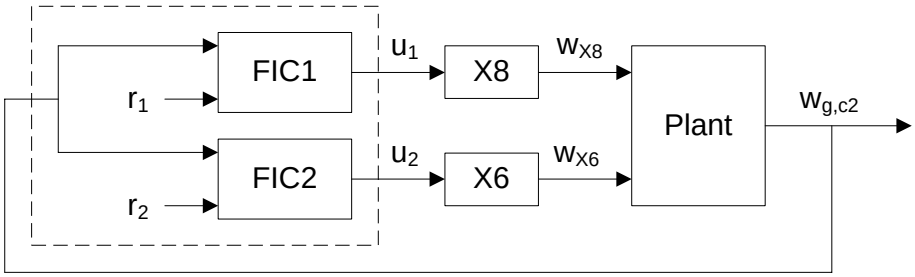

Figure 3.9: Control system structure of *DC1*. $w_{g,c2}$ is the gas flow rate through the second compressor stage. The overall SIMO flow rate controller is contained within the dashed box.

3.5.2 Constraint change feedforward by setpoint manipulation

The flow rate controller setpoints are computed as offsets from the gas flow rate constraint. The principle is illustrated in Figure 3.10. In order to accommodate for the choke valve stroke time as well as the transient flow rate response, the setpoint must be lowered in advance if the constraint is being lowered. This is solved using feedforward by setting the flow rate setpoint as given in equation (3.63), with c being the constraint offset, ST being the number of sampling points corresponding to the choke valve stroke time, and $\bar{w}_{g,c2,i}$ being the flow rate constraint at time sample number i

$$r_k = \min(\bar{w}^f_{g,c2,k}) - c \quad , \quad \bar{w}^f_{g,c2,k} = [\bar{w}_{g,c2,k} \quad \bar{w}_{g,c2,k+1} \quad \cdots \quad \bar{w}_{g,c2,k+ST}] \tag{3.63}$$

By considering the flow rate constraints in the time interval starting now and lasting ST samples into the future, there should be time for the choke valve to adjust to approximately the required opening in advance of any possible constraint change.

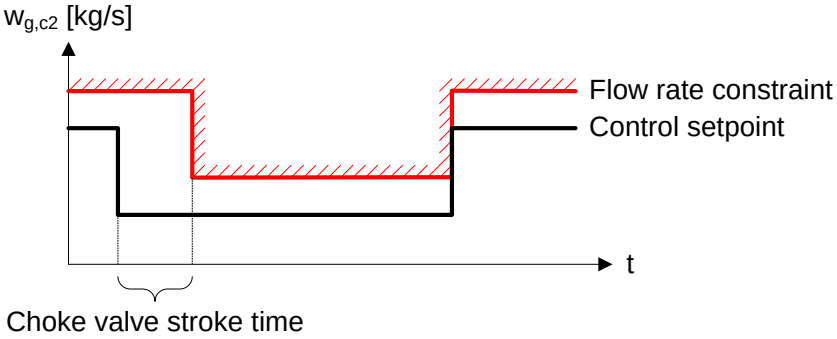

Figure 3.10: Constraint change handling principle

3.5.3 Disturbance feedforward

Known future disturbances can be compensated for using feedforward control. However, depending on the situation at hand, it may not be straight forward how the feedforward should be implemented when the target system is a PID controller. In our case, the choke valve stroke time poses a challenge, as we must start the choke valve compensation in advance in order to have the needed compressor capacity available when the known future disturbance actually occurs. Two different feedforward strategies will be examined. In the first approach, all of the feedforward data will be used. In the second approach, only the largest inflow changes will be fed forward, while the rest of the disturbance will be tackled using feedback control.

DC1 FF1 - First feedforward scheme

The first feedforward algorithm to be used by *DC1* is shown below, written in MATLAB code. `ii` is the current iteration number, the choke valve stroke time is *480s*, `measurement` is the gas rate measurement to be passed to the flow rate controller, `feedforwardData` is a vector consisting of the values of the disturbance estimate throughout the simulation run, and `maxFlowRateSingleWell` is the defined maximum gas flow rate from a well, used for scaling purposes. The latter value can be found in Table 2.3.

```
maxOnHorizon      = max(feedforwardData(ii:ii+480));
indexOfMax        = find(feedforwardData(ii:ii+480)==maxOnHorizon,1);
relIndexOfMax     = indexOfMax/480;
relMaxDisturbance = (maxOnHorizon-feedforwardData(ii))/maxFlowRateSingleWell;
if relIndexOfMax <= relMaxDisturbance
  measurement     = measurement + maxOnHorizon - feedforwardData(ii);
end
```

The idea behind the above algorithm is to examine the future disturbance data on a horizon equal to the choke valve stroke time. Depending on the size of the maximum disturbance up to the horizon, control action is performed at an appropriate time. See Figure 3.11. For instance, if the maximum disturbance relative to `maxFlowRateSingleWell`, `relMaxDisturbance`, is 1.0, control action will be taken immediately (that is, the measurement passed to the controller will be changed as specified in the algorithm). If the disturbance on the other hand for instance was 0.7, control action will be postponed until it has moved 0.3 times the choke valve stroke time closer to the current time on the horizon.

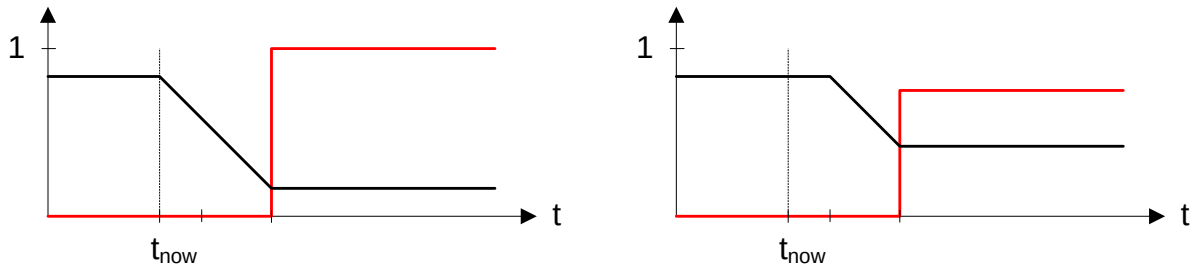

Figure 3.11: Disturbance feedforward principle as presented in Section 3.5.3. Black: Valve opening. Red: Relative size of predicted disturbance. Left: Large disturbance need immediate action. Right: Smaller disturbance allows us to postpone the reaction.

DC1 FF2 - Second feedforward scheme

In this feedforward approach, only the largest inflow disturbance changes will be fed forward, while the rest of the disturbance will be handled using ordinary feedback control. The idea is that the valves must be prepared for the largest flow rate disturbances due to the long valve stroke time, while it should be possible to capture the smaller flow rate changes using feedback control. Due to the inevitable difference between the predicted disturbances and the actual disturbances, additional feedback compensation is needed in any case.

The feedforward algorithm of *DC1* FF2 is shown below, written in MATLAB code. `minStepSize` can be set to a desired level. See FF1 for further variable explanations.

```
minStepSize          = 0.6*max(feedforwardData);
maxStepOnHorizon     = max(feedforwardData(ii:ii+480)) - feedforwardData(ii);
if maxStepOnHorizon >= minStepSize
    measurement      = measurement + maxStepOnHorizon;
end
```

3.5.4 Tuning

Using data from Table 2.3, it is easily verified that the well named *X8* has the highest GOR of the two controlled wells. Thus, the flow rate control will be mainly done through FIC1 by manipulating the valve of *X8*.

In the following, the tuning of the two PI controllers FIC1 and FIC2 in Figure 3.9 will be presented.

The proportional gain K_i of controller i was initially set roughly equal to the inverse of the process gain from u (valve opening) to y (gas mass flow rate) of well i. The reason for this was that a well producing large amounts of gas would need less control action in order to achieve a certain flow rate change, as its process gain was large in itself (it's the other way around for wells with less gas production). The gas flow rate gain of the different wells can be found in Table 2.3.[4] Since this only was a starting point, K was initially set equal to 1/20 for both controllers. It was since moved further back to 0.25/20 in order to remove some input oscillations.

PI controllers for flow rate control are often tuned using a short integral time. T_I of FIC1, which would be used for constraint control under normal conditions, was set to $10s$. T_I of FIC2 was set to $5s$. The particularly short integral time of FIC2 was chosen since fast action would be needed whenever FIC2 started choking down on *X6*, as the gas flow rate would be closing in on its constraint.

The controller setpoints of FIC1 and FIC2 were set as presented in Section 3.5.2, with their back-off set to 3.6 and 1.6 *kg/s*, respectively. In a real world, noisy environment, one should expect the need for using a larger back-off due to lower measurement quality. Note that the controller setpoints would be dynamically updated throughout the simulations in accordance with changing constraints. Their constraint back-off were however held at a constant level.

The controller tuning is summarized in Table 3.8.

Table 3.8: *DC1* flow rate controller tuning summary

Controller	*Controlling*	K	T_I	*Setpoint constraint back-off*
FIC1	*X8*	0.25/20=0.0125	$10s$	3.6
FIC2	*X6*	0.25/20=0.0125	$5s$	1.6

[4] As was pointed out in the beginning of Section 3.3 and quantified in equation (3.15), there is little difference between the gas outflow rate from the well and from the topside process.

Chapter 4

Simulation results

In this chapter, three simulation cases will be examined for each realized controller. The cases are as follows

1. *Startup of additional well.* A third well, simulated using OLGA, will be opened up for production after some time. Its choke valve opening will be set at a fixed level and held constant. This change in production will be known in advance and thus feedforward control will be applied. An inflow disturbance model will be used in order to illustrate the benefits of automatic control in relation to well startup. The disturbance model will contain a representation of the dynamic startup response of the third well, obtained from an earlier test run. See Section 2.4 for further details.

2. *Slugging well.* A third, slugging well will be introduced. The slugs will be represented using a pre-generated sawtooth inflow sequence. The disturbance will not be known in advance by the controllers, and in the case of the MPCs, at any given time, the disturbances detected by the integral action of the controllers will be assumed to be held at the present level for all future time. It will thus be handled as any other prediction error.

3. *Reduced gas processing capacity.* There will be a planned change in the second compressor gas rate constraint after some time. This constraint change will be known in advance, and the controllers will have to reduce the gas inflow rate accordingly. In a practical setting, this constraint change can be due to a number of reasons, such as repairs and maintenance work, for instance. One could also consider lowering the constraints a bit in advance of and during the startup phase of new wells (see *case 1*), in order not to break any physical process constraints. The constraint is reduced by 60% of the average peak gas flow rate from wells *X6* and *X8*, that is, 60% of an average well inflow (see Table 2.3 on page 8).

Plot scaling

The simulation plots in this chapter has been scaled as given in Table 4.1 when nothing else is specified.

Table 4.1: Simulation plot measurement scalings

Measurement	*Maximum deviation*
Sep1, Level oil	0.2 [m]
Sep1, Level water	0.2 [m]
Sep2, Level oil	0.2 [m]
Sep2, Level water	0.2 [m]
Sep1, Pressure	1.0 [bar]
Sep2, Pressure	0.25 [bar]

4.1 *MPC1* - Direct choke valve control

The measurements in the upcoming simulation results were scaled as given in Table 4.1.

The *case 1* simulations were performed using two different feedforward schemes *MPC1* FF1 and FF2, with FF1 having a more detailed startup model than FF2. See Section 3.3.2 for further details. The FF1 and FF2 results are presented in figures 4.1 and 4.2, respectively.

The two different *case 2* simulations were performed using two different costs on control input changes. In the first setup, see Figure 4.3, the standard costs as given in equation (4.1) were used, while in the second setup, see Figure 4.4, r_1 and r_2 were changed from the initial 250 to 1000.

The *case 3* simulation was performed two times, the latter of which was performed using an erroneous well model in order to demonstrate the importance of applying the correct model in the MPC. The model error was introduced by increasing the oil flow rate gain of *X8* by a factor of 1.5 in the linear MPC model, thereby making *X8* seem more economically profitable than *X6*, although it is the other way around in the actual OLGA well model. Both simulations were performed using the standard tunings as presented in Section 4.1.1. The simulation results are shown in figures 4.5 and 4.6.

Look to Section 5.1 for comments on the results.

4.1.1 Controller setup

The costs as defined in equation (3.21) were chosen as follows in the controller setups where nothing else is specified (q: oil production profit, r_i: input change cost, s_i: output change cost, $r_\mathcal{E}$: constraint softening cost)

$$q = 2 \quad , \quad \begin{bmatrix} r_1 \\ r_2 \end{bmatrix} = \begin{bmatrix} 250 \\ 250 \end{bmatrix} \quad , \quad \begin{bmatrix} s_1 \\ s_2 \end{bmatrix} = \begin{bmatrix} 1.0 \\ 0.1 \end{bmatrix} \quad , \quad r_\mathcal{E} = 1000 \tag{4.1}$$

The prediction and control horizons were chosen as given below

$$H_p = 2000s \quad , \quad H_u = 2000s \tag{4.2}$$

The MPC sampling time was set to 40 s, while the low level PID controllers were operating with a 1 s sampling time.

With a pressure increase from 8 to 80 bar, the flow rate of the second compressor is limited to 471.6 kg/s when operating at full speed, see Figure 1.1 on page 2. However, due to the

nonlinearity of the process together with the simplified topside model for the gas flow rate, a safety margin should be kept when introducing this constraint to the linear MPC. Therefore, the constraint $\bar{w}_{g,c2}$ was set to 468 kg/s. This rather small back-off worked quite well here, but in other cases, larger back-offs may be needed.

Being in a noise free environment, the Kalman filter for state estimation was set up with covariance matrices V and W as follows. The state covariance matrix X was initiated to the nonzero matrix $0.001I$. Otherwise, it can be seen from equations (3.35) and (3.36) that the state estimates would not be able to change from their initial values.

$$V = 1000I \quad , \quad W = 0.001I \tag{4.3}$$

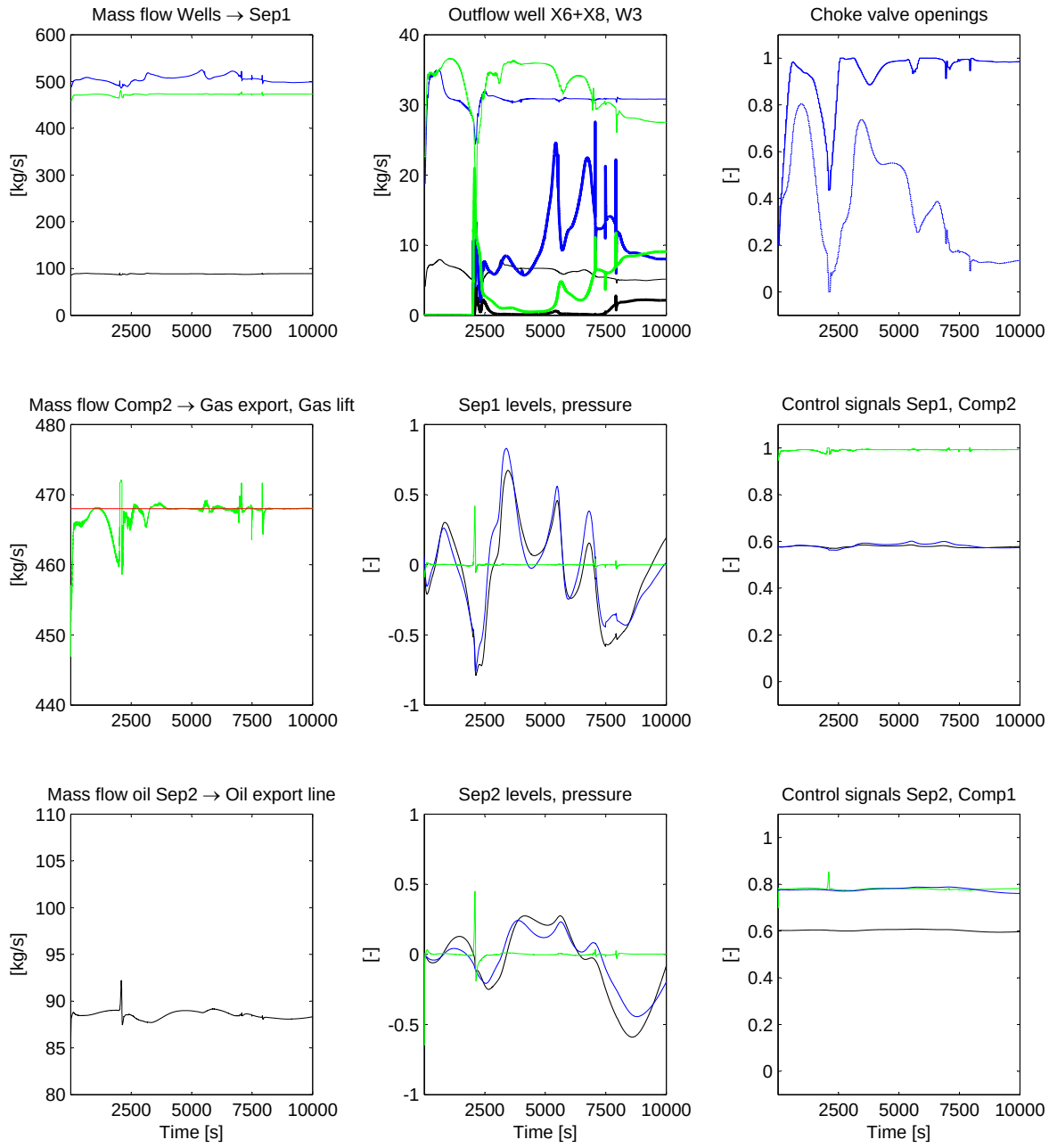

Figure 4.1: *MPC1* using feedforward scheme FF1. Startup of well *W3*. $\bar{w}_{o,s2} = 88.54$ [kg/s], $\text{var}(w_{o,s2}) = 0.22$ [(kg/s)^2]. Green-gas, black-oil, blue-water. Choke valve control signals: *X6* solid, *X8* dotted. *W3* bold.

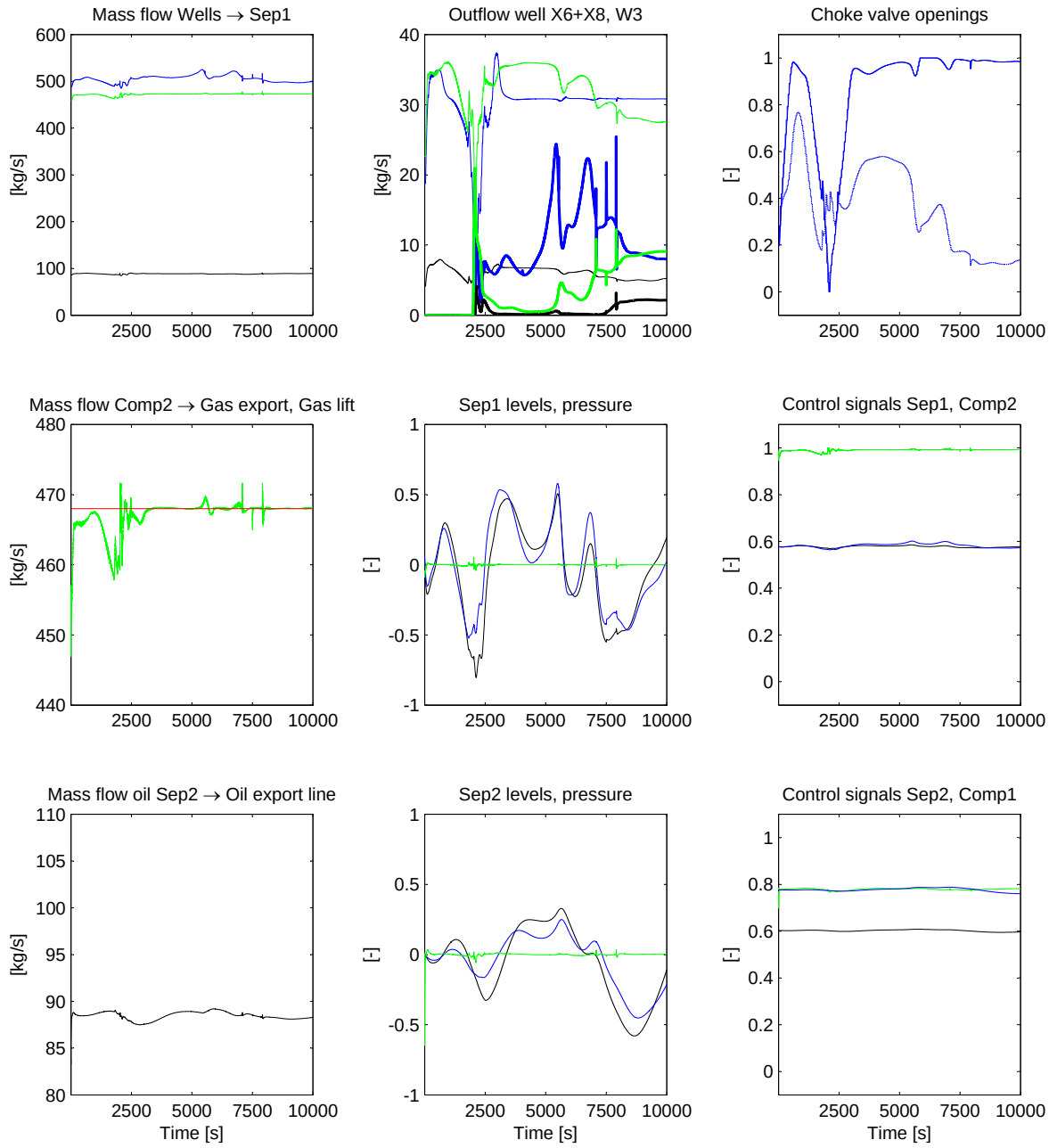

Figure 4.2: *MPC1* using feedforward scheme FF2. Startup of well *W3*. $\bar{w}_{o,s2} = 88.47$ [kg/s], $\text{var}(w_{o,s2}) = 0.19$ [(kg/s)^2]. Green-gas, black-oil, blue-water. Choke valve control signals: *X6* solid, *X8* dotted. *W3* bold.

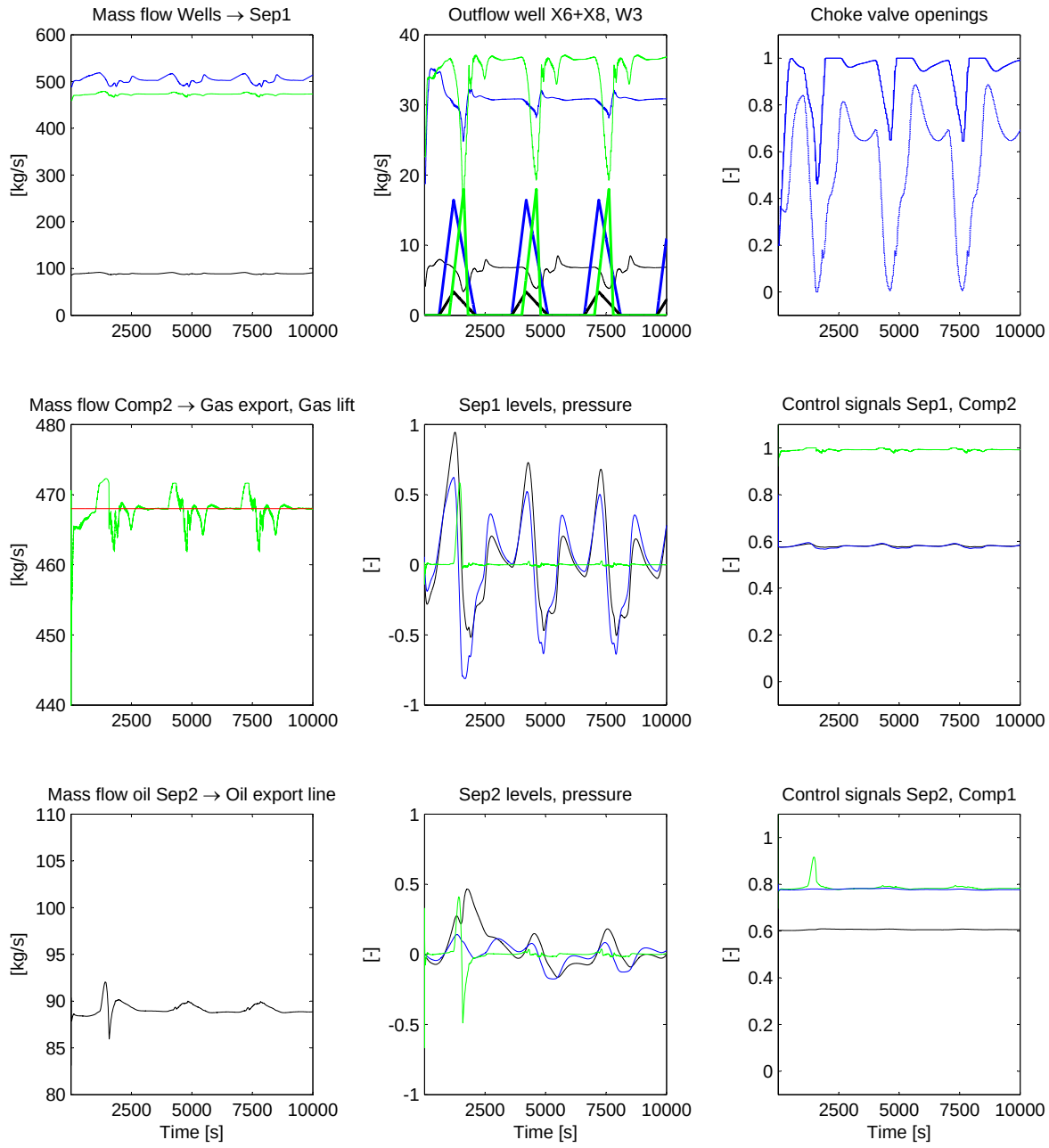

Figure 4.3: *MPC1.* Slugging well - Less cost on input change. $\bar{w}_{o,s2} = 89.19$ [kg/s], $\text{var}(w_{o,s2}) = 0.34$ [(kg/s)^2]. Green-gas, black-oil, blue-water. Choke valve control signals: *X6* solid, *X8* dotted. *W3* bold.

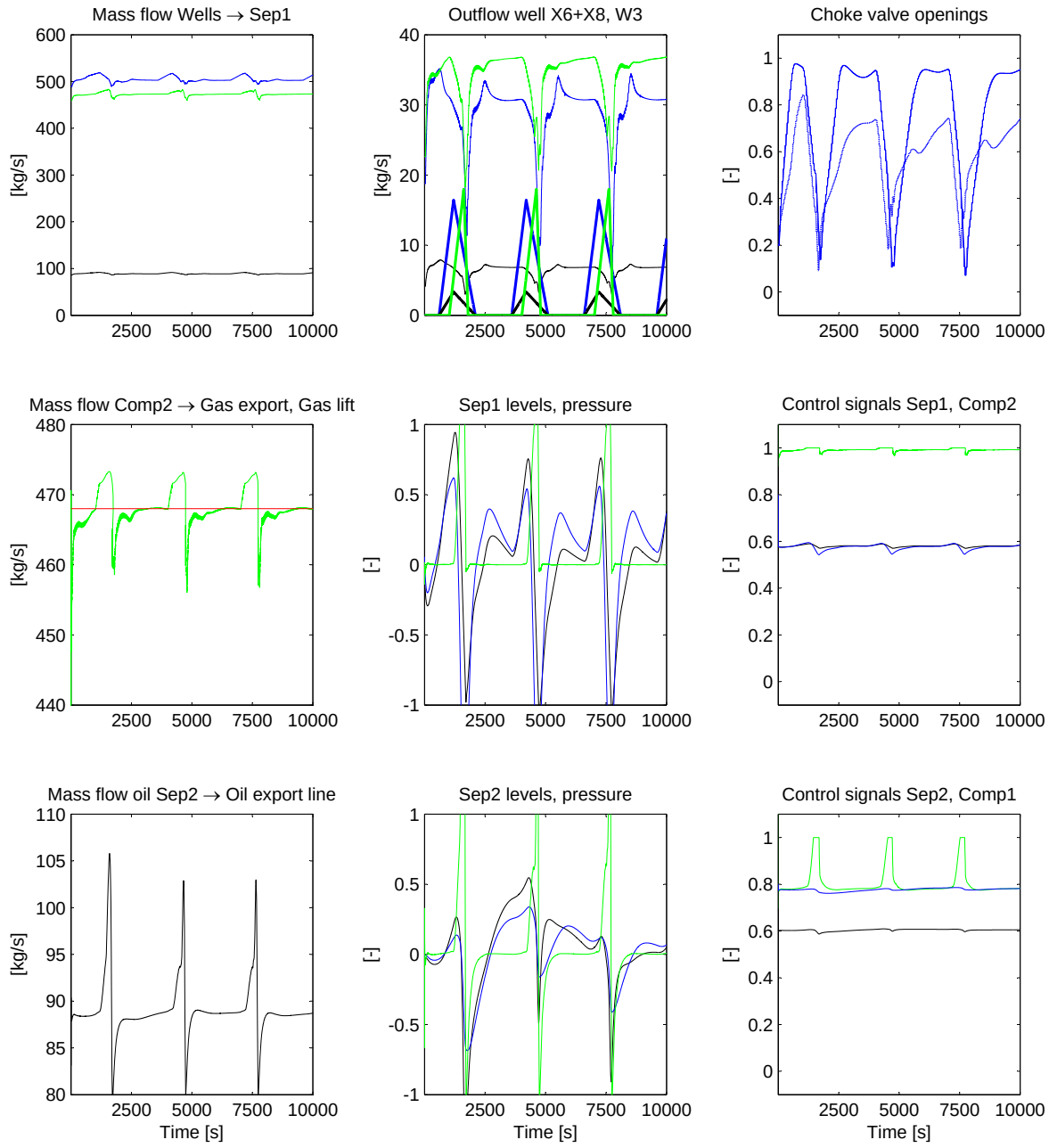

Figure 4.4: *MPC1.* Slugging well - More cost on input change. $\bar{w}_{o,s2} = 89.19$ [kg/s], $\text{var}(w_{o,s2}) = 10.96$ [(kg/s)^2]. Green-gas, black-oil, blue-water. Choke valve control signals: *X6* solid, *X8* dotted. *W3* bold.

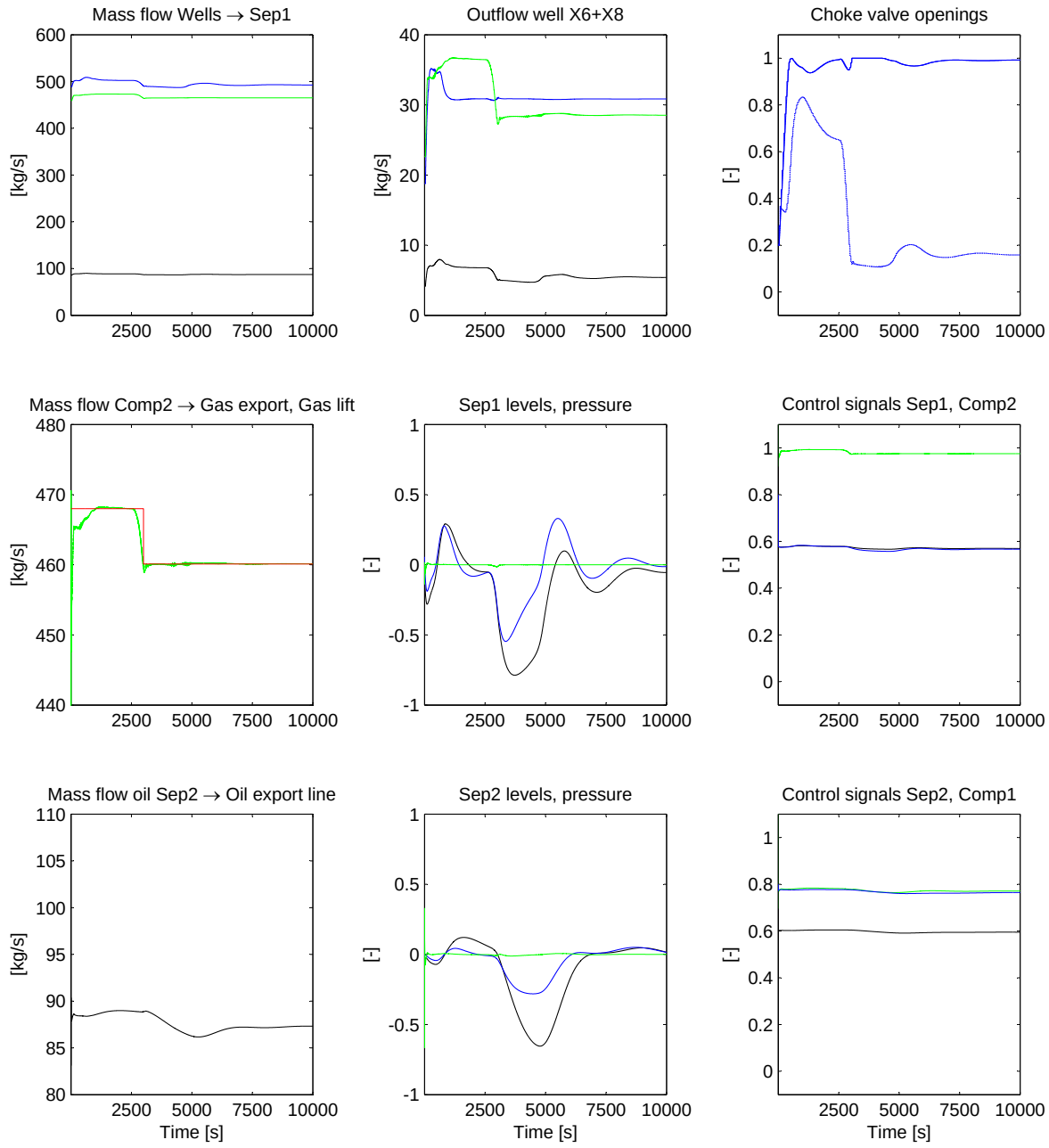

Figure 4.5: *MPC1.* Gas rate constraint change. Green-gas, black-oil, blue-water. $\bar{w}_{o,s2} = 87.58$ [kg/s], $\mathrm{var}(w_{o,s2}) = 0.81$ [(kg/s)^2]. Choke valve control signals: *X6* solid, *X8* dotted.

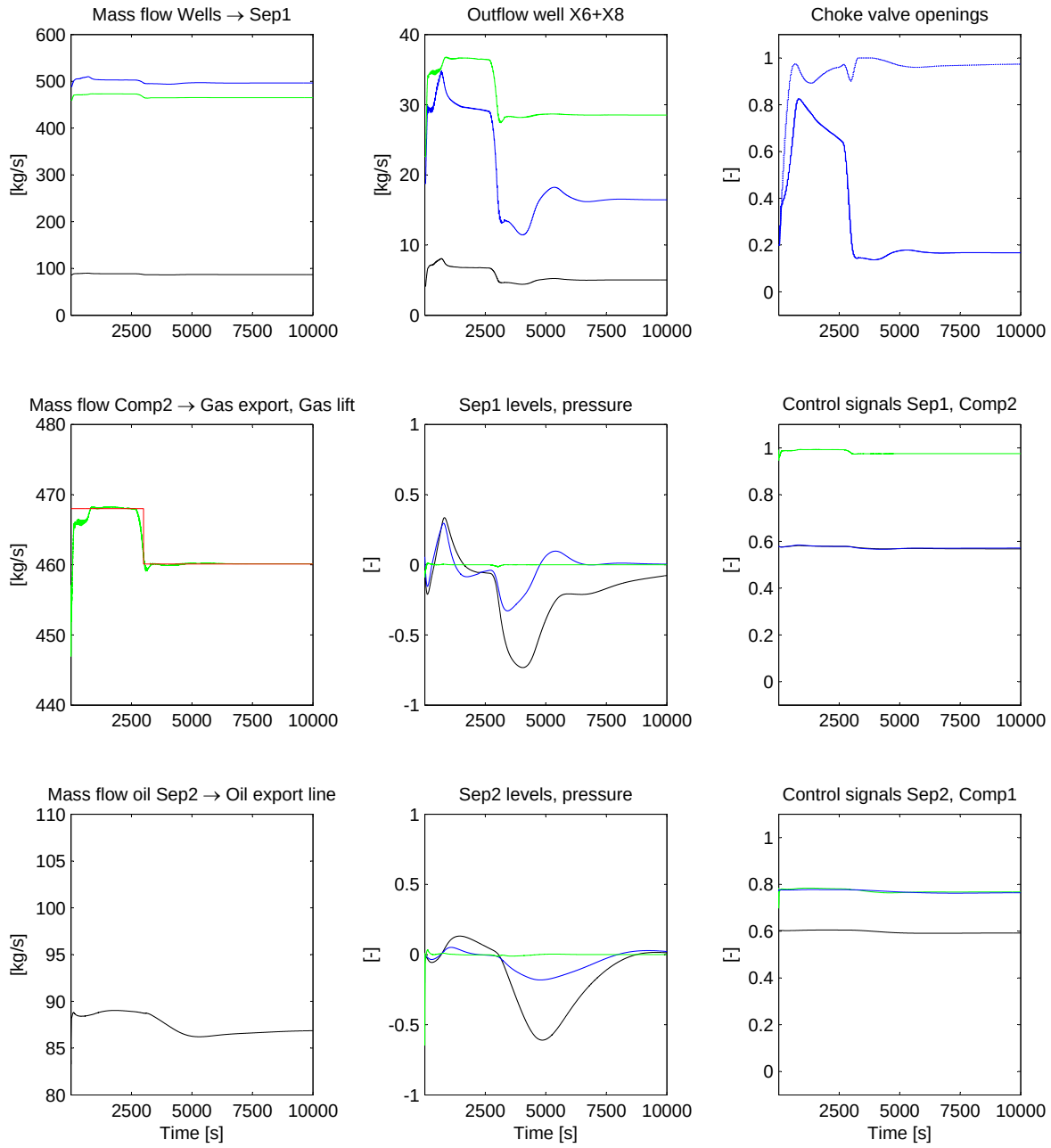

Figure 4.6: *MPC1.* Gas rate constraint change, with erroneous well model. Green-gas, black-oil, blue-water. $\bar{w}_{o,s2} = 87.32$ [kg/s], $\text{var}(w_{o,s2}) = 1.06$ [(kg/s)^2]. Choke valve control signals: *X6* solid, *X8* dotted.

4.2 *MPC2* - Direct choke valve and topside flow rate setpoint control

The measurements in the upcoming simulation results were scaled as given in Table 4.1 on page 44.

The results from simulation *case 1*, *2* and *3* are shown in figures 4.7, 4.8 and 4.9, respectively.

Look to Section 5.1 for comments on the results.

4.2.1 Controller setup

MPC1 was set up as presented in Section 4.1.1.

The costs of *MPC2*, as defined in equation (3.49), were selected as follows where nothing else is specified ($r_{2,i}$: input change cost, $p_{2,i}$: tank level setpoint deviation cost, $r_{\mathcal{E}2,i}$: constraint softening cost). In the middle column, the weights are scaled with respect to the approximately maximum expected flow rates and level deviations, for easier tuning

$$\begin{bmatrix} r_{2,1} \\ r_{2,2} \\ r_{2,3} \\ r_{2,4} \end{bmatrix} = \begin{bmatrix} 10000/88 \\ 5000/430 \\ 50000/88 \\ 5000/35 \end{bmatrix} = \begin{bmatrix} 114 \\ 12 \\ 568 \\ 143 \end{bmatrix}$$

$$\begin{bmatrix} p_{2,1} \\ p_{2,2} \\ p_{2,3} \\ p_{2,4} \end{bmatrix} = \begin{bmatrix} 5/0.2 \\ 5/0.2 \\ 0.5/0.2 \\ 0.5/0.2 \end{bmatrix} = \begin{bmatrix} 25 \\ 25 \\ 2.5 \\ 2.5 \end{bmatrix} \tag{4.4}$$

$$r_{\mathcal{E}2,i} = 10^4 \cdot \max_{j,l}(r_{2,j}, p_{2,l}) = 5.68 \cdot 10^6 \quad \forall i$$

The terminal cost (the costs of the last iteration on the horizon) was increased by a factor of 1000 in order to help enforcing convergence towards zero control input change and level deviation.

As in the case of *MPC1*, the *MPC2* prediction and control horizons were chosen as given below

$$H_p = 2000s \quad , \quad H_u = 2000s \tag{4.5}$$

Further, the *MPC2* sampling time was set to 40 s, while the low level PID controllers were operating with a 1 s sampling time.

The upper and lower tank level constraints were chosen such that all level deviations were smaller than 0.2 m, except for the upper water level constraints, which were limited to 0.18 m in order to stay clear of the tank weir top. Referring to the tank dimensions illustrated in Figure 3.1, it is clear that this is quite a conservative setting which could easily have been relaxed if needed.

The lower constraints on the control input (flow rate setpoints) were set to zero. The upper limits were calculated using the valve flow equation shown in equation (3.62), setting the valve opening $u = 1$, ρ equal to the average mass density of the phase flowing through the valve (approximated to 800 kg/m^3 for the oil valves and 1000 kg/m^3 for the water valves), while Δp was set equal to the steady state pressure difference over the valve in question. This yielded upper bounds $\{\bar{w}_{s1,o}\ ,\ \bar{w}_{s1,w}\ ,\ \bar{w}_{s2,o}\ ,\ \bar{w}_{s2,w}\} = \{320\ ,\ 750\ ,\ 204\ ,\ 46\}$ [kg/s]. The upper flow

rate bounds were needed in order to ensure that the MPC was not commanding greater flow rates than what was achievable in practice.

The Kalman filter for state estimation was set up with covariance matrices V and W similarly to that of *MPC1*. The state covariance matrix X was initiated to the nonzero matrix $0.001I$.

$$V = 1000I \quad , \quad W = 0.001I \tag{4.6}$$

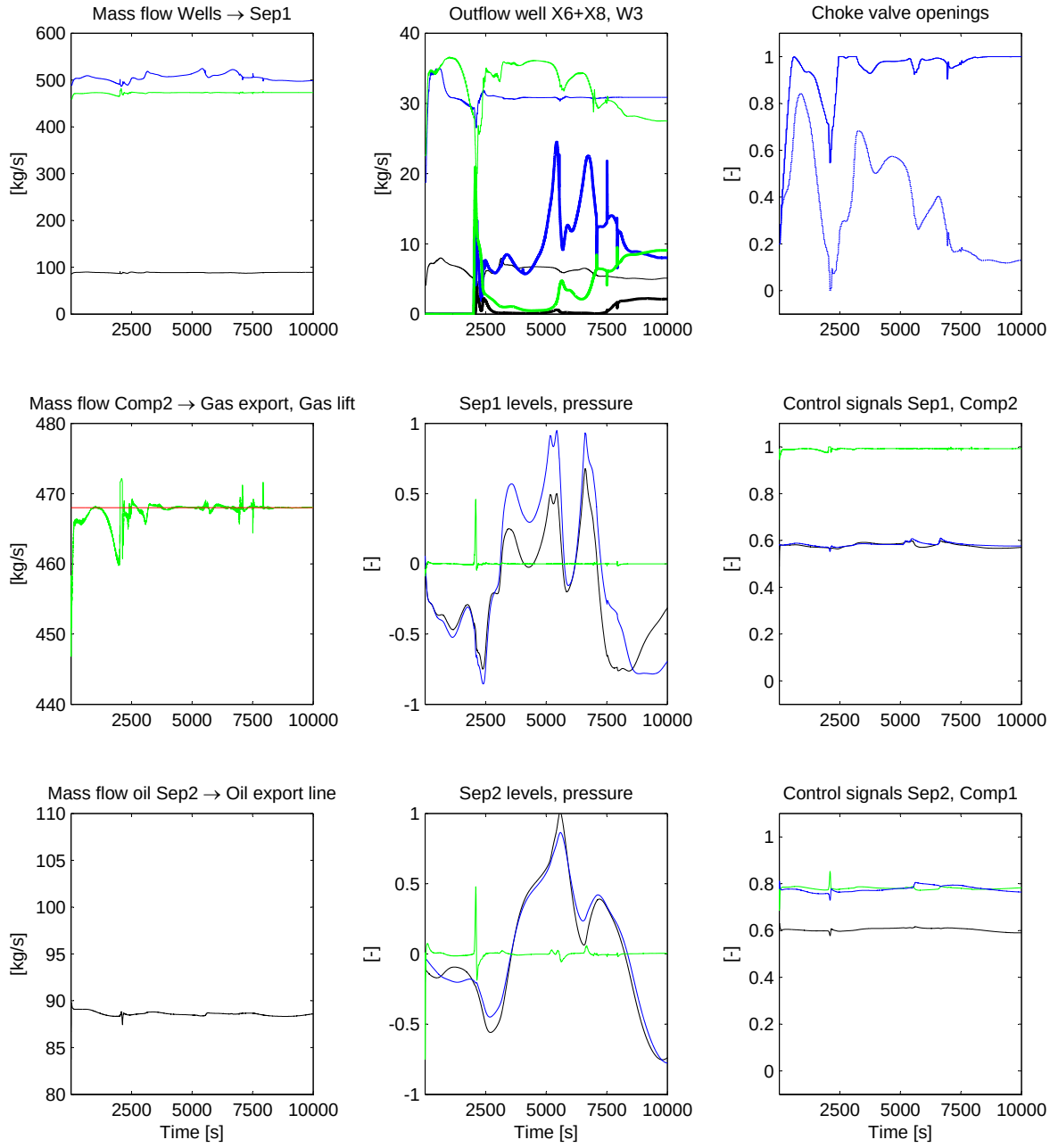

Figure 4.7: *MPC2*. Startup of well *W3*. $\bar{w}_{o,s2} = 88.55$ [kg/s], $\text{var}(w_{o,s2}) = 0.02$ [(kg/s)^2]. Green-gas, black-oil, blue-water. Choke valve control signals: *X6* solid, *X8* dotted. *W3* bold.

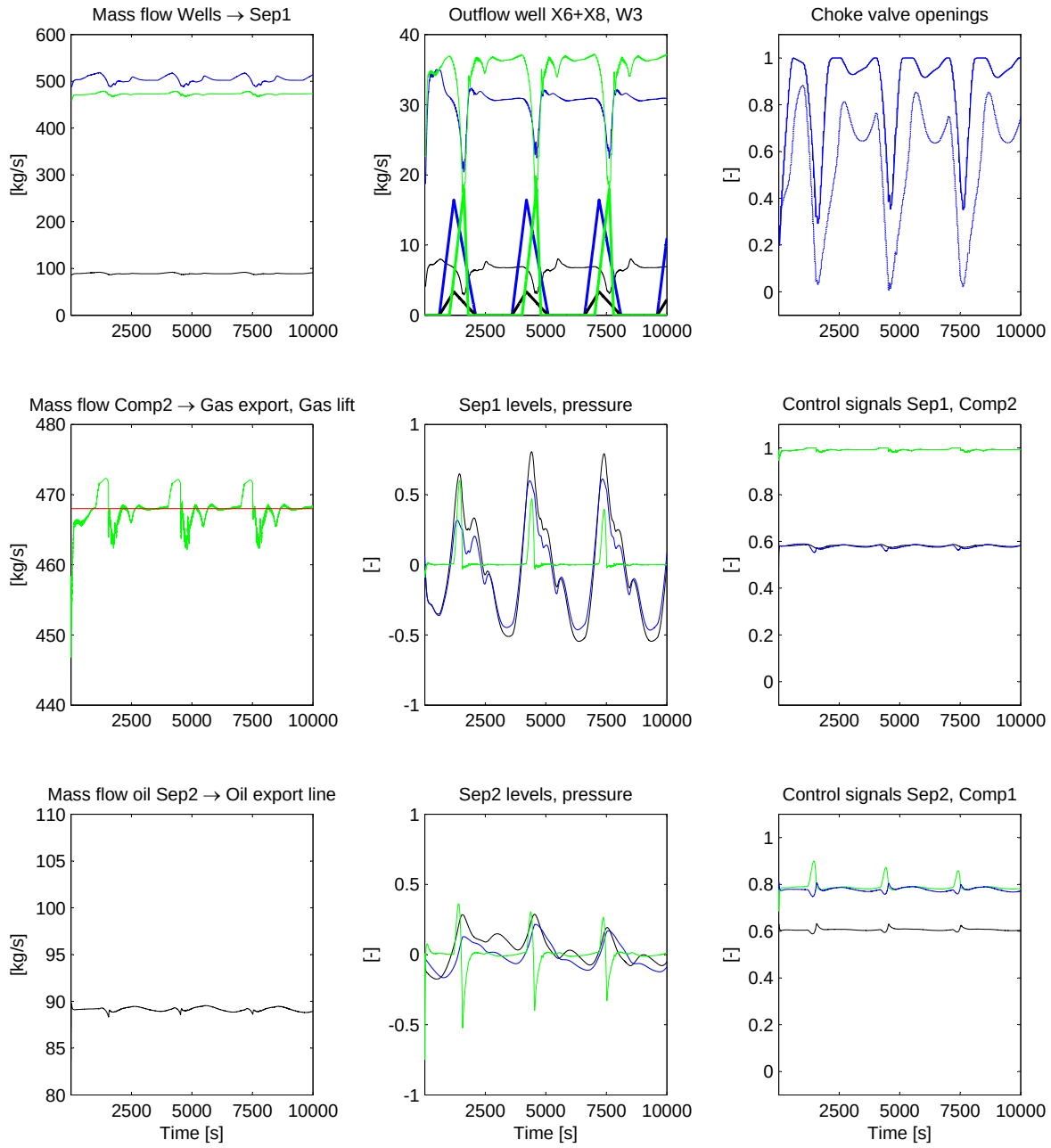

Figure 4.8: *MPC2.* Slugging well - Less cost on input change. $\bar{w}_{o,s2} = 89.14$ [kg/s], $\text{var}(w_{o,s2}) = 0.05$ [(kg/s)^2]. Green-gas, black-oil, blue-water. Choke valve control signals: *X6* solid, *X8* dotted. *W3* bold.

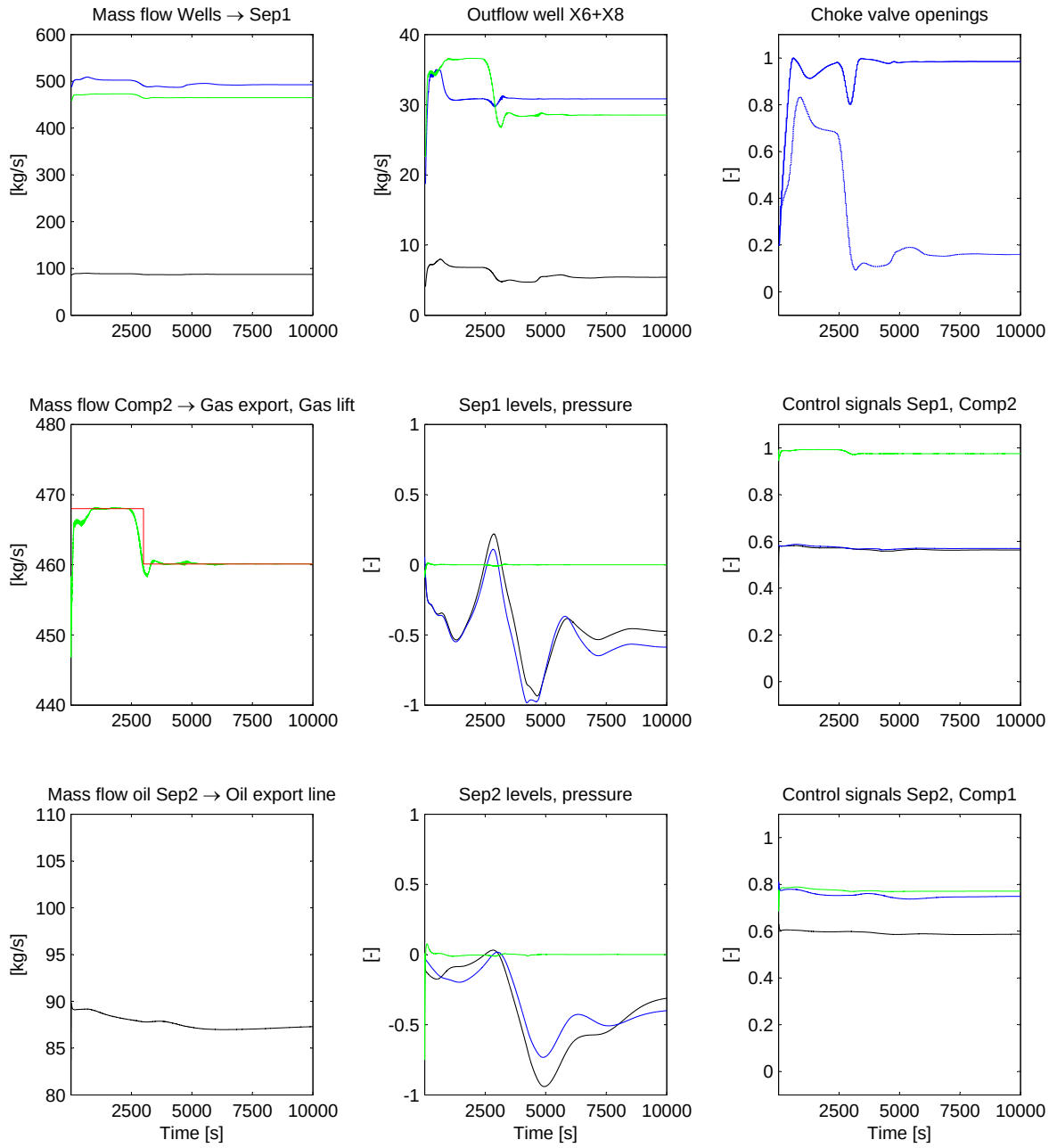

Figure 4.9: *MPC2.* Gas rate constraint change. Green-gas, black-oil, blue-water. $\bar{w}_{o,s2} = 87.50$ [kg/s], $\mathrm{var}(w_{o,s2}) = 0.28$ [(kg/s)^2]. Choke valve control signals: *X6* solid, *X8* dotted.

4.3 *DC1* - Decentralized choke valve control

The measurements in the upcoming simulation results were scaled as given in Table 4.1 on page 44.

As for *MPC1*, the *case 1* simulations of *DC1* were also performed using two different feedforward schemes, denoted *DC1* FF1 and FF2. The essential difference between the two schemes is that FF2 only feeds forward the larger expected inflow rate changes and leaves the rest to the feedback control. Look to Section 3.5.3 for further details on the different schemes. The results obtained using FF1 and FF2 are shown in figures 4.10 and 4.11, respectively.

In simulation *case 2*, two simulation runs were carried out. However, there is one main simulation result (Figure 4.12), with the other being included to illustrate the benefit of applying additional control action when closing in on the process constraint (Figure 4.13).

Figure 4.14 shows the results obtained in simulation *case 3* using the controller *DC1*. The constraint change handling principle is presented in Section 3.5.2.

Comments on the simulation results can be found in Section 5.1.

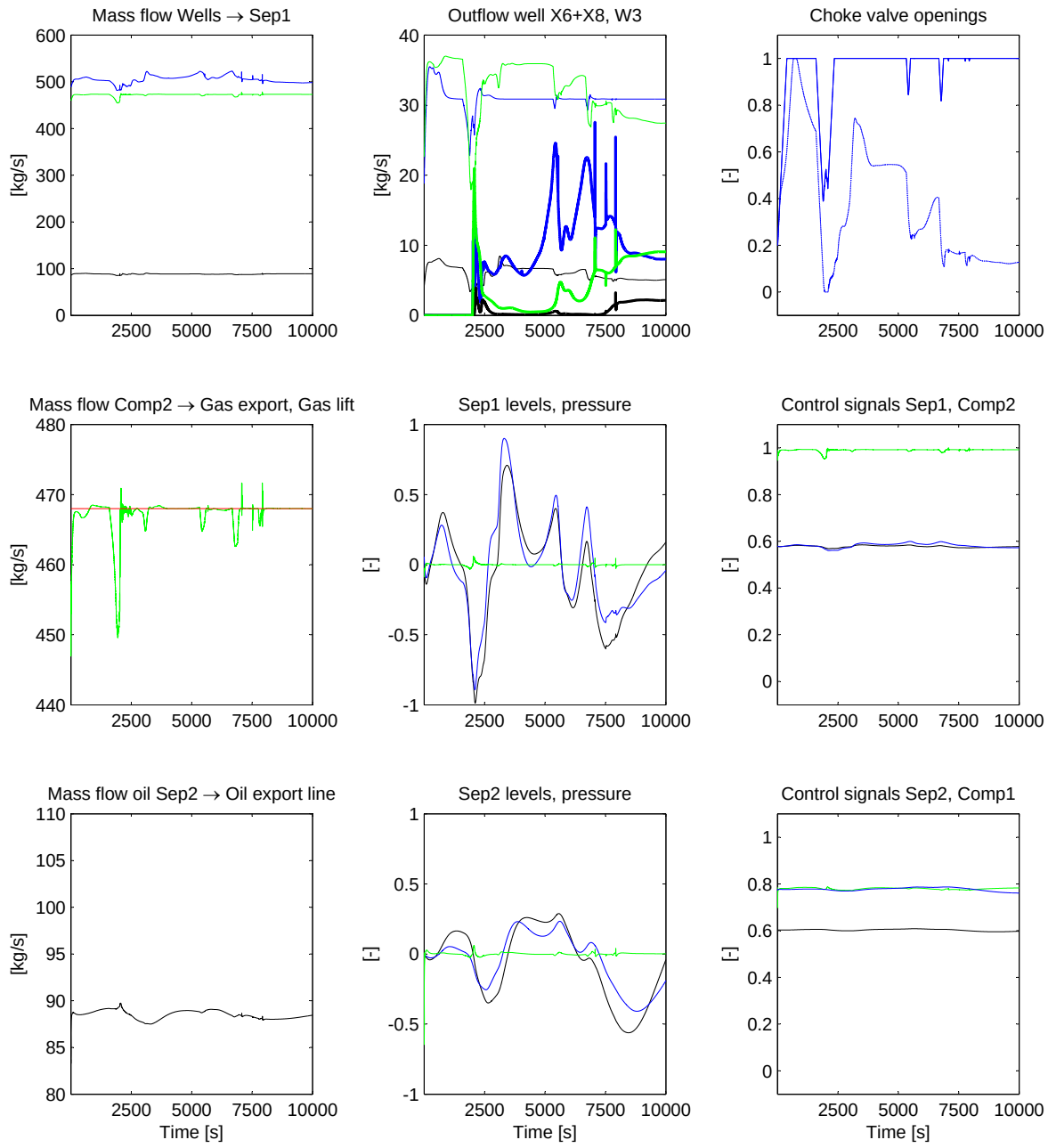

Figure 4.10: *DC1* using feedforward scheme FF1. Startup of well *W3* - *X6* and *X8* choke valves are controlled. $\bar{w}_{o,s2} = 88.50$ [kg/s], $\text{var}(w_{o,s2}) = 0.23$ [(kg/s)^2]. Green-gas, black-oil, blue-water. Choke valve control signals: *X6* solid, *X8* dotted. *W3* bold.

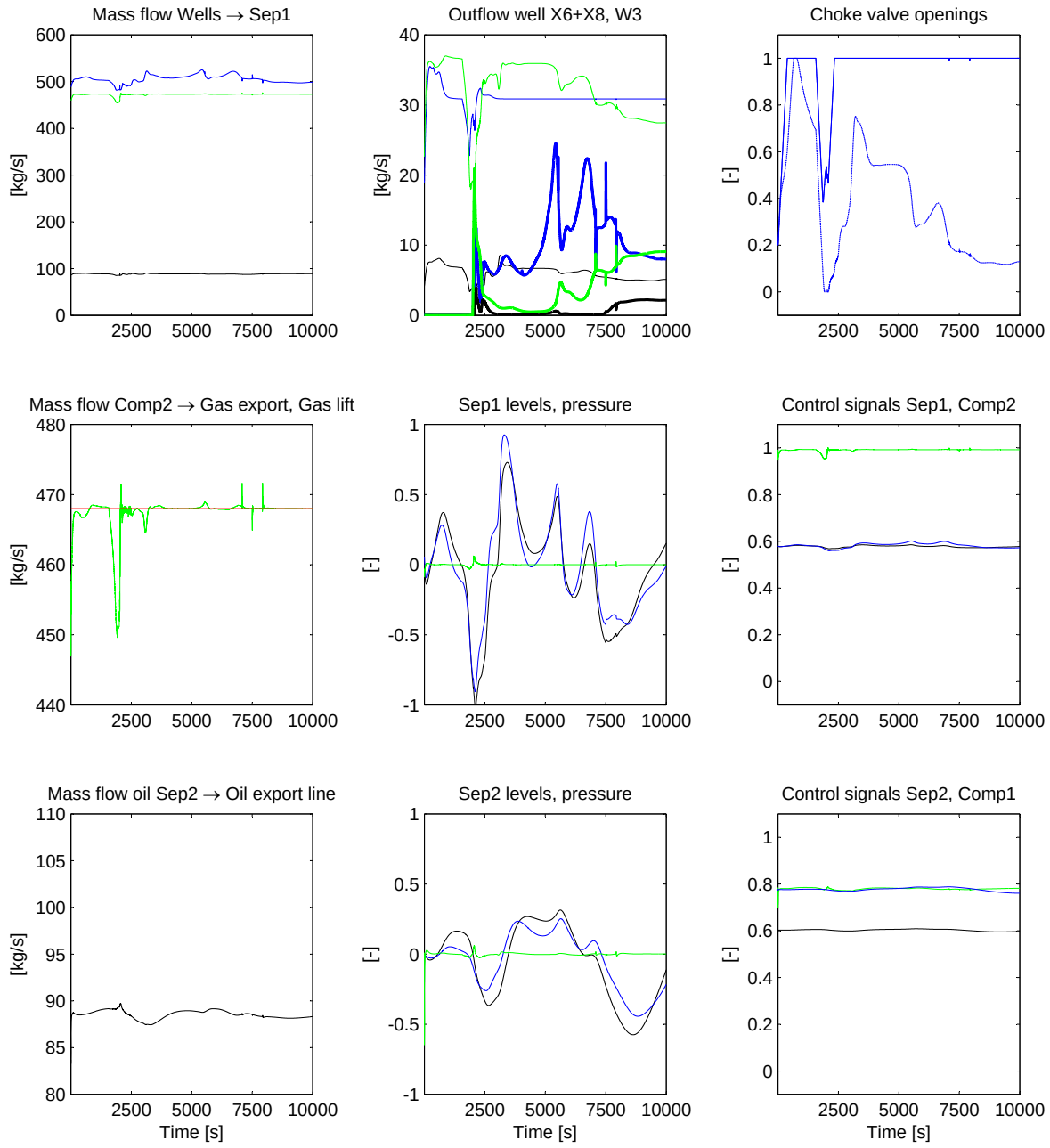

Figure 4.11: *DC1* using feedforward scheme FF2. Startup of well *W3* - *X6* and *X8* choke valves are controlled. $\bar{w}_{o,s2} = 88.55$ [kg/s], $\text{var}(w_{o,s2}) = 0.23$ [(kg/s)^2]. Green-gas, black-oil, blue-water. Choke valve control signals: *X6* solid, *X8* dotted. *W3* bold.

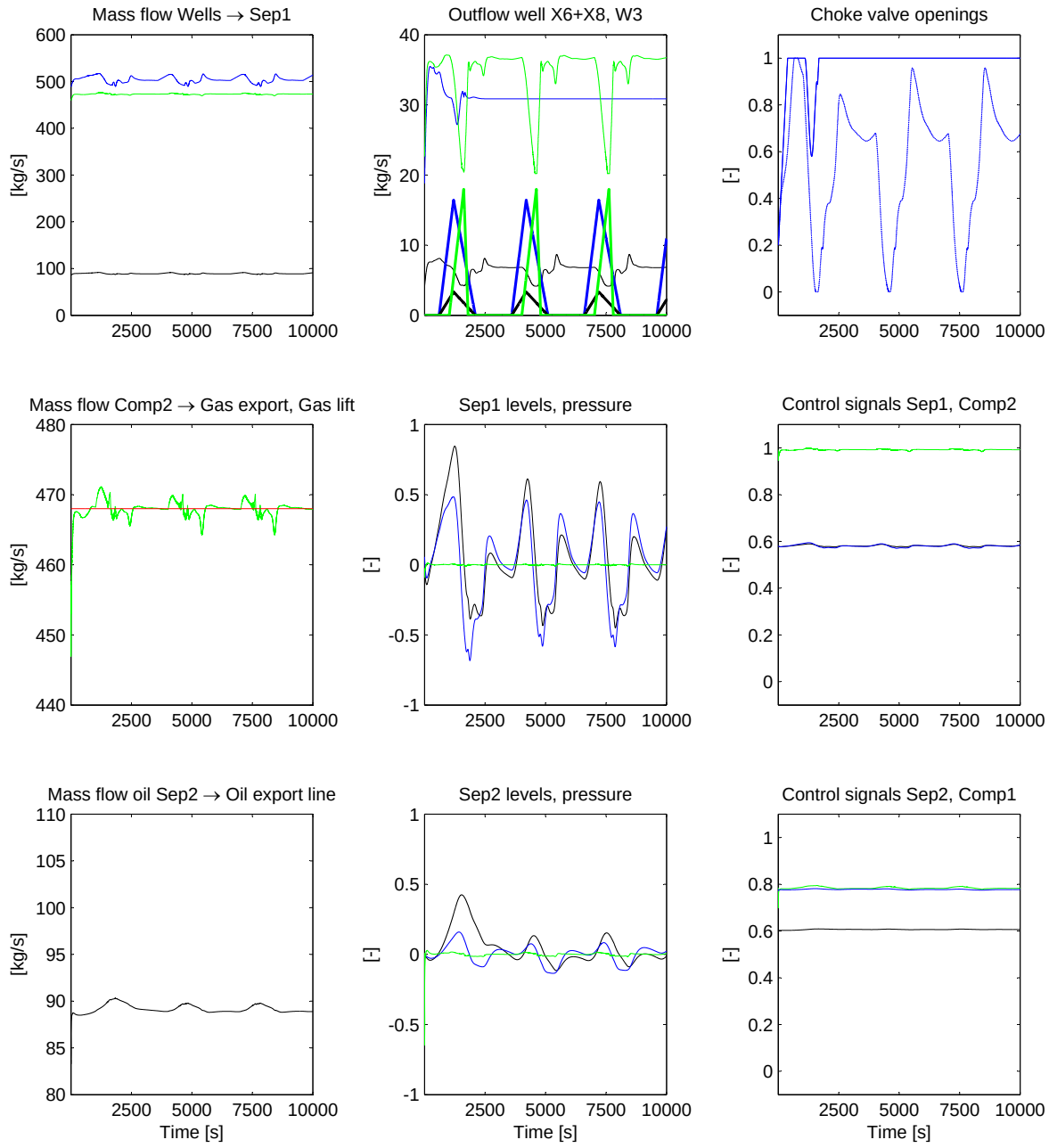

Figure 4.12: *DC1.* Slugging well - *X6* and *X8* choke valves are controlled. $\bar{w}_{o,s2} = 89.24$ [kg/s], $\mathrm{var}(w_{o,s2}) = 0.16$ [(kg/s)^2]. Green-gas, black-oil, blue-water. Choke valve control signals: *X6* solid, *X8* dotted. *W3* bold.

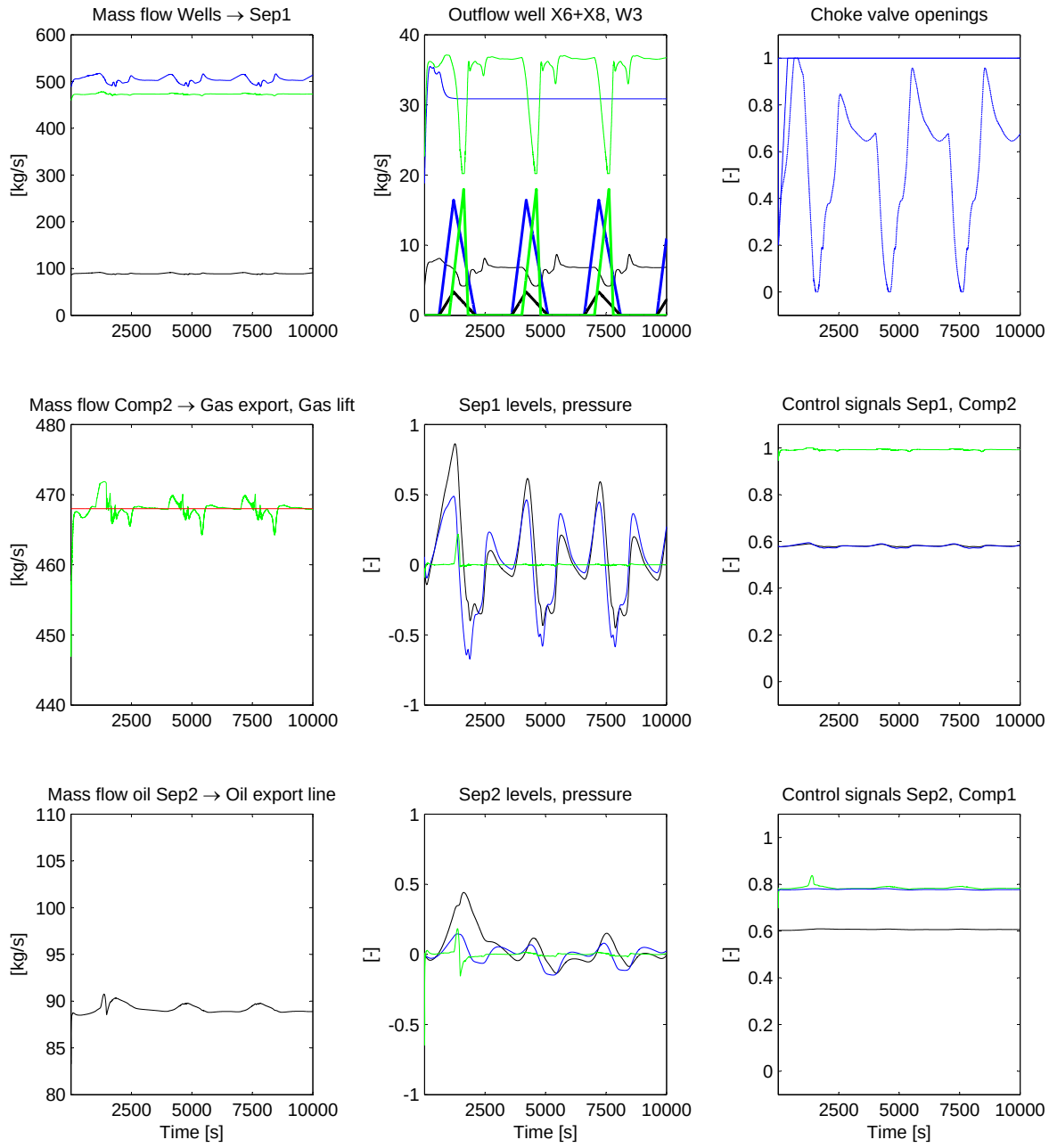

Figure 4.13: *DC1.* Slugging well - only *X8* choke valve is controlled. $\bar{w}_{o,s2} = 89.24$ [kg/s], $\text{var}(w_{o,s2}) = 0.18$ [(kg/s)^2]. Green-gas, black-oil, blue-water. Choke valve control signals: *X6* solid, *X8* dotted. *W3* bold.

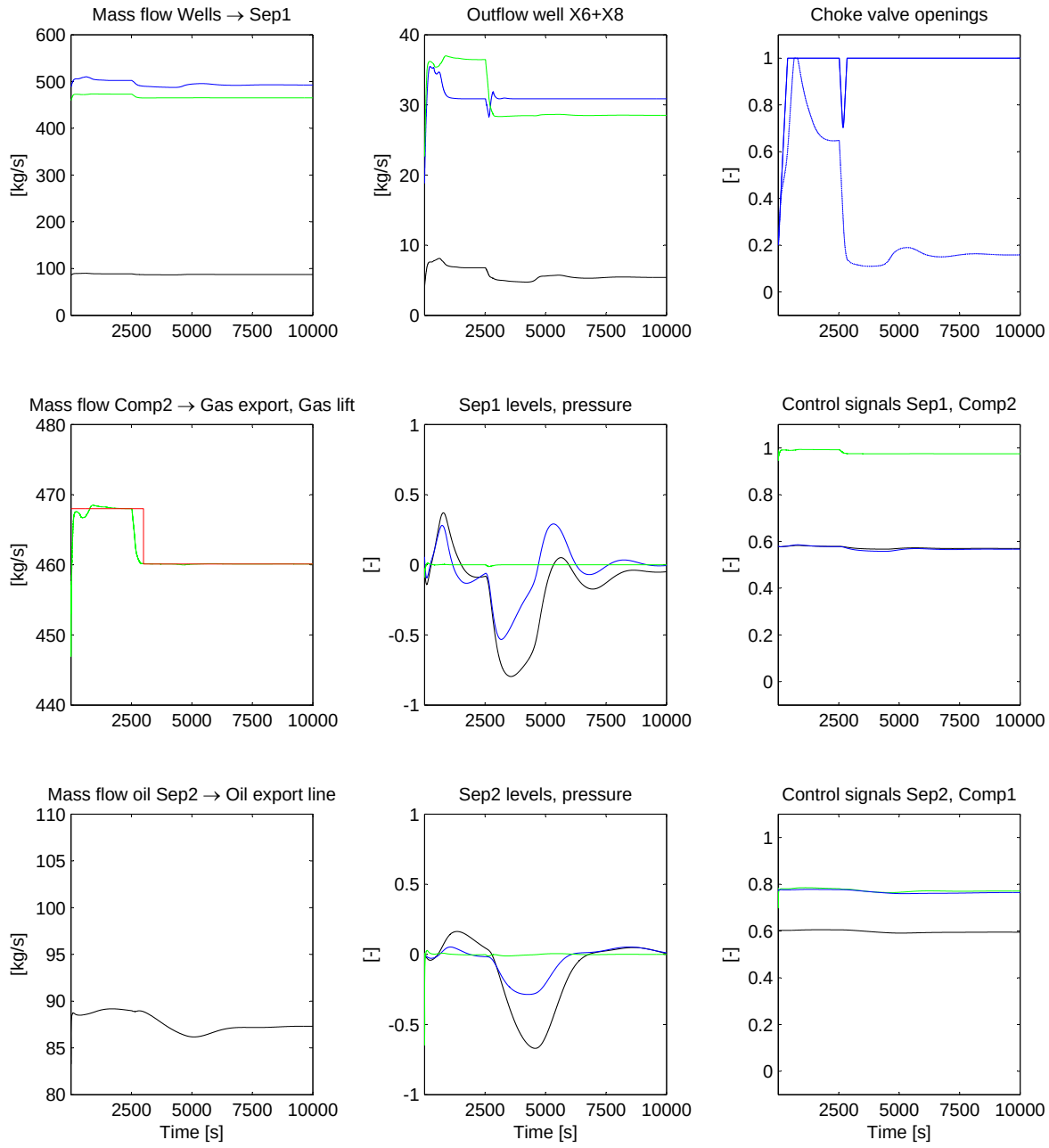

Figure 4.14: *DC1.* Gas rate constraint change - *X6* and *X8* choke valves are controlled. Green-gas, black-oil, blue-water. $\bar{w}_{o,s2} = 87.57$ [kg/s], $\text{var}(w_{o,s2}) = 0.89$ [(kg/s)^2]. Choke valve control signals: *X6* solid, *X8* dotted.

4.4 Manual choke valve control

The measurements in the upcoming simulation results were scaled as given in Table 4.1 on page 44.

Figures 4.15 and 4.16 show two different manual operating strategies for simulation *case 1*.

In the case of Figure 4.16, the flow rate of both wells are lowered in advance of the largest gas flow rate peak which occurs at the opening of the third well. Then, the choke valves are moved to the expected position of the steady state valve openings (we know the steady state valve openings by looking at the results of for instance *MPC1* in Section 4.1, while the operators must act from experience).

Figure 4.15 shows a choke valve handling strategy where the chokes are used a bit more actively, trying to keep closer to the gas rate constraint throughout the entire well startup interval.

Slugging wells are often dealt with by backing off from the process constraints when the wells are operated manually. The concept is that by setting the choke valves at sufficiently low openings, there should be room left for the disturbances when they occur. The result obtained using this strategy for simulation *case 2* is shown in Figure 4.17.

Simulation *case 3* is quite easily performed using manual control, see Figure 4.18. The difficulty would be that of timing the choke valve change, and also finding the right opening level to achieve a certain gas flow rate. In our case, this is achieved by looking at the *MPC1 case 3* results (see Figure 4.5), whereas the operators will have to rely on experience in order to get it right. Thus, the simulation results may be representing a somewhat best case scenario.

Once again, look to Section 5.1 for comments on the simulation results.

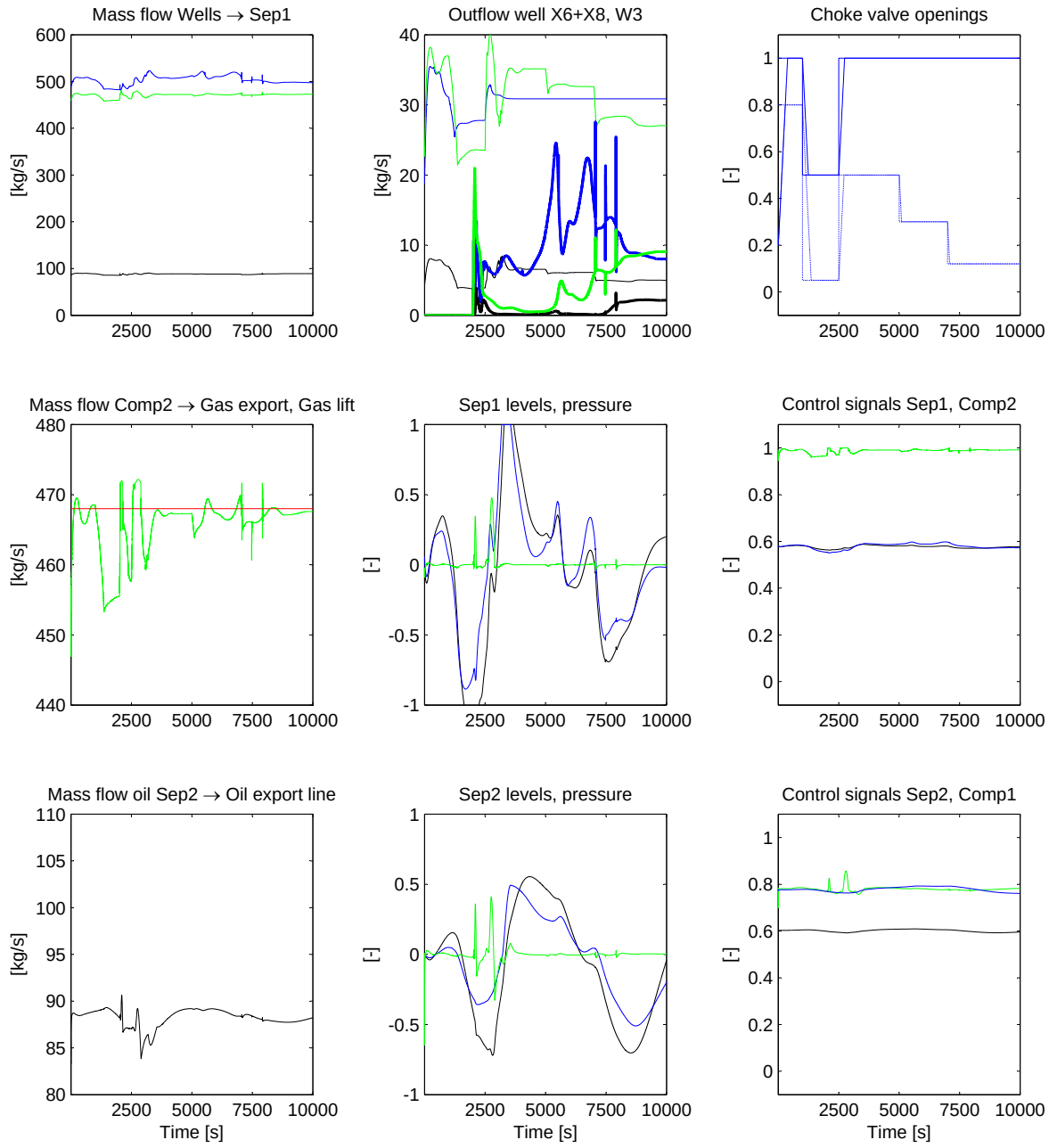

Figure 4.15: Manual choke valve control. Startup of well *W3*. $\bar{w}_{o,s2} = 88.20$ [kg/s], $\text{var}(w_{o,s2}) = 0.95$ [(kg/s)^2]. Green-gas, black-oil, blue-water. Choke valve control signals: *X6* solid, *X8* dotted. *W3* bold.

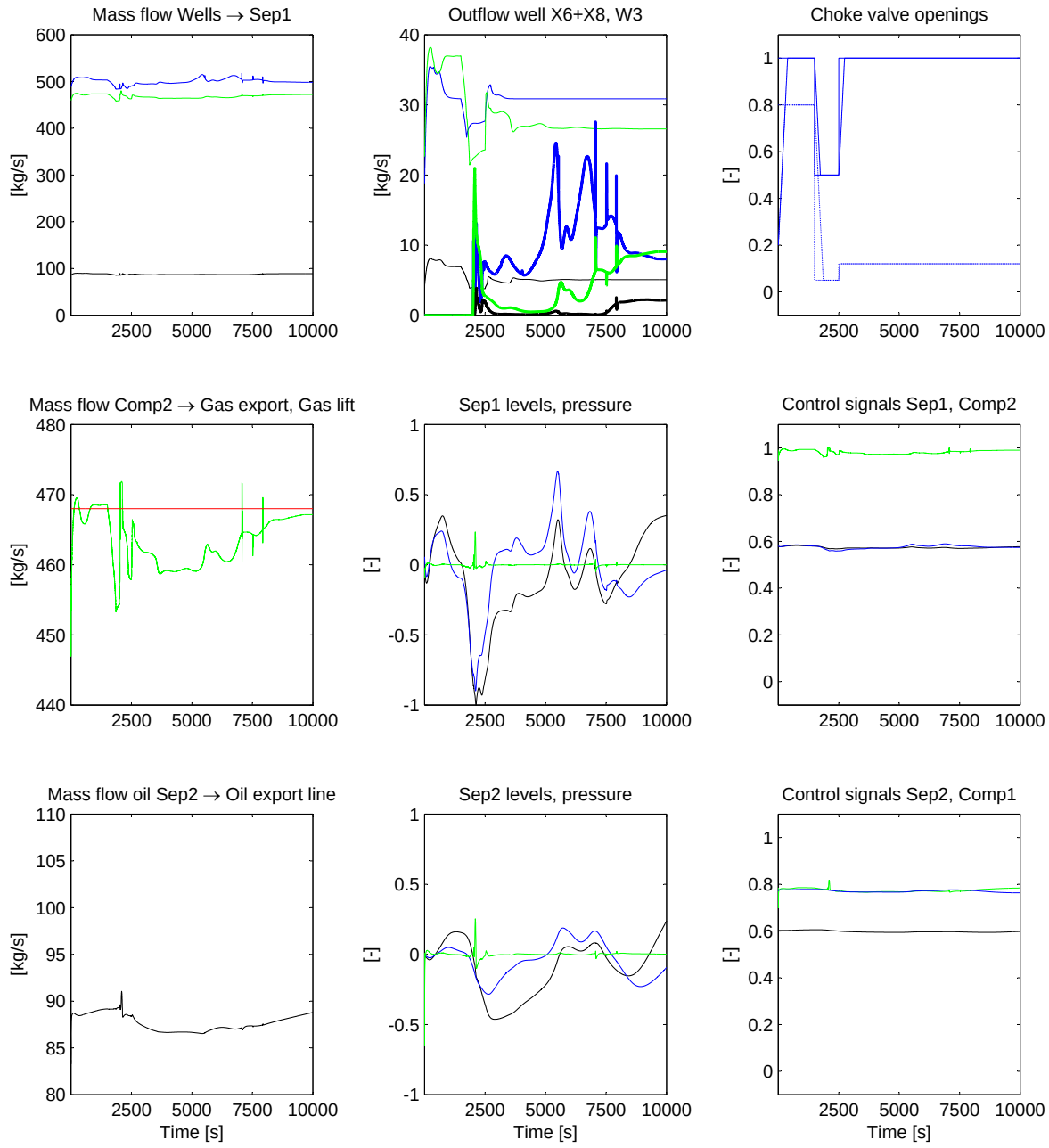

Figure 4.16: Manual choke valve control. Startup of well *W3*. $\bar{w}_{o,s2} = 87.62$ [kg/s], $\text{var}(w_{o,s2}) = 0.77$ [(kg/s)^2]. Green-gas, black-oil, blue-water. Choke valve control signals: *X6* solid, *X8* dotted. *W3* bold.

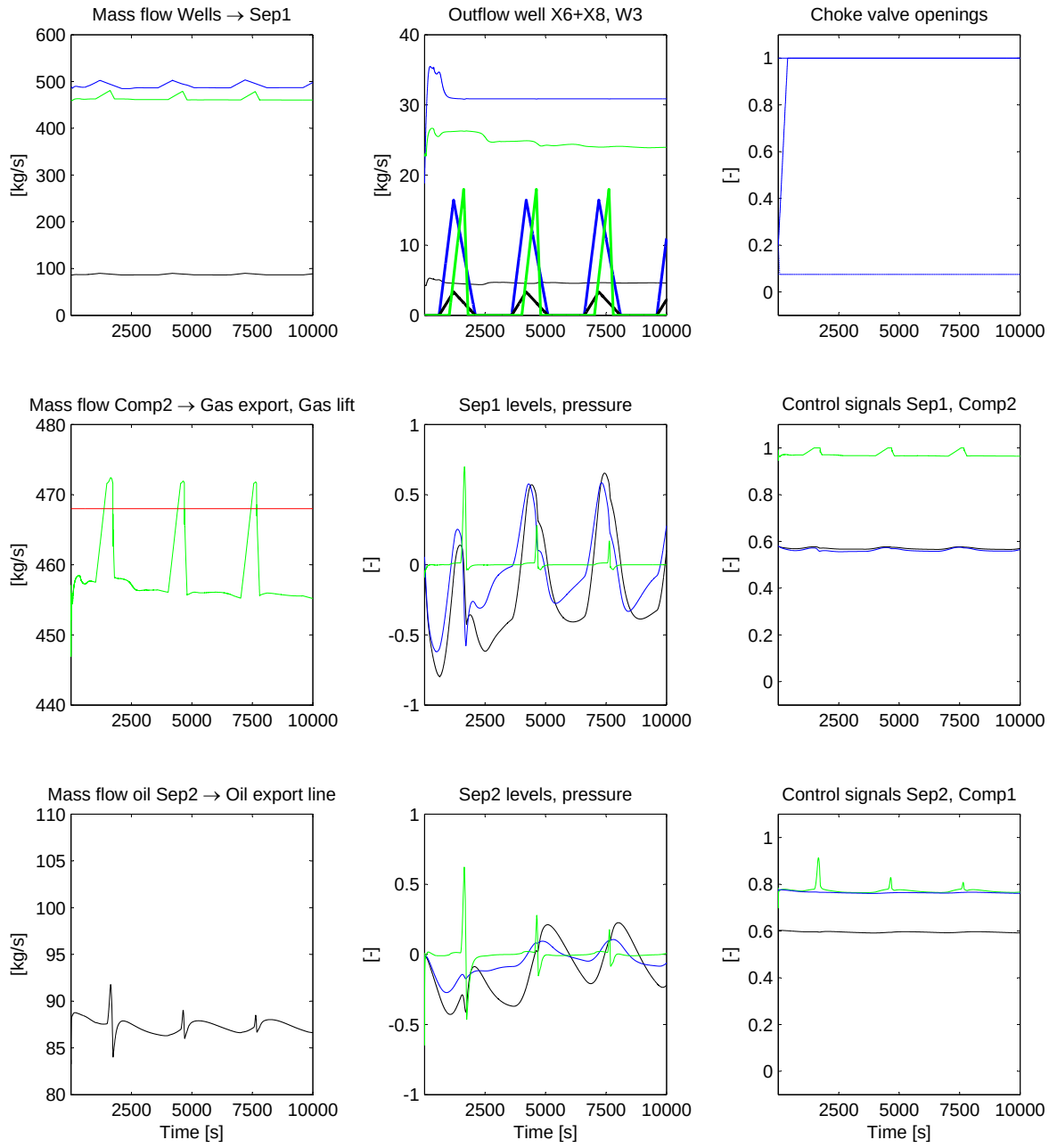

Figure 4.17: Manual choke valve control. Slugging well. $\bar{w}_{o,s2} = 87.27$ [kg/s], $\text{var}(w_{o,s2}) = 0.54$ [(kg/s)^2]. Green-gas, black-oil, blue-water. Choke valve control signals: *X6* solid, *X8* dotted. *W3* bold.

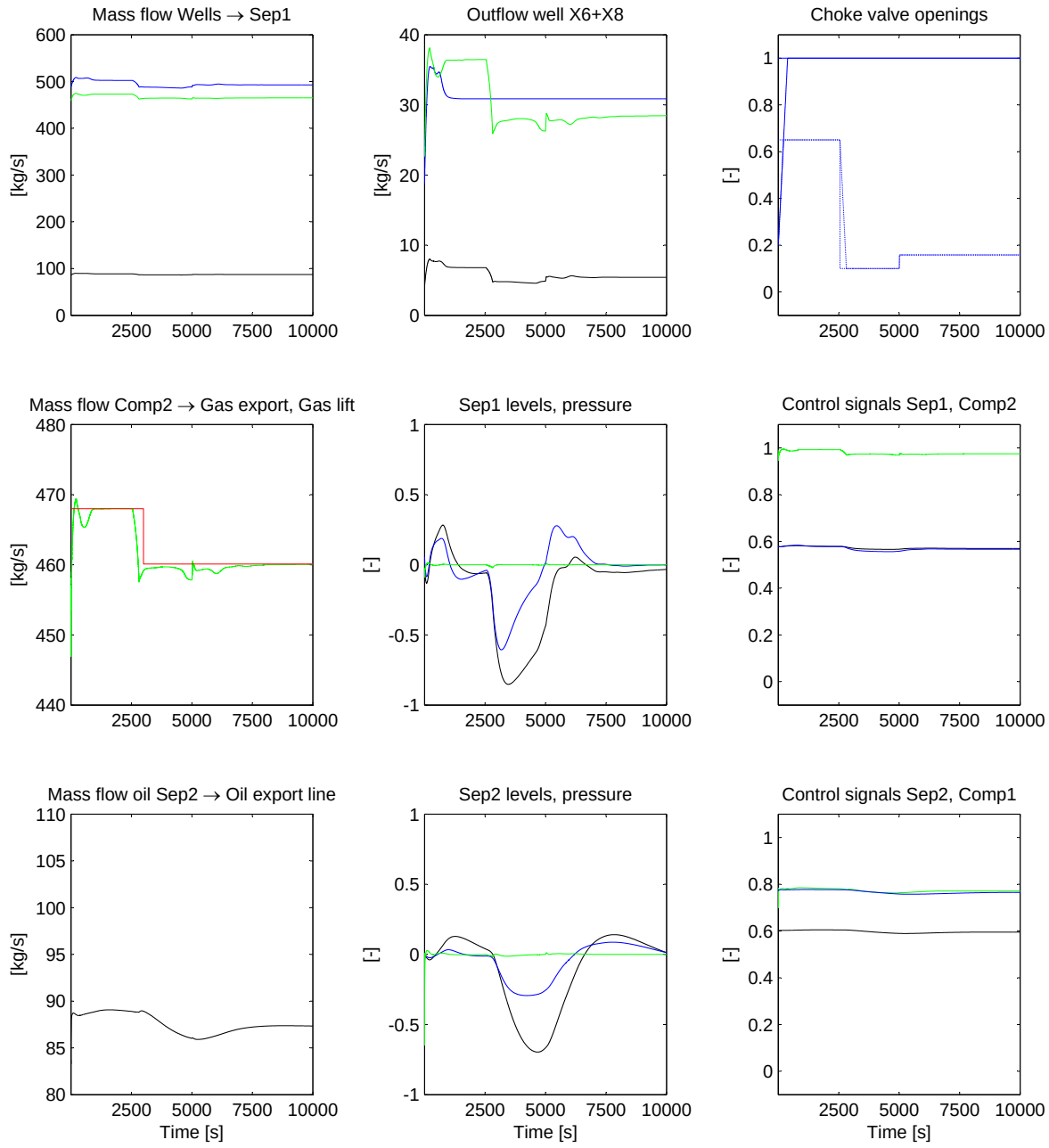

Figure 4.18: Manual choke valve control. Gas rate constraint change. $\bar{w}_{o,s2} = 87.48$ [kg/s], $\text{var}(w_{o,s2}) = 1.01$ [(kg/s)^2]. Green-gas, black-oil, blue-water. Choke valve control signals: *X6* solid, *X8* dotted.

Chapter 5

Discussion

5.1 Performance comparison

In Table 5.1 the performance of the various controllers are compared to the results obtained using manual control. $\bar{w}_{o,s2}$, the average oil outflow rate from the second separator tank, is used as a performance measure. The variance of $w_{o,s2}$ is also calculated for the various simulations. The data were obtained in the simulations of Chapter 4. Note that the first $1000s$ of the simulations were excluded from the calculations of $\bar{w}_{o,s2}$ and var($w_{o,s2}$) in order to avoid transient startup differences. The simulation results are commented in the sections below.

Table 5.1: Controller performance comparison. $\bar{w}_{o,s2}$ is the average oil outflow rate from the second separator tank. $w_{o,bias} = 81.90\ kg/s$ is the bias added during simulations representing the other wells as illustrated in Figure 1.2, and was merely used to fill the process capacity. (*: more aggressive, **: erroneous model)

Case	*Controller*	*Figure*	$var(w_{o,s2})$ $[(kg/s)^2]$	$\bar{w}_{o,s2}$ $[kg/s]$	$\bar{w}_{o,s2} - w_{o,bias}$ $[kg/s]$	*Increase over manual*
1 - Startup	MPC1, FF1	4.1	0.22	88.54	6.64	16%
	MPC1, FF2	4.2	0.19	88.47	6.57	15%
	MPC2	4.7	0.02	88.55	6.65	16%
	DC1, FF1	4.10	0.23	88.50	6.60	15%
	DC1, FF2	4.11	0.23	88.55	6.65	16%
	Manual*	4.15	0.95	88.20	6.30	10%
	Manual	4.16	0.77	87.62	5.72	-
2 - Slugging	MPC1	4.3	0.34	89.19	7.29	36%
	MPC2	4.8	0.05	89.14	7.24	35%
	DC1	4.12	0.16	89.24	7.34	37%
	Manual	4.17	0.54	87.27	5.37	-
3 - Constraint change	MPC1	4.5	0.81	87.58	5.68	2%
	MPC1**	4.6	1.06	87.32	5.42	-3%
	MPC2	4.9	0.28	87.50	5.60	0%
	DC1	4.14	0.89	87.57	5.67	2%
	Manual	4.18	1.01	87.48	5.58	-

5.1.1 Simulation case 1 - Startup of additional well

MPC1

Two feedforward schemes, denoted FF1 and FF2, were tested for *MPC1*. The schemes were presented in Section 3.3.2, and the simulation results obtained using FF1 and FF2 are shown in Figures 4.1 and 4.2, respectively.

MPC1 deals with the planned *W3* startup rather nicely in the case of both feedforward schemes, with *X6* and *X8* approximately inverting the *W3* gas inflow rate in both cases. By keeping the total gas outflow rate as close to its constraint as possible, the process throughput is maximized while the system is kept in the feasible region of operation.

Recalling that FF1 requires more modeling effort than that of FF2, it is interesting to note that apart from during the very initial phase of the *W3* startup, the flow rates achieved using the FF2 feedforward scheme is actually somewhat smoother than that of FF1. However, on the other hand, the FF1 average oil outflow rate is slightly higher than that of FF2.

MPC2

As Figure 4.7 shows, *MPC2* utilizes the buffering capacity of the separator tanks quite extensively. Also note that the tank levels are kept within the defined constraints at all times. Without the use of MPC integral action, the controller might have broken the constraints, due to the nonlinearity of the tank cross section. Further, we see that the levels of the second separator tank varies more smoothly than the levels of the first tank. The overall effect of the applied topside MPC is a smooth oil outflow from the second separator tank, which of course is an advantage for process equipment further downstream.

Comparing figures 4.1 and 4.7, we also see that the wells are operated quite similar in the case of *MPC1* and *MPC2*. This is as expected, since the MPC controlling the wells is set up practically in the same way in both cases, with the same cost function.

DC1

Figure 4.10 shows that the feedforward algorithm FF1 of *DC1* (presented in Section 3.5.3) worked quite well. There are very small pressure variations in the tanks. Also note that the choke valves start choking down prior to the disturbances, and by looking for instance at the peak of the gas inflow disturbance, we see that the down choking of the valves is timed quite well with the arrival of the disturbance.

The *DC1* feedforward algorithm FF2 was also presented in Section 3.5.3, and its simulation result is shown in Figure 4.11. It is pleasing to see that the simpler feedforward scheme works at least just as well as that of FF1, with a somewhat smoother gas flow rate and a slightly higher average oil outflow rate. As long as the choke valves are prepared for the most abrupt flow rate changes, the feedback control can take care of the smaller flow variations by itself, acting much in the same way as for the case of the slugging wells.

Manual choke valve control

Figure 4.16 shows an example of how an operator might be setting the choke valves during the startup of a third well. As the said figure illustrates, there is quite a lot of unused processing

capacity available during the well startup using this simple manual operating strategy (the topside gas outflow rate is generally far below its constraint).

Although it heightens the average oil outflow rate of the process, it also leads to less smooth flow rates and increased pressure variations in the tanks. This illustrates the difficulty of operating closer to the process constraints when using manual choke valve control.

Summary

The *case 1* simulations are shown in figures 4.1, 4.2, 4.7, 4.10, 4.11, 4.15 and 4.16.

The use of feedforward during well startup shows a good potential. It is also clear that much can be achieved by controlling the wells a bit more actively in the manual well control case. However, as Figure 4.15 illustrates, operating closer to the process constraints can be challenging when using manual choke valve control - the flow rates may become less smooth and the tank pressure variations may increase. Note that the measured performance increase will only be present until the newly opened well reaches stable production.

Figures 4.2 and 4.11 indicate that a lot can be achieved during startup of additional wells using ordinary feedback control (integral action in the case of the MPC). The prerequisite is that the largest abrupt disturbances are fed forward, either manually by setpoint or constraint manipulation, or automatically by the controller. This is because the choke valve stroke time is too long for the choke valve to be able to compensate for these disturbances instantaneously.

It is also worth pointing out that there is not a straight-forward answer to how one should implement feedforward in a PI controller regime. On the other hand, the ease of implementing feedforward is one of the big advantages of the MPC. However, the feedforward implementations for PI controllers presented in Section 3.5.3 proved to work to satisfaction in our simulation case.

By comparing the topside oil outflow rate variance achieved using *MPC2* to that of the other controllers, see Table 5.1, it is clear that a properly designed MPC can improve the utilization of the buffer tanks to a great extent, potentially leading to an almost constant topside outflow rate.

5.1.2 Simulation case 2 - Slugging well

MPC1

The slugging flow from well *W3* is illustrated in Figure 2.9. Two different MPC input change cost choices were used. In the first setup, used in Figure 4.3, the cost on input usage changes were relatively low compared to the setup used in the simulations of Figure 4.4, where r_1 and r_2 were changed from the initial 250 to 1000.

A relatively high cost on input changes yields a smoother control input. While a smooth control input is generally desirable, it may at the same time degrade the system performance. The effect of a too high input change cost is illustrated using the controller of Figure 4.4, which, compared to the controller of Figure 4.3, achieves a much poorer inflow disturbance rejection. The result is considerably larger tank pressure variations and less smooth topside process outflows in the setup used in Figure 4.4.

The controller of Figure 4.3 performs quite well, and is keeping the tank pressure at a rather constant level. This simulation case demonstrates the versatility of even a simple MPC when it is equipped with integral action.

It is worth noting that if the rise and fall time of the slugs become too short, any controller will eventually have to give up as the choke valve stroke times give an ultimate bound on what can be achieved with respect to inflow disturbance rejection by choke valve manipulation.

MPC2

MPC2 was able to smoothen out the effect of the unmeasured inflow disturbance from the slugging wells to a great extent, see Figure 4.8. It did however yield some pressure variations in the separator tanks. Recalling that the pressure control is managed by a decentralized control system alone, it is likely that this problem could have been reduced by additional controller tuning effort.

Looking at the said figure, it is apparent that the buffering capacity of the second separator tank could have been utilized even better. Note however that the cost function was tuned to perform well in all three simulation cases, and if it was tuned more specifically to this case, it might have performed less good in the other cases.

DC1

The controller used in Figure 4.12 handles the slugging well disturbance nicely, with practically no pressure changes in the separator tanks. Further, the oil outflow rate from the second separator tank is rather smooth.

In Figure 4.13, the *X6* choke valve has been left in a fully open position throughout the simulation. As is seen here, there is a slight pressure increase at one occasion. Comparing the two aforementioned figures, it becomes clear that FIC2 controlling the *X6* choke valve succeeds in its purpose of working against pressure increases in the tanks, and by acting only when absolutely needed, FIC2 ensures that *X6* will be at full production under normal operation and only choked down when needed.

Manual choke valve control

By backing off from the process constraints in order to have capacity for slugs entering the topside process, the operators must accept a lower production rate. Figure 4.17 illustrates the effect of this practice. Note that the loss will depend on the severeness of the slugs, as smaller disturbances will warrant for smaller back-offs. As can be seen, there are some tank pressure variations in addition to the lower production rate, and the outflow rates are not particularly smooth.

Summary

The *case 2* simulations are shown in figures 4.3, 4.4, 4.8, 4.12, 4.13 and 4.17.

The potential of achieving a performance improvement by using automatic control for slugging well compensation is quite apparent when looking at the figures of Table 5.1. It should however be noted that the improvement depends on the nature of the slugs. Smaller slugs may allow for a higher production rate also under the manual control regime. Likewise, more abrupt slugs may force the automatic controllers to a larger back-off from the process constraints nominally, thereby lowering the production rate towards that of the manual control case.

Also here, we note that the variance of the oil outflow rate from the topside process is particularly low for *MPC2*, which uses an MPC for topside flow rate control.

The gas flow rate out of the second compressor is somewhat less varying for *DC1* than for *MPC1* and *MPC2*. Even though the tank pressures, and thereby the compressor gas flow rates, were controlled using the same decentralized controllers in all cases, it is suspected that the MPC well controller could have performed better in those respects if the gas topside dynamics had been more thoroughly modeled. Another possibility is to have MPC involvement in the pressure and compressor control, but this may prove to be a challenge due to fast gas dynamics.

The simulation case with slugging wells is particularly interesting since the problem with slugging wells may persist for long periods of time once it first appears. Being able to operate closer to the process constraints throughout such disturbances could yield a significant economic gain.

5.1.3 Simulation case 3 - Reduced gas processing capacity

MPC1

Figure 4.5 illustrates that the MPC with a correct well model is capable of handling the planned constraint change nicely, keeping the flow rates at a high level as long as possible. Recalling that the steady state gain of the process is quite nonlinear (see Figure 2.3), it is pleasing to see that the second compressor gas flow rate is still kept below its constraint during the constraint change. This is not expected to have been possible without the help from the MPC integral action.

Figure 4.6 illustrates that also the MPC with an erroneous well model copes with the constraint change as such to satisfaction. However, by comparing figures 4.5 and 4.6, we see that the MPC has chosen to choke down on *X6* in the case with the erroneous linear MPC model, although this is actually the more profitable well. The consequence of this can be seen in Table 5.1, where we see a lowered average oil flow rate in the simulation of Figure 4.6. The loss may not seem too severe, but this is due to the two wells *X6* and *X8* producing somewhat similar amounts of oil (see Figure 2.6, remembering that in the MPC, the thin black line of *X8* is now increased by a factor of 1.5). If the difference between the wells had been greater, the loss would have increased too.

MPC2

As Figure 4.9 shows, *MPC2* yields a very smooth oil outflow also in simulation *case 3*. It does however result in quite a large tank holdup drop in the two separator tanks, and the holdup takes a long time to recover. This is not a big problem here, but if the topside inflow rates were further reduced due to a disturbance, the tanks would not be able to compensate for very long due to a lower holdup prior to the disturbance. One should however be able to better upon this situation by increasing the cost of level control deviations in the cost function of *MPC2*.

DC1

The gas flow rate constraint change in the simulation of Figure 4.14 results in a smooth and concise flow rate change, indicating that the setpoint manipulation strategy of equation (3.63) is a reasonable one. The flow rate is on target at the time of the actual constraint change. The overall system behavior is smooth. Note however that if the constraint change is large enough, there might be a need for an earlier initiation of the controller action in order to satisfy the constraint on time.

Manual choke valve control

Constraint change handling is quite easily performed using manual control, see Figure 4.18. One difficulty is however that the operator does not necessarily know which steady state valve opening is needed in order to reach a certain flow rate, so some adjustments will normally be needed. Note that there are some smaller variations in the compressor flow rates during the change. Other than this, the overall process flow rates are rather smooth during the transition. There is also the difficulty of timing the valve opening right in order not to start the valve opening change before it is strictly necessary.

Summary

The *case 3* simulations are shown in figures 4.5, 4.6, 4.9, 4.14 and 4.18.

Although there was a small gain in oil production when changing from manual to automatic control in simulation *case 3*, one of the main advantages of using automatic control is in this case considered to be that of the convenience factor, as timing the flow rate change with the arrival of an upcoming constraint change may be more easily achieved using automatic control.

The gas flow rate change is neatly timed with the constraint change using *MPC1* and *MPC2*.

One disadvantage with MPCs is demonstrated in the simulation of Figure 4.6. In this simulation, an error was introduced to the linear well model of the MPC, and as the said figure shows, *MPC1* chokes down on the most profitable well during the constraint change, due to the model identifying it as the less profitable one. For a comparison, look to the simulation of Figure 4.5, which is run with the correct well model. The resulting performance decrease in this particular simulation case can be found in Table 5.1. Although the loss was not too extensive here, it may be larger in other cases. One of the important lessons to be learned here, is that at least the mutual steady state gain between the different modeled wells should be correct in order to get the well choking priorities right.

The timing of the flow rate change when using a PI controller is largely dependent on the controller implementation, as the choke valve stroke time must be considered when deciding when to change the controller setpoint. In the case of *DC1*, it was decided to base the controller setpoints on the constraint one whole stroke time into the future, in order for the valve to be able to move over its entire opening range in time, should that be needed. This worked well in this case, but would have lead to an unnecessarily early valve opening change if the constraint change warranted only minor valve opening movements.

The realized topside oil outflow rate is quite smooth with all the different controller setups. However, the setup with the *MPC2* topside flow rate controller stands out as particularly smooth also in this case. *MPC2* achieved this by exchanging level deviation recovery speed for outflow smoothness.

5.2 Robustness

MPC1 and *MPC2* need a backup control system which will be used if the MPCs should fail for some reason. Being model based, they should also have a system for easy model updates, especially for updating the well model (at least the steady state gain for the different phase components of the individual wells). One possible effect of an erroneous MPC process model was demonstrated in the simulation of Figure 4.6. Look to the *MPC1* part of Section 5.1.3 for further comments on the simulation in question.

The *MPC2* topside PI flow rate controllers are dependent on flow rate estimates in order to function properly. It is clear that the performance of *MPC2* is closely linked to the quality of these estimates, at least for flow rate smoothing. With a lower estimate quality, one may consider a slower tuning of the flow controllers in order to avoid too much flow rate variations. Note that the simulations were performed using direct flow rate measurements in stead of estimates due to project time constraints. Thus, the simulation results may be considered to represent a best-case scenario.

The MPC integral action helps to robustify the MPCs by compensating for measurement prediction errors. It is highly likely that the realized linear MPCs would not have worked to satisfaction without integral action, much due to the extensive nonlinearity of the well flow rate steady state gains, as illustrated in Figure 2.2.

Further, the softening of process variable constraints is crucial to the feasibility of the MPCs. Without constraint softening, the MPCs would simply halt with an error message in the case of constraint violations. Thus, one could argue that the constraint softening is a very important step in the robustification of the MPCs. Note that control input set by the MPC alone need not be softened.

The PI controller based *DC1* has the advantage of not being dependent on a model during operation. The robustness properties of the PI controller is largely dependent on the parameter tuning and its applicability over the whole operational range of the process. However, *MPC1* and *MPC2*, *DC1* also needs a well priority system for deciding which wells which will be adjusted when the operational conditions change, and this priority setup should be easily updateable in order to avoid income loss.

Manual well control can be thought to be quite robust, as it only depends on the human operator and the choke valves, with in principle very little hardware and software in between. It does however depend on the experience and readiness of the operator, and may cause process shutdowns due to human failure.

All of the realized automatic controllers depend on a flow rate measurement in the gas compression train. This measurement may be infested with a considerable amount of noise. Consequently, one may consider using a flow rate estimator for cleaning up this measurement. Note however that the flow rate measurement in question is already used in closed loop in actual topside processes for controlling the recycle flow rate for compressor surge avoidance (the gas recycle loops are not included in the model used in this project). Thus, this measurement may be of adequate quality already. Also, considering the slow choke valve dynamics, one could consider using an average gas flow rate measurement for feedback in stead of using the instantaneous flow rate directly.

5.3 Other comments

Although *DC1* generally performed to satisfaction in the simulations carried out in this report, the situation may change in a case with a larger number of wells, as realizing a decentralized well choking priority scheme for a large number of wells may not be straight forward. One possibility for simplifying the decentralized control design in such a situation is to bundle the wells into a small number of priority groups and treat the groups as one well each, thereby reducing the problem size.

As a side note, the situation discussed above is where the MPCs are expected to really outshine their competition, as the implementation of the MPC should be just as easy for many as for few wells. Note however that with an increasing number of wells, the work required to keep the

well models (at least the steady state gains of the different phases in each well) up to date will increase as well.

Chapter 6

Conclusion

The objective of this thesis was to design and compare the performance of a decentralized and an MPC based control system for integrated automatic well and topside process control.

The work of this thesis can mainly be separated into three parts, namely

- Topside process and well model establishment and interconnection
- Controller design
- Simulation study and result assessment

6.1 Models

The topside process model and two OLGA well models were provided by Hydro at project startup. However, the well models needed some tweaking, as was also the case for the decentralized topside control system. The MATLAB platform model and the OLGA well models were connected through the OLGA MATLAB Toolbox. By using the pressure of the first separator tank as a boundary condition in the OLGA model, it was ensured that the model connection would be two-way interactive.

6.2 Controller design

One decentralized controller and two MPCs were designed in the work of this thesis. As part of the design, linear models of the topside process and the wells needed to be established. The basic properties of the different controllers are summarized in Table 6.1. Two different feedforward schemes were tested for both *MPC1* and *DC1*, the difference in both cases being that the simpler feedforward scheme only fed forward the largest abrupt predicted inflow rate changes, leaving the rest to feedback control. Interestingly, the simpler schemes performed just as well as the more detailed feedforward schemes.

Table 6.1: The realized controllers

Controller	*Well control*	*Topside control*	*Introduction*	*Illustration*
MPC1	MPC	Decentralized PI	Section 3.3	Figure 3.2
MPC2	MPC	MPC for PI setpoint control	Section 3.4	Figure 3.5
DC1	Decentralized PI	Decentralized PI	Section 3.5	Figure 3.7

6.3 Simulation results

For the simulation study, three disturbance scenarios were defined in cooperation with Hydro. The cases, which were presented in the beginning of Chapter 4, are listed below. Note that in the first and third simulation cases, feedforward is being used by the controllers.

1. Startup of third dynamic well
2. Slugging third well
3. Reduced gas processing capacity

The simulations were performed using the realized controllers as well as on a system with manual well control, thereby enabling a performance comparison with the results obtained using today's control conventions. The simulation results were discussed in Chapter 5, with a quantified performance comparison given in Table 5.1.

6.3.1 Outflow smoothness

Using the same decentralized topside control system, *MPC1* and *DC1* performed comparably with respect to the topside oil outflow rate smoothness. *MPC2* achieved a considerably lower variance in the oil outflow rate due to better separator tank buffering volume utilization. The manual well control system resulted in larger outflow variations than its competition due to less smooth well outflow rates, despite using the same topside control system as *MPC1* and *DC1*.

6.3.2 Oil throughput

In terms of oil throughput, the performance of the production system was optimized by maximizing the gas flow rate through the second topside compressor stage, which was identified as the process bottleneck. In order to avoid tank pressure build-ups, this meant keeping the compressor gas flow rate close to an upper flow rate constraint.

The automatic controllers performed quite similarly throughput-wise. Having subtracted the inflow bias (see Figure 1.2), which was merely added to fill the process capacity, the production system showed an oil throughput increase in the area of around 15% and 35% in simulation *case 1* and *2*, respectively, when comparing to the manual well control simulations. Note that the *case 1* production increase will only last until the newly opened well reaches stable production, while the increase seen in *case 2* may last for as long as the flow rates of the slugging well stay unstable. In simulation *case 3*, the throughput increase is more negligible. Here, the automatic controllers are considered to be more of a convenience factor, providing an easy way of timing the flow rate change to the arrival of the constraint change.

6.3.3 Remark

An important remark is that although the simple *DC1* control system seems favorable with its comparable performance to that of *MPC1* and *MPC2* while at the same time requiring a lot less modeling effort, it should be noted that its throughput may decrease relative to that of its competition as the number of controlled wells increases, since designing a decentralized well choking priority scheme may not be straight forward with a large number of wells. One possibility is bundling the wells into a small number of priority groups, and treat the groups as one well each. The implementation of the MPCs is not expected to increase in complexity when the number of wells increases, except for the extra well modeling effort. Consequently, it is expected that there will be an increased performance difference in favor of the MPCs in a system with a larger number of wells.

6.4 Conclusion summary

It has been demonstrated that there is a potential for a significant economic gain using an automatic integrated control system for the wells and topside process of modern day production systems for oil and gas.

DC1 showed a similar gain as *MPC1* and *MPC2*, despite its simpler structure and modeling requirements. It is however expected that the MPCs may outperform *DC1* as the number of wells increases, due to possible difficulties in designing an optimal decentralized well priority scheme in the case of *DC1* with an increased number of wells. Also note that feedforward from known disturbances is generally more easily realized in an MPC than in a decentralized controller.

Finally, we note that by applying a supervisory MPC to the topside control system, *MPC2* achieved significantly smoothened topside outflow rates, compared to what was achieved in the case of *MPC1* and *DC1*.

Chapter 7

Further work

Topside flow rate estimators

For *MPC2*, one of the next steps could be to implement the topside flow rate estimators which are needed by the topside PI flow rate controllers. Stange (2006) may be a place to look for ideas on how to approach this problem.

Larger number of simulated wells

A simulation study with a larger number of simulated wells may also be of interest, enabling the testing of different well priority schemes for the decentralized well controller. It is expected that the MPCs will perform better than the decentralized controllers in a simulation case with a larger number of wells.

Extremum seeking

One should choke down on the least profitable wells first when needed. One way of identifying those wells adaptively online is to apply an extremum seeking scheme to the system, slowly perturbing the control inputs slightly and observing the effect on some selected measurements or combinations thereof (for instance the ratio between the gas train outflow rate and the second separator tank oil outflow rate). The concept of extremum seeking is presented in Krstic and Wang (2000). Note that extremum seeking may be best suited for use with the decentralized well control scheme.

A few issues does however need to be addressed if extremum seeking is to be applied. First, input constraints must be dealt with, as it is not clear how one should perturb the input when it is pushing against its upper and lower constraints. Secondly, there is the problem of parameter constraints, as the parameter which is sought for, the choking split fraction, is constrained between choking 100% on one well and 100% on the other well, but there is no facilities for constraining the parameter estimate which is found in the extremum seeking algorithm. Thus, the estimate may wind up past the constraint. In this case, the algorithm may correctly find the optimum being to choke mainly on one well, but may not be able to detect later changes in the optimum once it saturates.

Input blocking

During simulation runs of *MPC2*, it was observed that the topside MPC used about 10% of the CPU time, with the well controlling MPC and the OLGA model splitting most of the remaining time about equally (note that the MPCs were running with a $40s$ sampling time, while the minimum sampling time of the OLGA model, internally in OLGA, was $1.25s$, and the topside model simulation and the low level controllers were running at $1s$ sampling time).

One could consider applying input blocking a while into the MPC horizon, particularly for the well controlling MPC, constraining the control input to stay at the same values for several consecutive iterations, thereby cutting optimization time. Note that this means that the constraint on the input rate of change need to be incremented for the input blocked iterations.

MATLAB MPC Toolbox

It seems that the MATLAB MPC Toolbox only supports quadratic reference tracking with positive costs with respect to the measurements in the cost function. It would seem that this doesn't comply very well with our defined cost function for the production well controller, which tries to maximize the oil flow rate measurement (one can look at this as maximizing the flow rate deviation from a thought zero reference).

However, if desired, it should be possible to use the MATLAB MPC Toolbox as the MPC implementation environment by applying a small change to the cost function. By defining a somewhat unrealistically high flow rate reference for the oil flow rate, it would still in effect be maximized.

Bibliography

M. Krstic and H.H. Wang. Stability of extremum seeking feedback for general nonlinear dynamic systems. *Automatica*, 36(4):595–601, 2000.

J. M. Maciejowski. *Predictive Control with Constraints*. Prentice Hall, 2002.

S. Skogestad. Tuning for smooth PID control with acceptable disturbance rejection, 2006. Refined version of the paper 'Lower limit on controller gain for acceptable disturbance rejection', presented at IFAC-symposium Adchem 2003, Hong Kong.

S. Skogestad. Control structure design for complete chemical plants. *Computers & Chemical Engineering*, 28(1):219–234, 2004.

M. Stange. *Estimering av strømningsratene inn og ut av en trefaseseparatortank ved bruk av Kalmanfilter*. Norsk Hydro ASA, Summer internship report. Supervised by Alstad, V., 2006.

Appendix A

Topside process key parameters

The tables below hold parameter values used in the topside process model. The model was presented in Section 2.1.

Table A.1: Parameters separator tank 1

Parameter	*Value*	*Unit*
Diameter	3.1540	m
Length	8.4667	m
Weir height	1.0000	m
Weir position	5.5350	m
Temperature	350	K
$K_{v,o,1}$	0.0150	$\sqrt{\frac{kg \cdot m^3}{s^2 \cdot Pa}}$
$K_{v,w,1}$	0.0300	$\sqrt{\frac{kg \cdot m^3}{s^2 \cdot Pa}}$
$p_{ext,w,1}$	$1.75 \cdot 10^5$	Pa

Table A.2: Parameters separator tank 2

Parameter	*Value*	*Unit*
Diameter	3.1540	m
Length	5.8922	m
Weir height	1.0000	m
Weir position	5.5350	m
Temperature	350	K
$K_{v,o,2}$	0.0200	$\sqrt{\frac{kg \cdot m^3}{s^2 \cdot Pa}}$
$K_{v,w,2}$	0.0040	$\sqrt{\frac{kg \cdot m^3}{s^2 \cdot Pa}}$
$p_{ext,w,2}$	$1.00 \cdot 10^5$	Pa
$p_{ext,o,2}$	$1.00 \cdot 10^5$	Pa

Table A.3: Parameters compressor 1

Parameter	*Value*
c_0	8.0000
c_1	0.0600
c_2	-0.0080
N_{max}	1.4000
N_{min}	0.4000

Table A.4: Parameters compressor 2

Parameter	*Value*
c_0	130.0000
c_1	0.0600
c_2	-0.0010
N_{max}	1.4000
N_{min}	0.4000
$p_{ext,g}$	$80.00 \cdot 10^5$ $[Pa]$